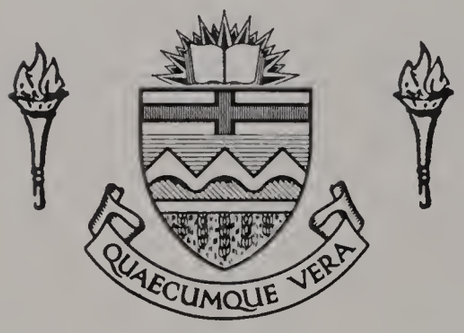

THE UNIVERSITY OF ALBERTA

RELEASE FORM

NAME OF AUTHOR ZBIGNIEW KAZMIERCZAK

TITLE OF THESIS SEISMIC CRUSTAL STUDIES IN SASKATCHEWAN

DEGREE FOR WHICH THESIS WAS PRESENTED MASTER OF SCIENCE

YEAR THIS DEGREE GRANTED 1980

THE UNIVERSITY OF ALBERTA

SEISMIC CRUSTAL STUDIES IN SASKATCHEWAN

by

ZBIGNIEW KAZMIERCZAK

A THESIS

SUBMITTED TO THE FACULTY OF GRADUATE STUDIES AND RESEARCH

IN PARTIAL FULFILMENT OF THE REQUIREMENTS FOR THE DEGREE

OF MASTER OF SCIENCE

IN

GEOPHYSICS

DEPARTMENT OF PHYSICS

EDMONTON, ALBERTA

FALL, 1980

THE UNIVERSITY OF ALBERTA

FACULTY OF GRADUATE STUDIES AND RESEARCH

The undersigned certify that they have read, and recommend to the Faculty of Graduate Studies and Research, for acceptance, a thesis entitled SEISMIC CRUSTAL STUDIES IN SASKATCHEWAN submitted by ZBIGNIEW KAZMIERCZAK in partial fulfilment of the requirements for the degree of MASTER OF SCIENCE in GEOPHYSICS.

ABSTRACT

Seismic refraction techniques have been employed in crustal studies of southern Saskatchewan. Two receiver sites and five shotpoint locations yielded the seismic data from five profiles ranging from 207 to 381 km in length. Seismic data have been subjected to a number of processing steps. Power spectral estimates indicate that the body wave energy is confined always between 2 and 20 Hz.

Travel time results of the first compressional waves with an analysis of the computed models lead to the following conclusions. (1)There is support for the existance of one or more major crustal faults in southern Saskatchewan running in the N.S. direction. The vertical displacement along the *Moho discontinuity* at about 103°W is at least 8-10 km. (2)Of a similar nature a crustal fault seems to exist on the Leross/Cabri profile at a longitude of 105°W. (3)The depth to the *Mohorovičić discontinuity* in southern Saskatchewan varies from 40 to more than 50 km. (4)The pattern of crustal thickness changes in southern Saskatchewan indicates the existance of Precambrian block faulting with north-south trends in the east and possibly complex N.E.-S.W. trends in the west. An identification of secondary arrivals was attempted using both the observed and computed travel times as well as an analysis of the ground motion and the apparent velocities across the recording line. The results of previous seismic surveys in the area are summarized and comparison of the crustal models is made.

The operational, instrumental and theoretical aspects of the work are discussed.

ACKNOWLEDGEMENTS

I would like to express sincere appreciation to my supervisor Dr. E.R.Kanasewich who originally proposed the project to me and who provided guidance and assistance throughout the entire study.

I would like to thank Dr. G.L.Cumming who supplied me with much information used in many phases of my work.

I would like to thank Mr. C.H.McCloughan for sharing with me his experiance with computer software matters and for his assistance in much of the preliminary processing of the data.

I wish to express my appreciation to the University of Alberta for financial support in form of a Graduate Teaching Assistantship throughout the entire programme.

Table of Contents

LIST OF TABLES

LIST OF FIGURES

1. INTRODUCTION

1.1 Brief Historical Review of Crustal Studies

Seismic crustal studies go back to the beginning of this century when Mohorovičić (1910) recorded earthquakes at some stations located within the range of several hundred kilometers from the epicentre. This led to the first profile which assumed the existence, below a sedimentary cover, of a crustal layer about 30 km thick with P and S waves velocities of about 5.6 and 3.3 km/s respectively. The discontinuity at its base (*Moho* or *M discontinuity*), in which the P wave velocity increases to about 8 km/s, is now generally considered as the boundary between the crust and underlying mantle.

A single layer model was challenged by Conrad (1925) who divided the crust into a two-layered system. The discontinuity (*Conrad* or *C discontinuity*), located at a depth of about two thirds of the crustal thickness, separated an upper layer ('*granitic layer*' as suggested by Jeffreys(1937)) from a lower one (classified as '*intermediate*' by Jeffreys) in which the velocities rose to some 6.5 and 3.6 km/s for P and S waves respectively.

Since that time a great deal of reliable data from artificial blasts have been accumulated allowing seismologists to determine the structure in much more detail. In the light of recent findings Jeffreys' hypothesis of varying crustal composition from acidic at the top to

basic at the bottom seems to hold, however, the problem of layering is more complex. The overwhelming amount of data supports the idea that the crust is multi-layered. The number of layers, their composition and the depths at which they occur appears to be a local phenomenon. Only the *M discontinuity* can be correlated in all parts of the world and areas in which it cannot be observed are found to be tectonically anomalous.

The most extensive crustal studies have been carried out in Central Europe, North America and the USSR. Many local crustal models have been derived using travel time curves and amplitude data. The use of synthetic seismograms makes it possible to discriminate between different models which on the basis of travel time observation alone were considered to be eqivalent.

A survey of the regions where more detailed velocity-depth functions have been obtained was made by Heacock (1971). More recently, detailed seismic refraction studies in the USA have been carried out by Braile *et al.* (1974) and Keller *et al.* (1975). At the same time in Central Europe, detailed intepretations of crustal seismic data have been attempted by many authors (Mueller *et al.*, 1973, Edel *et al.*, 1975, Meissner *et al.*, 1976, Prodehl *et al.*, 1976, and Mueller, 1977).

A typical example of a finely layered structural model of the crust is presented in Fig.1.1. It was proposed by Mueller (1977) and is based primarily on data from Central

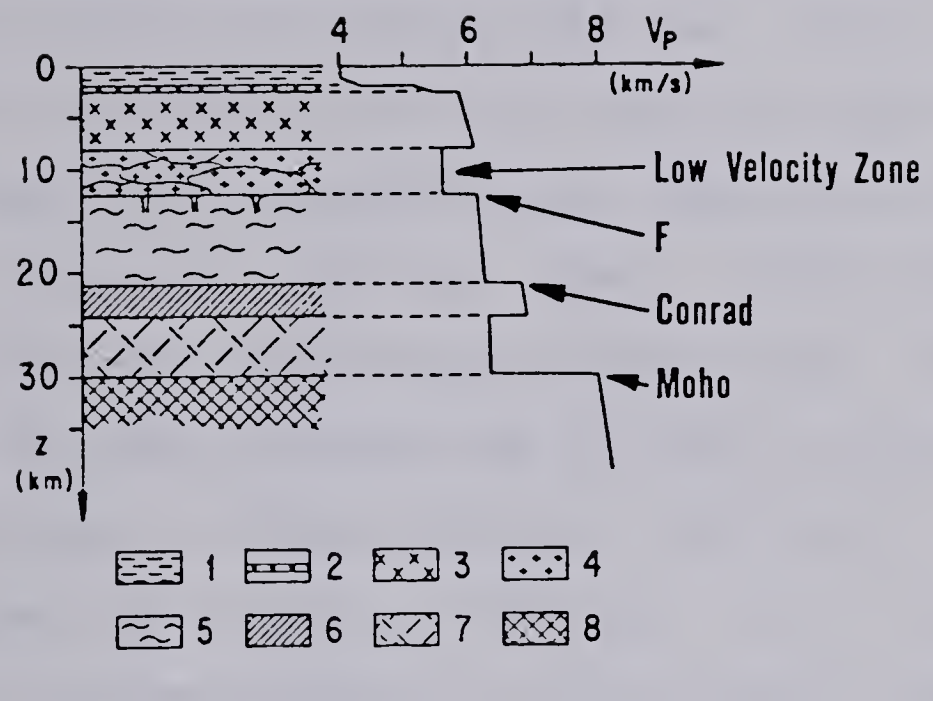

Fig.1.1. Schematic model of the continental crust (after Mueller, 1977).
1.Cenozoic sediment (near-surface low-velocity layer).
2.Mesozoic (and Paleozoic)sediment.
3.Upper crystalline basement consisting of metamorphic rocks such as gneisses and schists (zone of positive velocity gradient).
4.Laccolithic zone of granitic intrusions (sialic low-velocity zone).
5.Migmatites (middle crustal layer).
6.Amphibolites (high-velocity tooth).
7.Granulites (lower crustal layer).
8.Ultramafic (uppermost mantle).

Europe. The most significant features of the model are as follows:

1. The upper crystalline basement has a much smaller velocity gradient than has been predicted from laboratory measurements. Increasing pressure in the interstices of the low-porosity basement seems to be responsible for this phenomenon (Mueller, 1977).
2. The sialic low-velocity zone at a depth of about 10 km is associated with a semicontinuous laccolithic zone of granitic intrusion having lower velocities and densities than the surrounding basement rocks. Also in that zone the water content and the pore pressure, not the temperature, is likely the most significant factor in the observed processes (Mueller, 1977). The lower boundary of the zone appears to be relatively sharp and can be considered as being identical to the *F discontinuity* introduced by Liebscher (1962, 1964) which is eqivalent to the *G discontinuity* quoted in the Russian literature (Polshkov *et al.*, 1973).
3. The middle and lower crustal layers are characterized by a relatively low average velocity in which the *Conrad discontinuity* has been reduced to a few kilometers thick high-velocity tooth (Mueller, 1977).
4. A large velocity jump occurs at the crust-mantle transition zone which seems to be relatively sharp and well defined worldwide. There are some strong suggestions that the topmost part of the mantle is

laminated (Clowes and Kanasewich, 1970). This would explain the observed normal incidence reflections and the P_n velocity anisotropy.

Seismic crustal studies in Canada have been carried out for over 40 years. It was on December 27, 1938, when the first recorded rockburst took place in a mine at Kirkland Lake, Ontario. This and subsequent events initiated the Dominion Observatory's rockburst programme which led to the first crustal profile in the country (Hodgson, 1947). Long range modern studies with controlled explosions and high-fidelity recording began however in 1958 with the first reversed refraction profile in the world as carried out by Richards and Walker (1959) in southern Alberta. There was also an unreversed profile from the Ripple Rock, British Columbia, explosion on April 5, 1958. Now a number of groups both from the Universities and the Government carry out some form of seismic crustal studies.

The results of various refraction and reflection experiments with the seismic models that have been derived were summarized by Kanasewich (1966) and Berry (1973). Berry and Mair (1977) discussed the validity of the various crustal models and compared results from three tectonic provinces. The locations of seismic survey lines in Canada and some of the results obtained are shown in Fig.1.2. From published papers some general conclusions can be drawn:

1. The P or compressional velocity of the mantle (called P_n for the n-th layer) at the Moho discontinuity varies

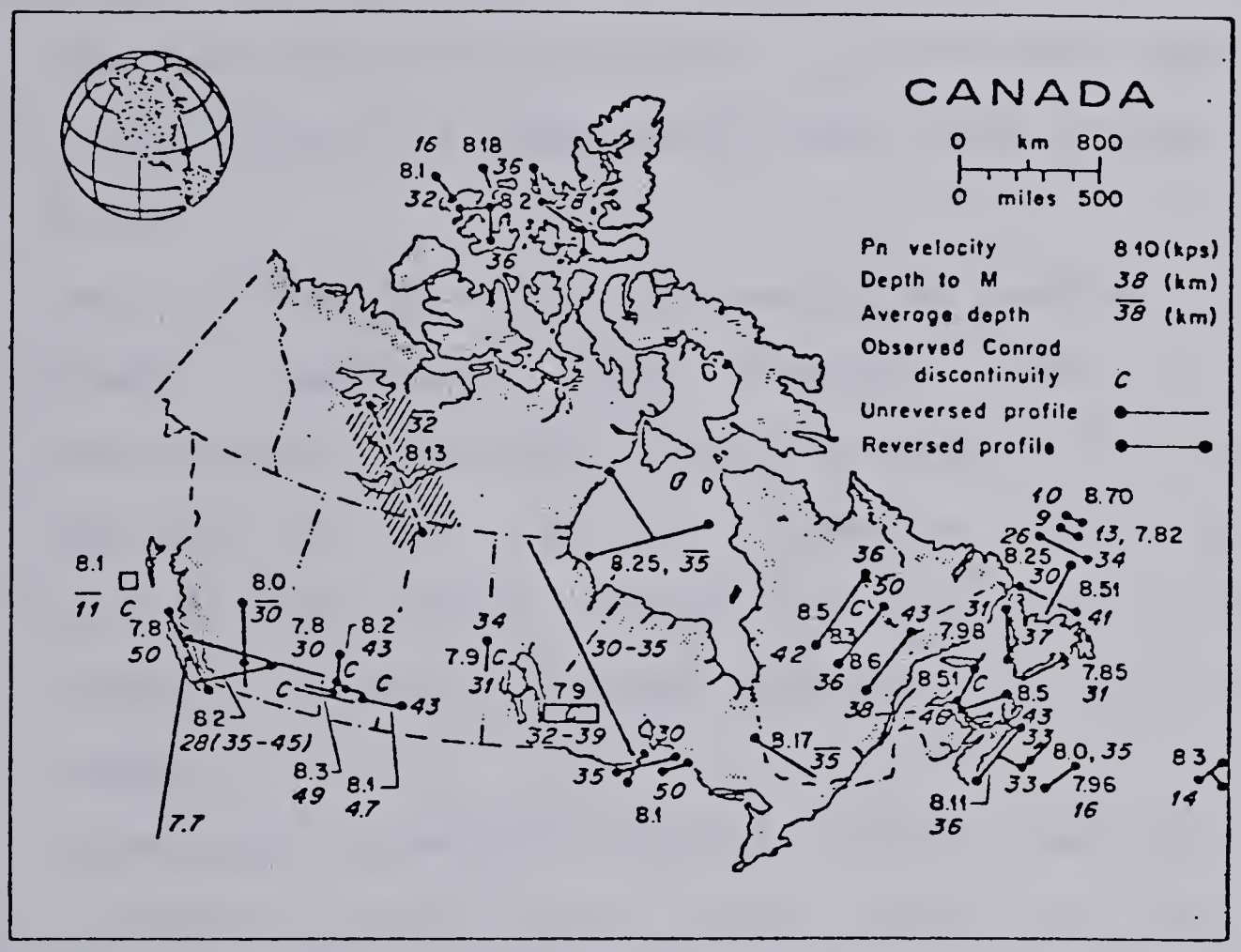

Fig.1.2. The most important crustal features and upper-mantle P-wave velocity as determine by seismic refraction and reflection experiments (after M.J.Berry, 1973).

widely depending on the region from a value possibly as low as 7.7 km/s beneath Vancouver Island to 8.6 km/s and higher in the extreme eastern parts of the shield and in some areas of the Atlantic coast.

2. The crustal thickness on the continent also varies widely from 30 km up to over 50 km, with higher values below Vancouver Island, south Prairies, the Lake Superior and some eastern parts of the shield. There is no indication of a continental crust being thinner than 29 km.

3. The *Riel discontinuity*, (Kanasewich and Cumming, 1965, Clowes, Kanasewich and Cumming, 1968) a deep intra-crustal reflector and refractor, is widely reported on the Prairies. It may be present in some areas of the eastern shield and the Arctic coast, however, it has not been reported in the rest of Canada.

Recent detailed seismic studies in North America such as the COCORP project (Oliver *et al.*, 1976, Schilt *et al.*, 1979) and COCRUST project (Green *et al.*, 1979) have revealed some fine structure within the crust. The exact picture, however, requires more extensive seismic surveys and is still the matter of analysis and discussions. An example of the possible complexity of velocity-depth functions is shown in Fig.1.3. The results presented come from an experiment which attempted to determine the velocity structure of the crust along three profiles located in two geological

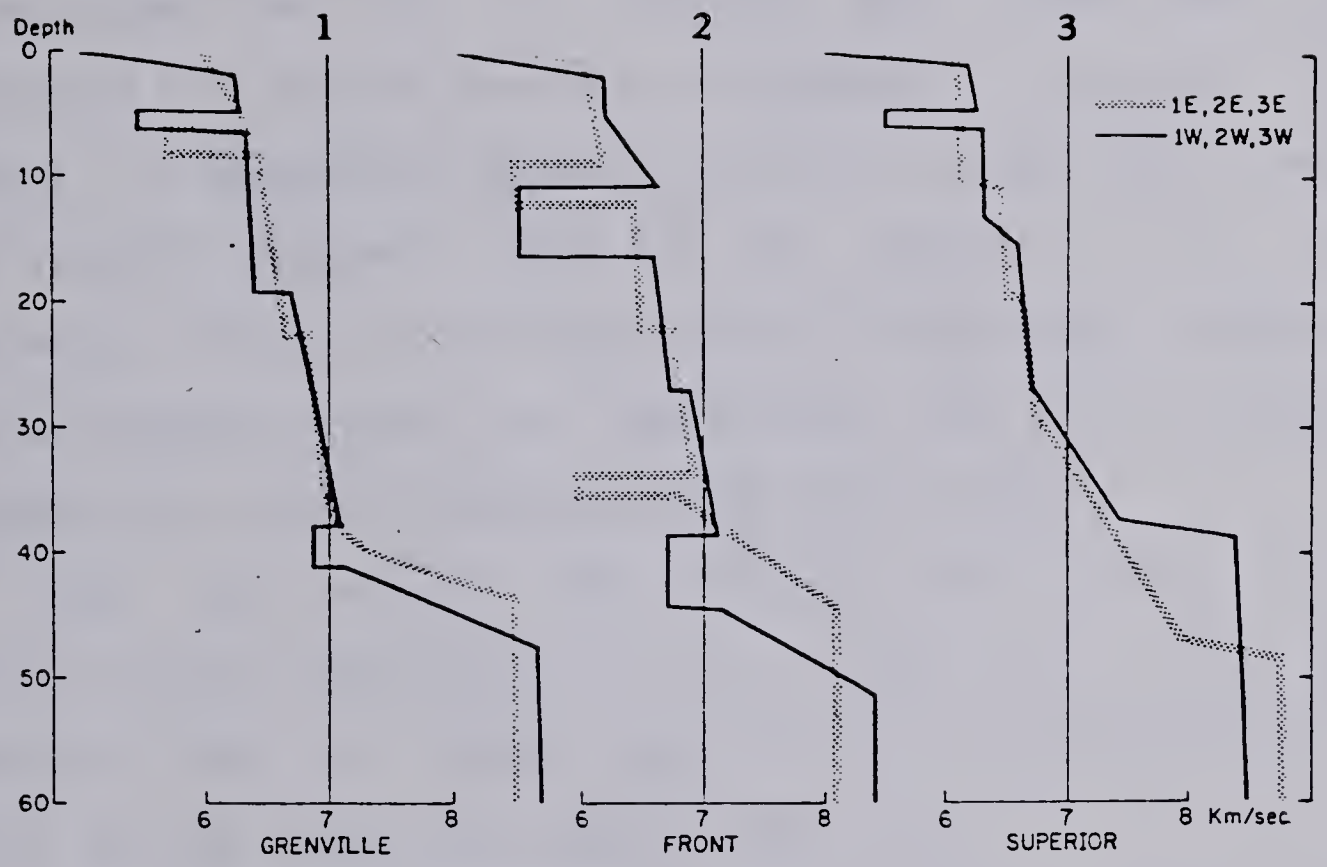

Fig.1.3. The six P-wave velocity models obtained for the three reversed profiles of the Grenville-Superior refraction experiments. The solid lines represents profiles derived from eastern shotpoints, while the stippled lines represent profiles derived from western shotpoints (after Berry and Fuchs, 1973).

provinces (Grenville and Superior) and at the boundary between them (Berry and Fuchs, 1973).

The family resemblance of the six models suggests that the main features are a generally valid representation of the real crust in the region. The velocity of the upper crust is appropriate to granite, while that of the lower crust is represented best by an increase with depth that is not necessarily a smooth function. Furthemore, some small scale lateral inhomogenity appears to exist in the lower crust. A low velocity channel seems to be present in all cases becoming thicker and deeper under the boundary between the two provinces and can be correlated with the pronounced low-gravity anomaly centred along the boundary.

One can notice the striking similarities in the velocity-depth functions of Fig.1.1 and Fig.1.3. This might indicate that at least some of the fine features of the crust may be common on a world-wide scale.

Berry and Mair (1977) list four factors which mostly determine the velocity structure of the crust:

1. The tectonic type of an area which includes the geochemistry of the rocks and their orogenic history.
2. The water content both in the form of hydrated minerals or in a free form as pore fluid.
3. The past and present values of stress.
4. The past and present temperature regime.

Thus, knowing the factors for a certain region, one might expect that the velocity-depth function will follow a

certain theoretical pattern. However, we would like to deduce the converse. Ideally the seismic velocity structure should tell us the history of the region, the lithology at various depths, as well as the variation of such physical parameters, as stress, porosity, permeability, and temperature with depth.

1.2 The Main Geologic and Geophysical Features of the Superior-Churchill Boundary Zone

Geologically Canada is divided into a number of regions(Fig.1.4.). The area of the 1979 seismic refraction profile is in southern Saskatchewan and south-western Manitoba. It is placed entirely within the Interior Platform, which is the part of the North American craton that subsided slightly in the past and now is covered by Phanerozoic sedimentary rocks. To the north and east the craton outcrops forming the Precambrian Canadian Shield consisting of a number of structural provinces. To the west of the Interior Platform the craton is bordered by the Cordilleran Orogen, a geosyncline composed mainly of Phanerozoic and late Precambrian rocks which have been deformed at various times (Douglas, 1968).

1.2.1 The Superior-Churchill boundary zone in northern Manitoba

Fig.1.4. Geological regions of Canada (from *Geology and Economic Minerals of Canada*, 1970).

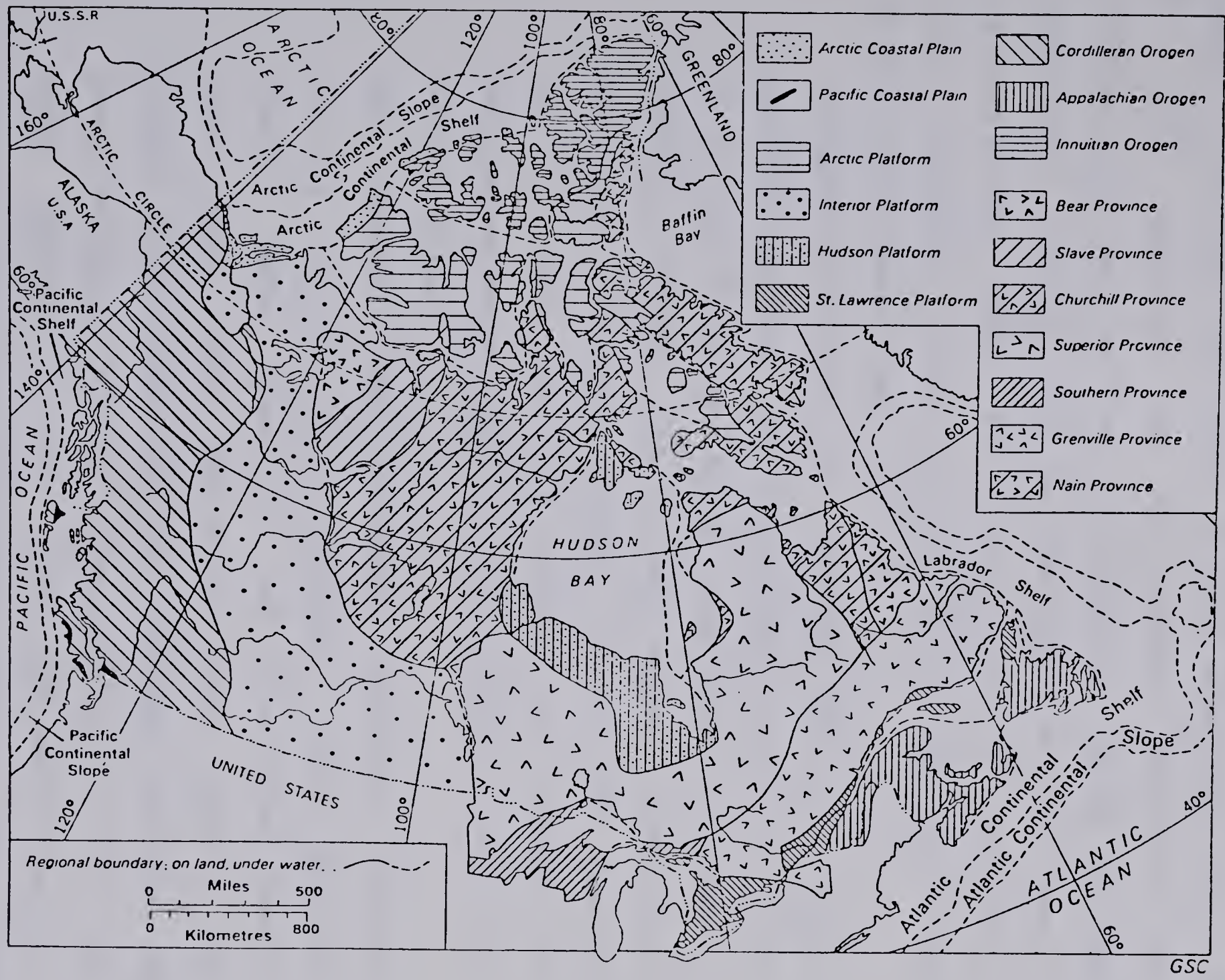
U.S.S.R
ARCTIC OCEAN
160°
ARCTIC CIRCLE
ALASKA U.S.A
Arctic Continental Slope
Arctic Continental Shelf
Arctic
120°
100°
80°
60°
GREENLAND
Baffin Bay
60°
Pacific Continental Shelf
140°
OCEAN
PACIFIC
HUDSON BAY
Pacific Continental Slope
UNITED STATES
120°
100°
Labrador Shelf
Shelf Slope
Atlantic Continental Slope
Atlantic Continental Shelf
ATLANTIC OCEAN
40°
60°
Arctic Coastal Plain
Pacific Coastal Plain
Arctic Platform
Interior Platform
Hudson Platform
St. Lawrence Platform
Cordilleran Orogen
Appalachian Orogen
Innuitian Orogen
Bear Province
Slave Province
Churchill Province
Superior Province
Southern Province
Grenville Province
Nain Province
Regional boundary: on land, under water
0 Miles 500
0 Kilometres 800
GSC

The boundary between the Superior and the Churchill tectonic provinces has been under investigation since 1939, however, its extent and nature is still uncertain. Green *et al.* (1977) postulate that the boundary zone in northen Manitoba comprises the Pikwitonei province and the Wabowden subprovince, however, they form two separate identities, as outlined by Bell (1966, 1971). The geology and geophysics of norhern Manitoba is outlined in Fig.1.5. and Fig.1.6. and can be briefly summarized as follows.

1. The Superior province is dominated by E.W. trending granite/greenstone and granite/gneiss belts (Wilson, 1971); both formations being extensively intruded by granitic plutons. Gravity and magnetic anomalies as well as the lithology, bedding, folding and faulting tend to follow the E.W. pattern of the belts. The average radiometric age of rocks is 2300 to 2800 m.y. (Kenoran ages).
2. The boundary zone-Pikwitonei province, trending N.E.-S.W., is dominated by granulate facies gneisses, layered mafic granulites and hypersthene bearing granite (Bell, 1971). The Nelson River gravity high anomaly is coincident with the Pikwitonei province. The granulite facies exhibit characteristic *'bird's eye maple'* pattern of small ovoid high and low magnetic anomalies. Rocks yield radiometric ages at least 2300 to 2800 m.y. with some strong indications of being older.

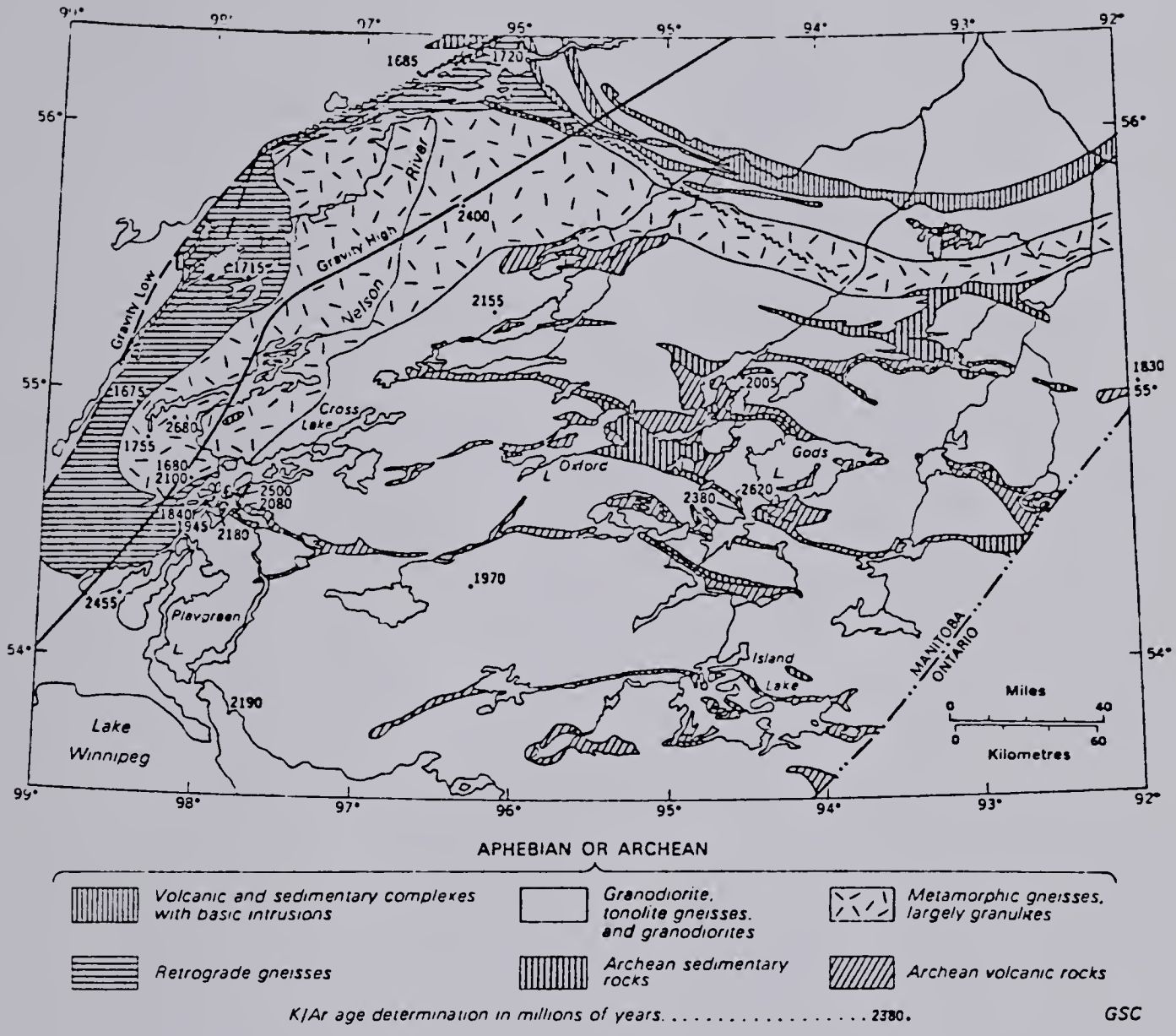

Fig.1.5. Geology of the Superior-Churchill boundary zone in northern Manitoba (from *Geology and Economic Minerals of Canada*, 1970).

Fig.1.6. Main geophysical and structural trends of the Superior-Churchill boundary zone in northern Manitoba (from *Geology and Economic Minerals of Canada*, 1970)

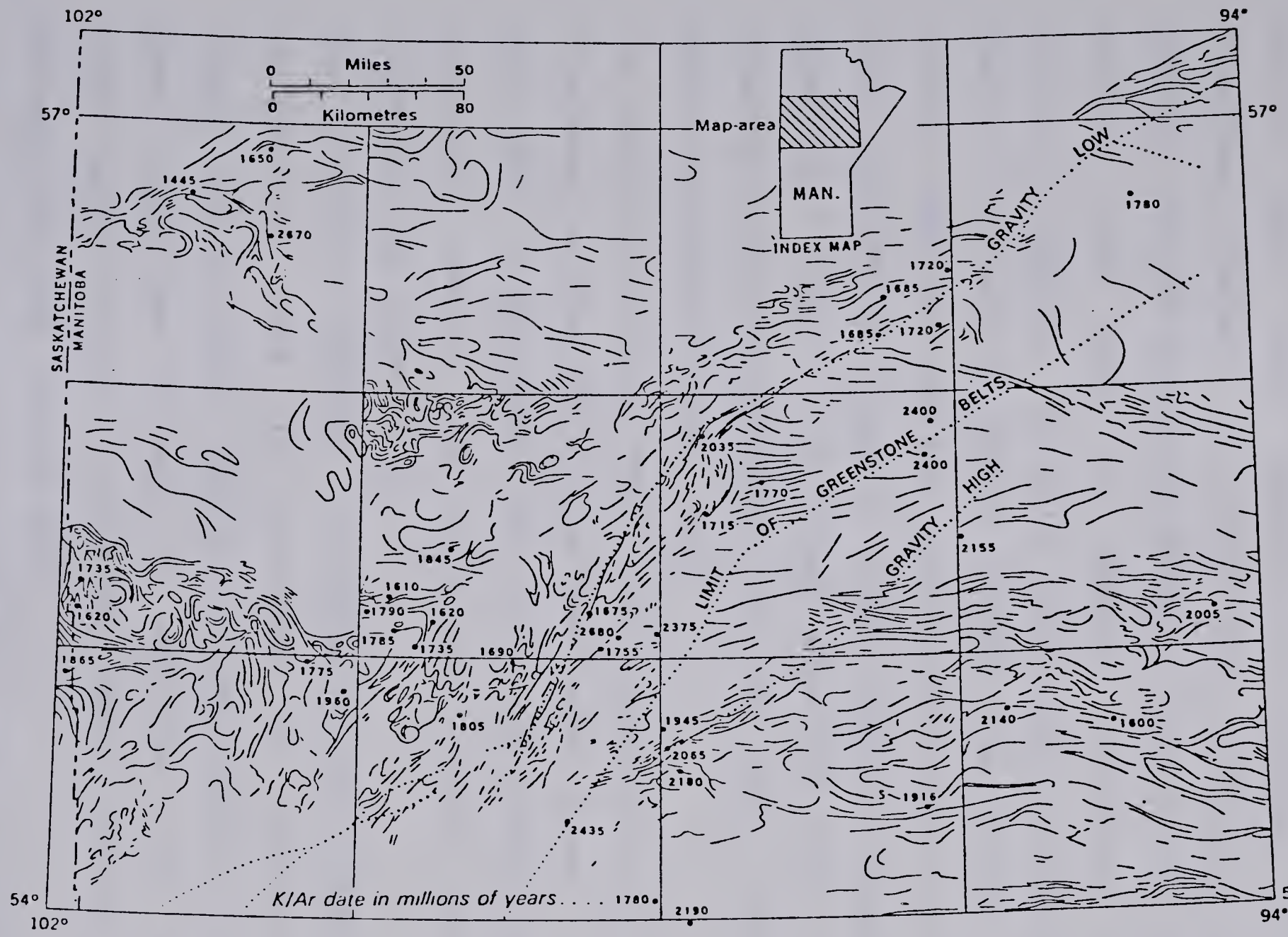
102°
94°
57°
54°
0 Miles 50
0 Kilometres 80
Map-area
MAN.
INDEX MAP
SASKATCHEWAN
MANITOBA
LOW GRAVITY
BELTS
GREENSTONE
HIGH
LIMIT OF GRAVITY
1650
1445
2670
1780
1720
1685
1685
1720
2400
2035
2400
1770
1715
2155
1735
1620
1610
1790
1620
1845
1675
2680
1785
1735
1690
1755
2375
2005
1865
1775
1960
1805
1945
2065
2180
1916
2140
1600
2435
2190
KIAr date in millions of years 1780

3. The boundary zone-Wabowden subprovince has been referred to as *'Thompson nickel belt'*. It is very important economically because it contains one of the world's major nickel deposits. It trends, like the Pikwitonei province, in a N.E.-S.W. direction with layered gneisses being the dominent type of rock. They enclose linear belts of sediment, volcanics and peridotite bodies from which the nickel is extracted. There is a very prominent gravity low anomaly of similar magnitude and direction as the adjacent Nelson River gravity high anomaly. High intensity magnetic anomalies, usually of broad elongated form, are observed across the gneisses. The rocks yield Kenoran ages(Cranstone and Turek, 1976).

   The boundary between the Wabowden subprovince and the Pikwitonei province is a major fault zone (Assean Lake fault zone) in the north (Bell, 1971) and a metamorphic transition zone in the south and central regions (Cranstone and Turek, 1976).

4. The Churchill province is covered mostly by granitic and gneissic rocks. The geological and geophysical trends are variable. The gravity and magnetic fields show a significant decrease in magnitude. The rocks yield Hudsonian ages in the range 1600 to 1900 m.y. in the east but older further west.

1.2.2 The Superior-Churchill boundary zone in southern Manitoba and Saskatchewan

South of latitude 54°35'N the boundary zone disappears beneath the Phanerozoic sediment and its southward extension is based primarily on gravity and magnetic data and their patterns as compared to these in northern Manitoba. Moving south the gravity high broadens and eventually near latitude 53°N becomes impossible to trace. Further south there are a number of high anomaly axes that may be related to the Nelson River high. The *'birds's eye maple'* magnetic pattern across the Pikwitonei province is not seen south of the Phanerozoic sediment but elongated N.E.-S.W. magnetic anomalies can be traced to the limit of the federal-provincial aeromagnetic map coverage near latitude 52°N. Using newly acquired ground and aero magnetic data Green *et al*. (1977) compiled a magnetic map of S.W. Manitoba and S.E. Saskatchewan (Fig.1.7.). There are three distinct magnetic zones on it:

1. An Eastern region where high amplitude E.W. trending magnetic anomalies are typical of the Superior province.
2. A Central region where high amplitude anomalies trend N.E.S.W to N.S.
3. A Western region of relatively low amplitude anomalies trending N-S

The gravity for that area is less obvious, however, observable anomalies show essentialy a similar pattern. On the basis of the new data Green *et al*. (1977) postulate that:

Fig.1.7. Compiled aeromagnetic map of S.W. Manitoba and S.E. Saskatchewan. Contour intervals are 100 nT and black spots are the areas with high amplitude anomalies that cannot be contoured at this scale. Values correspond to flight elevation of 0.16 km above ground. The thick lines show boundaries between three magnetic regions; the dash-dot line delineates the western extension of the low magnetic relief zone (bz-boundary zone), and the dashed line outlines the area of low amplitude, medium to long wavelenght magnetic anomalies.

A-Neepawa anomaly.

B-Oak Lake anomaly.

CC, DD, EE, and FF are a group of positive and negative anomalies trending N.W.-S.E. (from Green *et al.*, 1977).

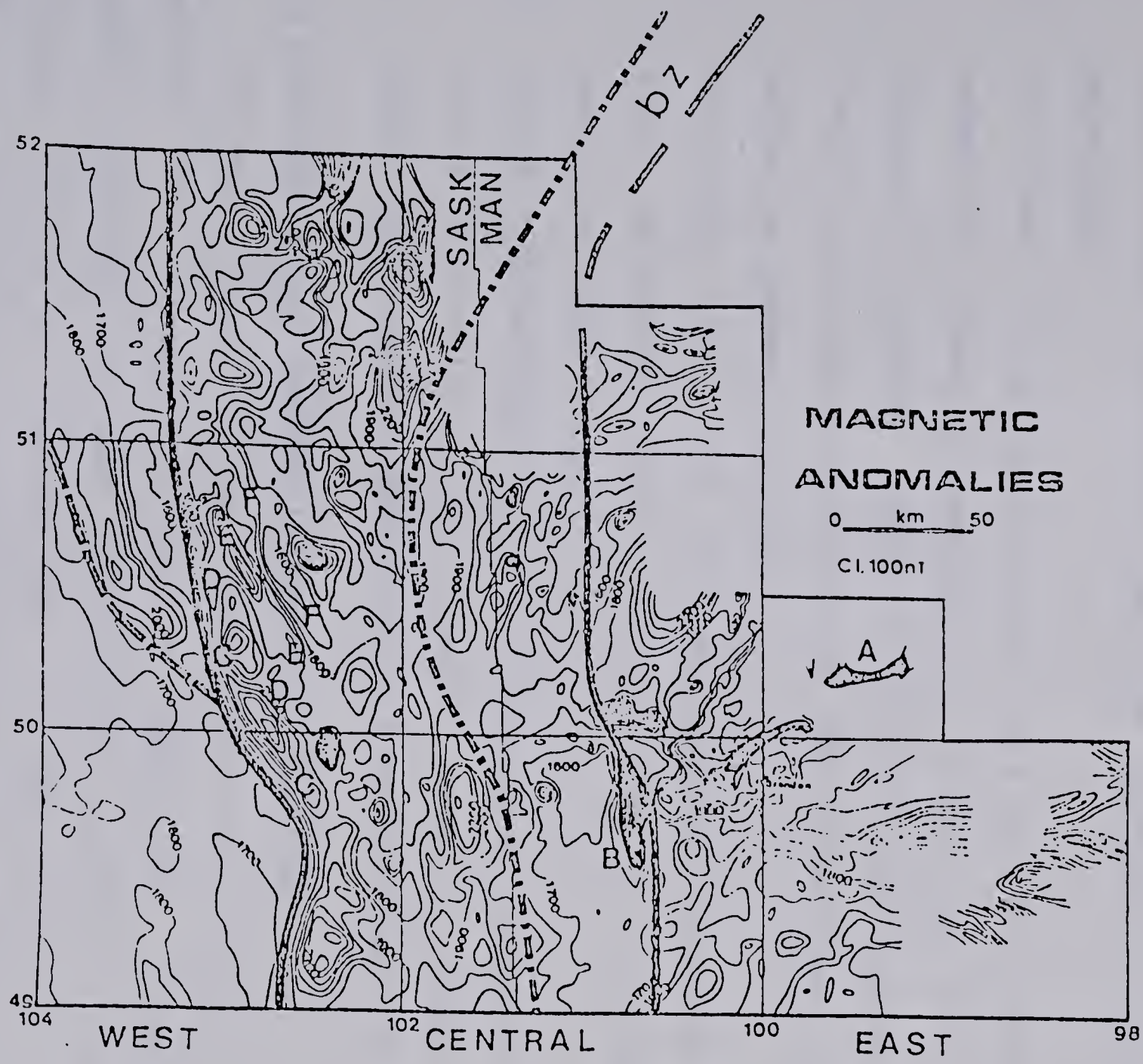
52
51
50
49
104
102
100
98
SASK
MAN
bz
1600
1700
1800
1900
2000
2100
A
B
C
D
MAGNETIC
ANOMALIES
0 km 50
CI. 100nT
WEST
CENTRAL
EAST

1. The Superior province lies to the east of eastern solid line in Fig.1.7.
2. The adjacent low magnetic relief zone (between solid and dashed-dotted lines in Fig.1.7.) is the boundary zone between the Superior and the Churchill tectonic provinces.
3. The zone of high amplitude N.E.-S.W. and N-S striking anomalies, extending from south of Flin Flon to the Canada-U.S. border, might indicate the continuation of the Flin Flon-Snow Lake granite and greenstone belt below the sedimentary cover.
4. The sharp truncation of these anomalies to the west, along the western solid line in Fig.1.7., probably indicates a major fault.
5. Central Saskatchewan is a large area of low magnetic relief. A similar quiet magnetic zone is observed across the Kisseynew gneiss belt in northern Manitoba.

1.3 Previous Seismic Refraction Works in the Area

The southern part of the Interior Platform has been the location for a number of seismic experiments. Several seismic profiles had been obtained for southern British Columbia, Alberta and Saskatchewan by the University of Alberta Geophysics group between 1962 to 1969. Various parts of these profiles have been interpretated and discussed by Weaver (1962), Maureau (1964) and Chandra (1966). Cumming and Kanasewich (1966) summarized the results of the profiles in a final report under a contract with the Project Vela

Uniform. In general, they obtained approximately 47 km as the crustal thickness in southern Alberta and 8.2-8.3 km/s as the upper-mantle velocity. The studies also revealed the existance of sub-basement refractor with velocity of about 6.5 km/s and an intermediate layer reflector (*Riel discontinuity*) below wich the velocity was about 7.2 km/s (Cumming and Kanasewich, 1966)

A general preliminary interpretation of the seismic data from these profiles was attempted by Kanasewich *et al.* (1969). Chandra and Cumming (1972), using some additional information, reinterprated all the available refraction data in an attempt to derive a crustal structured profile from Greenbush Lake, British Columbia to Swift Current, Saskatchewan along latitude 50°30′N. The eastern section of their model (SuffieldSwift Current) is shown in Fig.1.8.

In addition to the refraction studies detailed reflection techniques have been used successfully in the area (Kanasewich and Cumming, 1965, Clowes *et al.*, 1968, Clowes and Kanasewich, 1970). The profiles show a surprisingly complex structure including steeply dipping horizons (up to 20°) and a large topographic relief of 8 km over a horizontal distance of 25 km (Clowes *et al.*, 1968). Combined refraction and reflection data have revealed an existance of a number of major steeply dipping faults in the middle and lower crust which penetrate the *Moho discontinuity*.

The Churchill-Superior boundary zone in southwestern

Fig.1.8. Crustal models of S.W. Manitoba and southern Saskatchewan derived from seismic refraction surveys prior to 1979. The solid lines show values obtained from the coverage for a given refractor, while the dashed lines represent interpolated values.

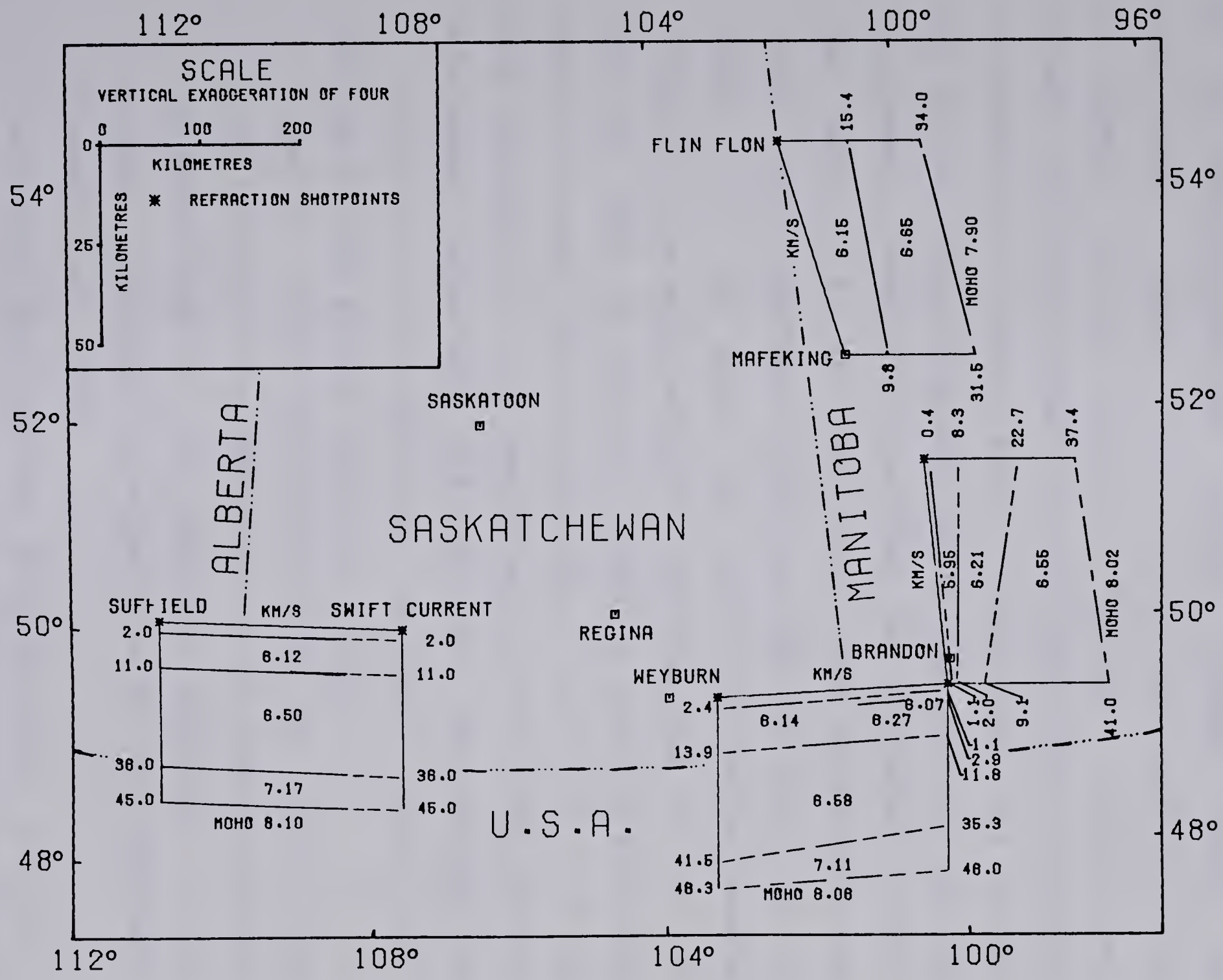
112°
108°
104°
100°
96°
54°
52°
50°
48°
SCALE
VERTICAL EXAGGERATION OF FOUR
0
100
200
KILOMETRES
0
25
50
KILOMETRES
REFRACTION SHOTPOINTS
FLIN FLON
15.4
94.0
KM/S
6.15
6.65
MOHO 7.90
MAFEKING
9.8
31.5
SASKATOON
ALBERTA
SASKATCHEWAN
MANITOBA
0.4
8.3
22.7
37.4
KM/S
6.95
6.21
6.55
MOHO 8.02
SUFFIELD
KM/S
SWIFT CURRENT
2.0
11.0
6.12
6.50
38.0
7.17
45.0
MOHO 8.10
2.0
11.0
38.0
45.0
REGINA
BRANDON
WEYBURN
KM/S
2.4
6.14
6.27
8.07
1.1
2.0
9.1
41.0
13.9
1.1
2.9
11.8
6.58
35.3
41.5
7.11
48.0
48.3
MOHO 8.08
U.S.A.

Manitoba and southeastern Saskatchewan was the target of a cooperative seismic survey in July 1977. This was undertaken by an Inter-Universities Crustal Studies Group, an association composed of geophysicists from the Universities of Alberta, British Columbia, Manitoba, Saskatchewan, Toronto and Western Ontario and the Earth Physics Branch of the Department of Energy, Mines and Resources. The project and the preliminary data and results have been described and discussed by Green (1977) and Green and Stephenson (1978). Some aspects of data analysis have been described by Mann (1979), and a final report was presented by Green *et al.* (1979). Fig 1.8. shows the locale of the two reversed refraction/wide angle reflection profiles, one in the N.S. and the other in the E.W. directions crossing each other south of Brandon. Various size shots, from 363 to 1119 Kg, were detonated at the ends of each profile. The geophones were spaced, on average, at 7.7 Km apart, and a maximum shot to receiver distance was 245 Km. The interpertation of data led them to some general conclusions (Fig.1.8.).

1. There is a significant thickning of the crust within the boundary from about 41 Km in the Superior province to about 48 Km in the Churchill province. A major crustal fault might be responsible for this phenomenon. (Green *et al.*, 1979).
2. The crustal model derived from the E.W. profile is similar to these described for eastern Saskatchewan and southern Alberta (Fig.1.8.) which suggests that the

Churchill province might extend westward up to the foothills.

3. The crustal structure derived from the N.S. profile is similar to published crustal models of the Superior province.
4. Velocities for N.S. and E.W. profiles are broadly similar.
5. The strongly refracting horizon with the velocity of about 7.0-7.22 km/s is evident only for the Churchill province.

An early seismic survey in the Churchill-Superior boundary zone was conducted in 1961. Two groups from the University of Saskatchewan and the University of Manitoba made an unreversed refraction profile, extending south from the shotpoint at the North Star Mine, near Flin Flon, to the village of Mafeking (Fig.1.8.). The crustal structure in the area is characterized by a pronounced gravity anomaly. The project and initial data interpretation was described by Hall and Brisbin (1961). In 1964 some additional records, with improved equipment, were taken along the same line and using the same shotpoint. By combining the reinterpretated old data with new set of data Hall and Brisbin (1965) were able to use the converted head waves method to determine the crustal structure along the profile (Fig.1.8). Their main conclusions were as follows.

1. A *Manitoba Conrad discontinuity* ranges from a 15.5 km depth near Flin Flon to something just under 10 km

depth near Mafeking. The *Moho discontinuity* is located at the depth 34 and 31 km respectively.

2. The velocities obtained were: 6.15 km/s for the upper crustal layer, 6.65 km/s for the intermediate crustal layer, and 7.90 km/s for the upper mantle.
3. The crustal model derived from the profile does not satisfactorily explain the observed gravity anomalies. Near-surface Precambrian masses, covered by a thin layer of Paleozoic rocks, are belived to be responsible for the disagreement.

2. TECHNICAL ASPECTS OF THE PROJECT

2.1 Description of Profile

In August 1979 the COCRUST (formerly the Inter-Universities Crustal Studies Group) carried out its second cooperative seismic refraction survey in southwestern Manitoba and southern Saskatchewan. Its first objective was the continuation of studies of the Churchill-Superior boundary zone to obtain information on the crustal structure of the Churchill province, just west of the boundary zone. There was some hope of finding more about a possible major crustal fault running in a N.S. direction to correlate with as a prominent feature on the magnetic map (Fig.1.7). Among other factors which influenced the decision for conducting a survey in the southern part of the transition zone, as opposed to the northern part were the following.

1. Easy access for shooting and recording due to a complete network of available roads.
2. An unconsolidated surface layer allowing easy drilling.
3. A great number of bore hole data from oil companies supplying information on the Phanerozoic sediment.

Within the COCRUST group the University of Alberta had a two-man crew recording the same blasts to the west of the main COCRUST sites. Fig.2.1. shows the sites of their short recording line as well as shotpoint locations.

The technical details of the University of Alberta profiles are summarized in Table 1. The geometry of the

Fig.2.1. Location of the 1979 COCRUST refraction survey with shotpoints and the University of Alberta recording sites. The Superior-Churchill boundary zone and major crustal fault are delineated after Green *et al*. (1979).

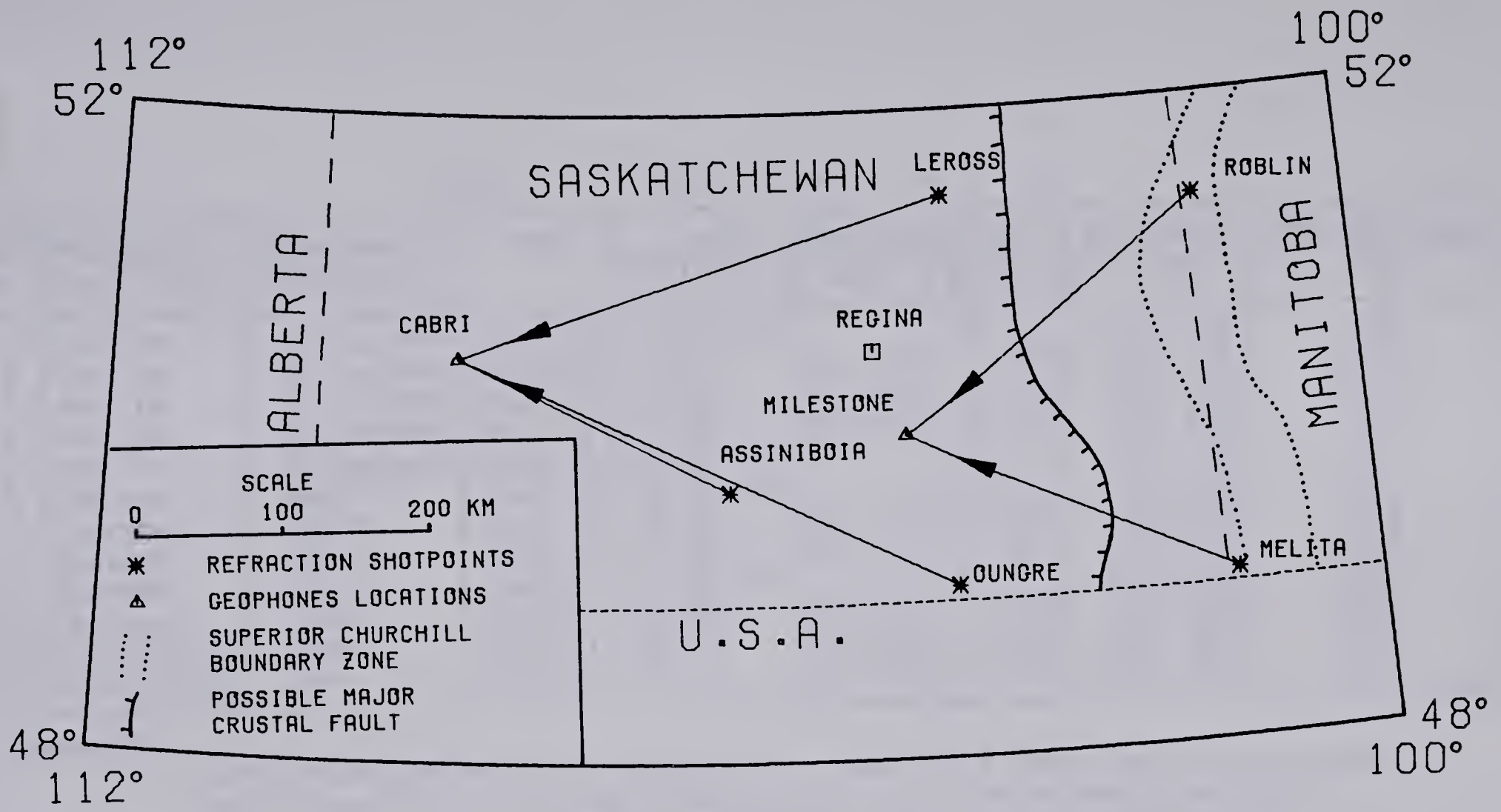
112°
52°
100°
52°
SASKATCHEWAN
ALBERTA
MANITOBA
LEROSS
ROBLIN
CABRI
REGINA
MILESTONE
ASSINIBOIA
OUNGRE
MELITA
U.S.A.
SCALE
0
100
200 KM
REFRACTION SHOTPOINTS
GEOPHONES LOCATIONS
SUPERIOR CHURCHILL BOUNDARY ZONE
POSSIBLE MAJOR CRUSTAL FAULT
48°
112°
48°
100°

TABLE 1. Description of profiles

Shot No	Shotpoint Location	Receiver's Location	Date	Local time of shot				Distance Km	Charge size Kg
				Hr.	M.	Sec.	Accur.		
1	Roblin	Milestone	Aug.15	05	59.97		±0.01	272.595	400
2	Melita	Milestone	Aug.15	06	31	06.183	±0.003	260.344	200
3	Melita	Milestone	Aug.15	07	31	04.488	±0.003	260.344	1000
4	Melita	Milestone	Aug.16	06	31	02.925	±0.003	260.344	425
5	Roblin	Milestone	Aug.17	06	00.97		±0.01	272.595	1200
6	Leross	Cabri	Aug.18	06	01.97		±0.01	350.695	350
7	Oungre	Cabri	Aug.18	06	31	03.145	±0.003	381.684	400
8	Oungre	Cabri	Aug.19	07	31	02.819	±0.003	381.684	983
9	Leross	Cabri	Aug.20	06	00.97		±0.01	350.695	1249
10	Oungre	Cabri	Aug.20	06	31	02.582	±0.003	381.684	250
11	Assiniboia	Cabri	Aug.21	06	01	03.458	±0.003	207.193	250
12	Assiniboia	Cabri	Aug.21	21	01	02.749	±0.003	207.193	1375

Comments:

1. Distances between shotpoints and receivers have been calculated with respect to the recording site with three geophones, two for measuring horizontal components and one for measuring vertical component.

Fig.2.2. Geometry of the recording line used by the University of Alberta at two recording sites.

GEOMETRY OF RECORDING LINE

MILESTONE

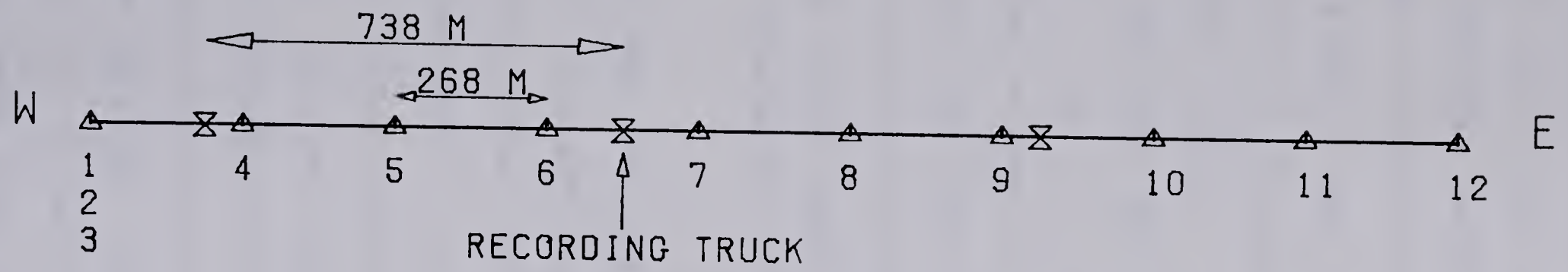

CABRI

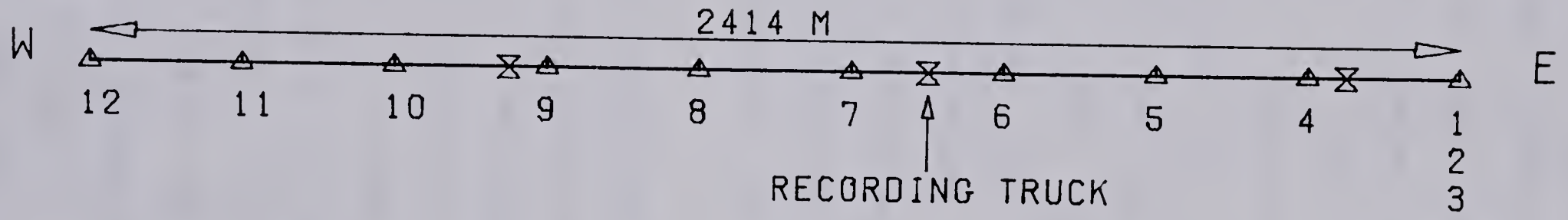

△ GEOPHONES
⧖ CABLE TERMINALS

GEOPHONE 1 - HORIZ. N.S.COMPONENT
GEOPHONE 2 - HORIZ. E.W.COMPONENT
GEOPHONES 3 TO 12 - VERT.COMPONENT

refraction lines is shown in Fig.2.2. The spreads consisted of 12 seismometers spaced 268 m apart, except for seismometers No 1, No 2, and No 3 which were placed at the same site. The total length of the recording line was 2414 m. Geophones 3 to 12, measuring the vertical component of the seismic signal, were model TI S-36 with a natural frequency of 2 Hz. Seismometers 1 (measuring the horizontal N.S. component) and 2 (measuring the horizontal E.W. component) were Hall Sears model S-10 type with the natural frequency of 1 Hz. All spreads were laid out along a straight line in the E.W. direction. The first was located beside a gravel road starting (seismometers 1, 2, and 3) at the crossroad three miles east of Milestone. The second was located along a minor country road starting (seismometers 1, 2, and 3) approximately 3.5 miles south and four miles west of Cabri.

The latitudes and longitudes of receivers were obtained from 1:50000 topographic maps (Lang-Saskatchewan 72H/16 and Shackleton-Saskatchewan 72K/10 for Milestone and Cabri spreads, respectively). A reading accuracy of 0.5 mm yielded the longitude with an accuracy of 1.28" (about 25 m), and the latitude with an accuracy of 0.82" (about 25 m). The geographic coordinates of seismometer 12 for Cabri and 1 to 3 for Milestone have been read from the maps; for the rest they have been obtained using the geometry of recording line. A total of 12 shots were detonated in five locations (Fig.2.1) The charge sizes varied from 200 to 1375 kg (Table

1.). Times of shots, latitudes, longitudes and other shot parameters were supplied by Dr.Z.Hajnal, who was in charge of the project. All shotpoint-receiver distances have been calculated using a geodetic computer program by supplying the geographical coordinates as input data.

2.2 The Recording System

The recording system employed was of digital type. Out of twenty available channels, fourteen were used to record the seismic signals and the source time. Channel 7 recorded WWVB radio time signal and channel 14 recorded the tone break when the shot was detonated. Channels 1 to 6 and 8 to 13 were used to record signals coming from seismometers 1 to 6 and 7 to 12, respectively. In the 1979 survey the absolute time signal from WWVB was of particular importance since the shotpoints were far beyond the radio range of the recording sites, therefore, channel 14 could not record the transmitted shot instants and contained only noise. All these channels have been recorded on both tape recorder and photographic paper. In the first case an 800-BPI (bytes per inch) 9-track unit with tape velocity of 6.25 ips was used yielding 5000 character (=byte) per second transfer rate (Allsopp *et al.*, 1972). In the second case an analog type of display by means a galvanometer type recording camera was used. Despite its obvious drawbacks, as compared to digital recording, this proved to be a useful tool in some instances allowing a first direct examination of the recorded signals.

It also made processing the digital data on tapes more efficient.

The main segments of the complete digital system are shown in Fig.2.3. The tape recorder is a model #7830-9 with write-only transport manufactured by Peripheral Equipment Corporation. The multiplexer, A-to-D converter and 5 KHz crystal clock, along with some additional circuitry, are contained in a modified model #120 Data Acquisition System (Allsopp *et al.*, 1972). One to 20 channels are available for recording with a maximum of 4096 words per channel and a block time of 22.94 sec. When a longer record time is required (as in long-distance refraction case) several blocks may be written in sequence, with an interval of 0.096 sec. of lost data between each block. The analog to digital convertor has a resolution of 14 bits (13 bits plus sign), and a dynamic range of 84 db. The sampling rate is 2500 data words per sec. (data words were two 8-bit bytes long i.e. they were written in integer *2 form). Thus for 14 channels, the sampling rate is 14/2500 =0.0056 sec. Consequently the Nyquist frequency is 89.3 Hz.

Fig.2.4. shows a diagram of the amplifier circuit. A signal at its input passes through an 18 db gain transformer which drives the fixed gain 40 db preamplifier. The latter feeds the main amplifier through a high-pass two-pole Bessel filter which ensures a minimum-phase shift. If required, however, this filter can be bypassed. From the main amplifier output the gain can be controled from 0 to 60 db

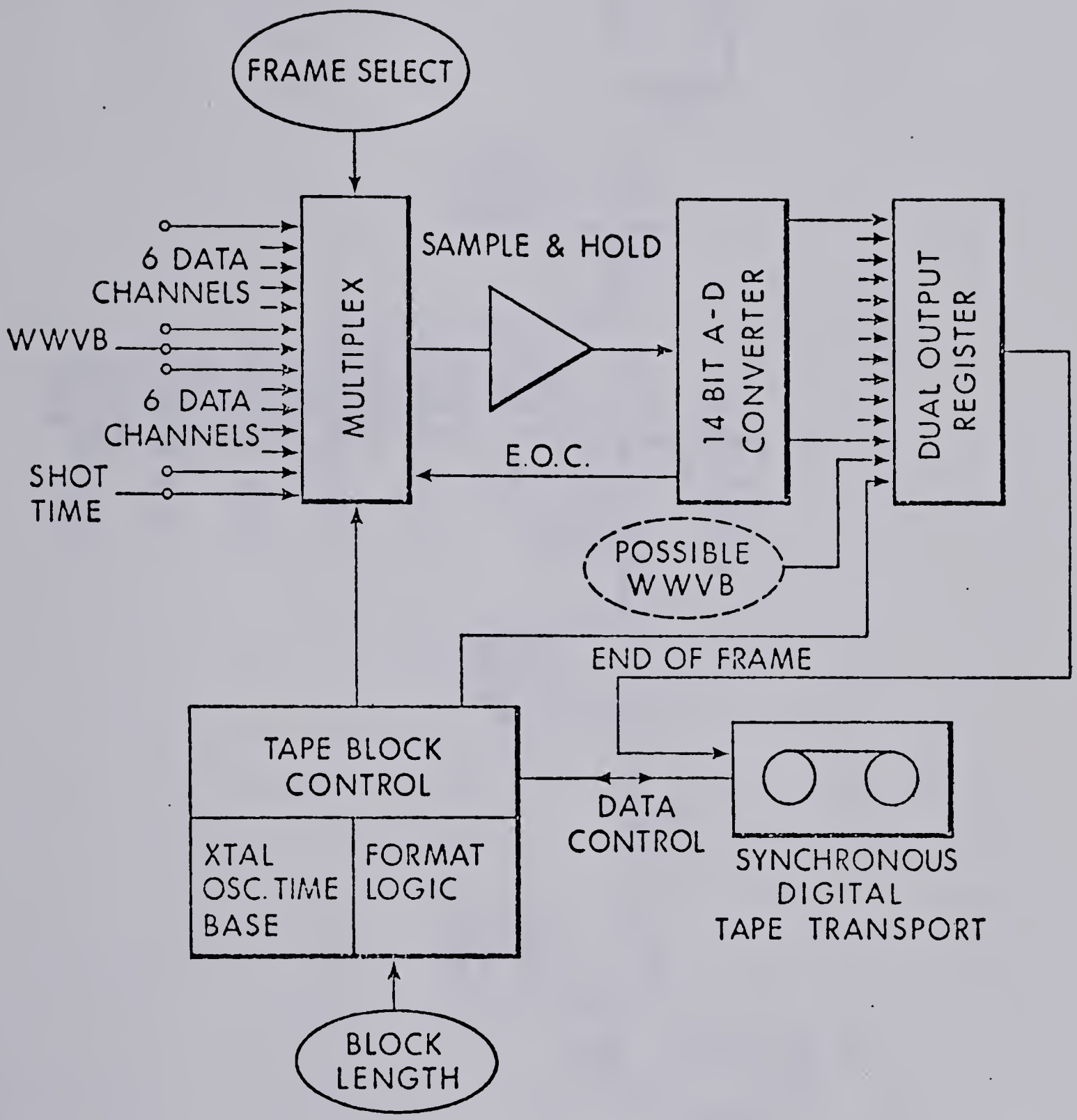

Fig.2.3. The digital recording system (after Allsopp *et al.*, 1972).

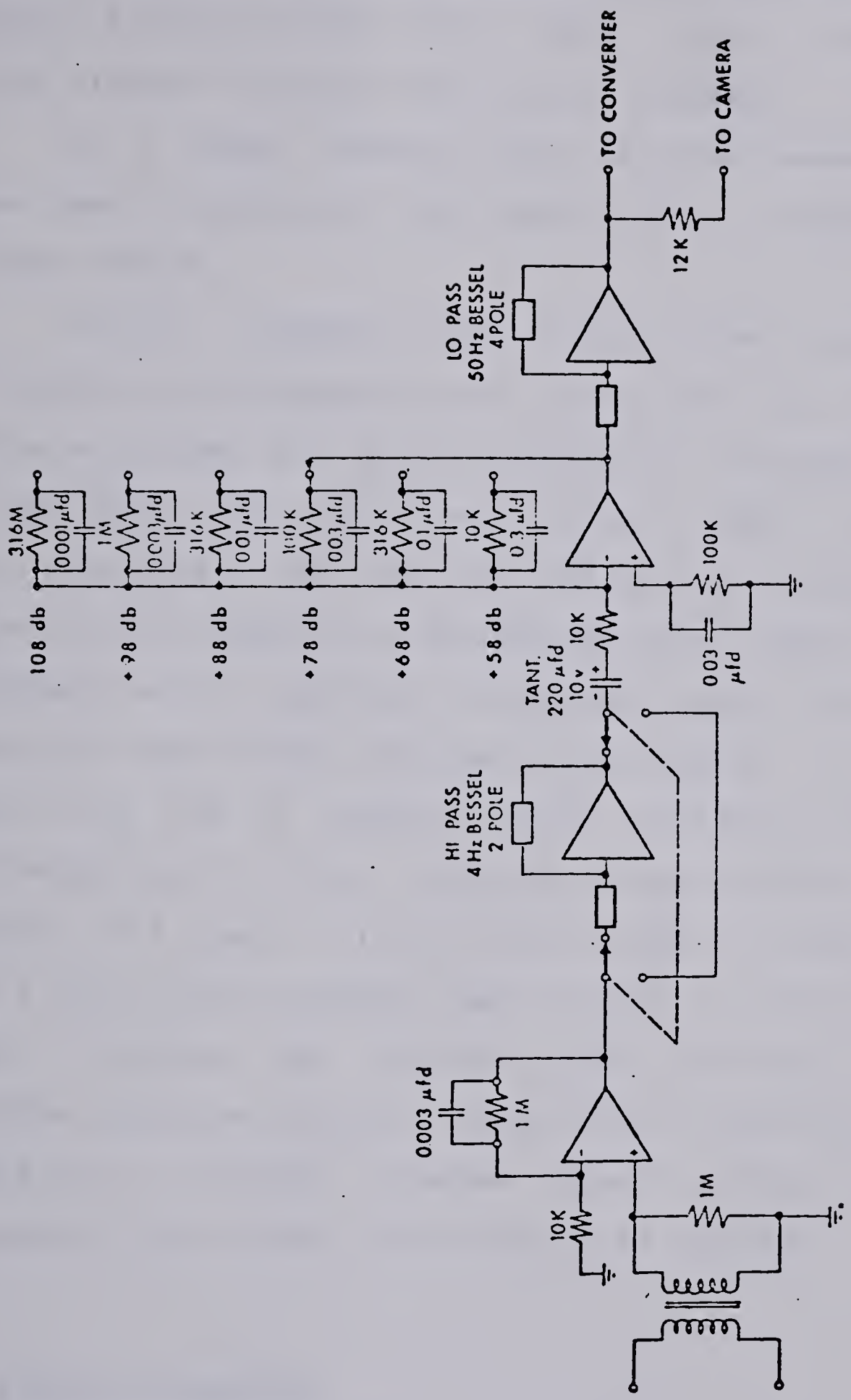

Fig.2.4. The amplifier circuit (after Allsopp *et al.*, 1972).

with increments of 10 db, signal passes through a four-pole Bessel aliasing filter with a 50-Hz corner, what ensures high attenuation above the Nyquist frequency.

As a power source a small gasoline-powered generator was used to supply all requirements of the complete system (about 300 W).

Fig.2.5. presents the analog seismic data recorded directly on photographic paper (upper part) and the digital data as plotted on a Calcomp plotter at the computing center (lower part). For the former, channel 7 (WWVB time signal) is displayed at the top, followed by noisy channel 14 (time tone) and 12 channels in descending order (channel 1 at the bottom) which recorded the seismic signals. The digitized data is shown without the two time channels. It is clear, that the use of magnetic tape recording offers a big advantage over a direct recording on photographic paper by means of a camera. In the field one can minimize the amount of filtering and automatic gain control. If desired one can then introduce the optimum amount of these on playback. Another important feature, especially in exploration, is the ability to produce extended record sections which are powerful aids in the interpretation of the data.

2.3 Data Processing

During the 1979 refraction survey all the data were written in block lengths of 2048 samples (=4098 bytes) per channel. This yielded 28672 words as the total block size

Fig.2.5. The seismic data as recorded directly on photographic paper (upper part) and the same data set after digitization plotted by computer (lower part). The two bottommost traces display the horizontal components and the rest are vertical component data.

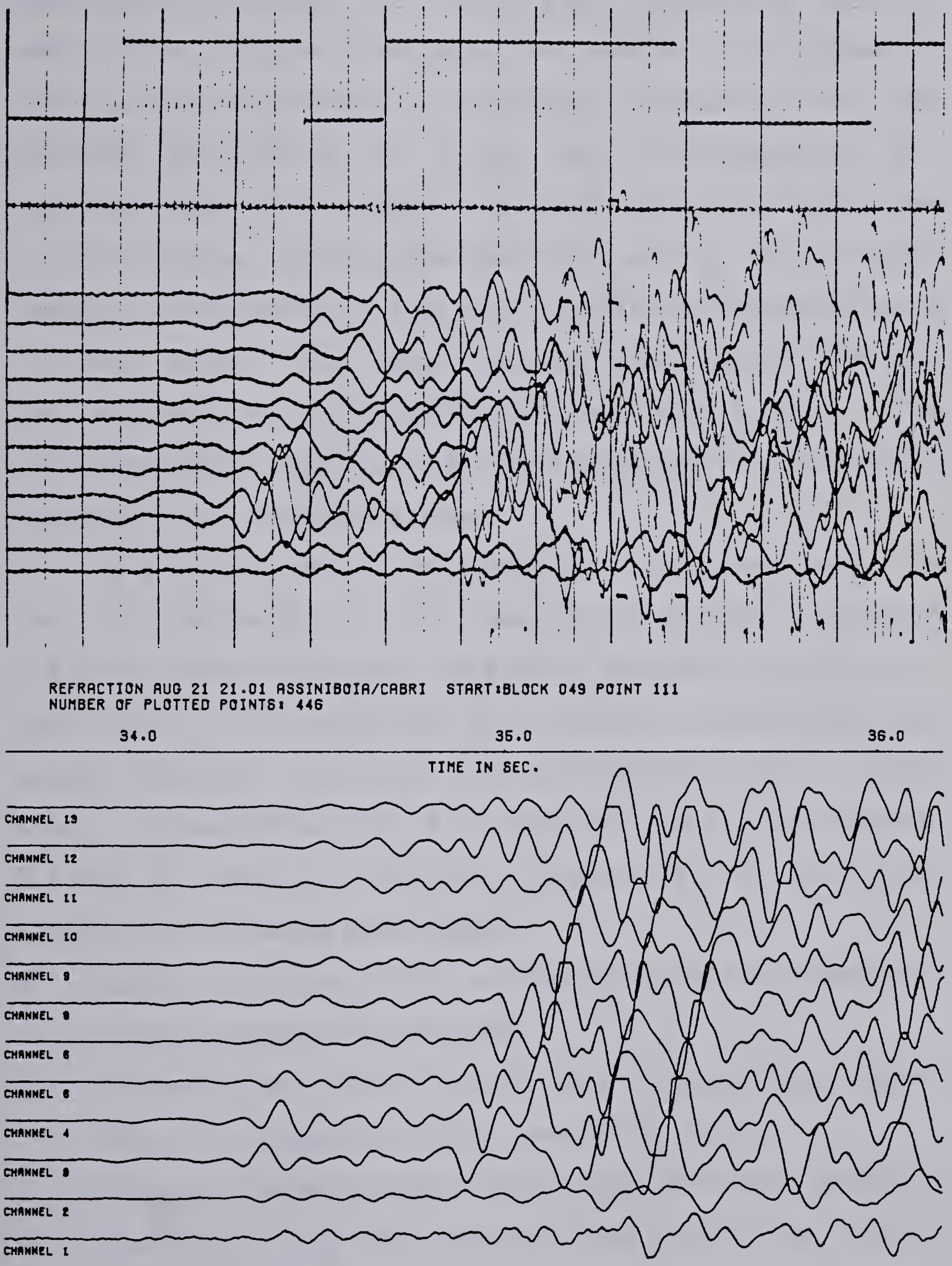
REFRACTION AUG 21 21.01 ASSINIBOIA/CABRI START:BLOCK 049 POINT 111
NUMBER OF PLOTTED POINTS: 446
34.0
35.0
36.0
TIME IN SEC.
CHANNEL 13
CHANNEL 12
CHANNEL 11
CHANNEL 10
CHANNEL 9
CHANNEL 8
CHANNEL 6
CHANNEL 6
CHANNEL 4
CHANNEL 3
CHANNEL 2
CHANNEL 1

(14 channels *2048=28672 integer *2 words =57344 bytes). This long block length placed rather severe demands on the tape-computer system. The first step, therefore, was to rewrite the field recorded data in a shorter block format to increase the efficiency of future data processing. This was achieved by placing 12 files, each corresponding to 1 recorded shot, onto a single tape with each file consisting of 336 blocks. Setting the new block size at 128 words per channel, this yielded a total of 1792 multiplexed data words in each block. The total recorded time interval for each shot was 240.8 sec. (128*336*0.0056 sec. =240.8 sec.). The unfiltered data from this tape have been used in a number of instances for various analyses.

In analysis, the 12 seismometers in each recording line can be considered only as a one recording point, so that 5 different shotpoints and 2 receivers locations (see Fig.2.1. and Table 1.) yielded only 5 refraction time-distance data points. However, the use of many seismometers along a short line, instead of only 3 (1 to measure a vertical component, 2 and 3 to measure horizontal components) at one site, offers the following advantages:

1. Reduces the possibility of recording failure because of single seismometer problems.
2. Increaces the reliability of data by comparing records from all seismometers and *'averaging'* data.
3. Yields some additional information about the nature of the signal (e.g. the apparent velocity of the seismic

pulse along the line).

The recorded data have been subjected to a number of data processing techniques which are described in the next sections.

2.3.1 Moveout correction

Generally moveout can be defined as the difference in the arrival time of a particular phase at different seismometer positions. Arrival times differ because of:

1. Normal moveout which is the difference due to variable source to receiver distance.
2. Dip moveout which is a time difference due to reflector or refractor dip.
3. A *static* time difference which is the same for all phases and is due to near-surface or weathering velocity variation.

In applying normal moveout correction, traces 3 to 12 were moved with respect to a base station (seismometers 1, 2, and 3) with one stacking velocity of 8 km/s. Thus the alignment of first arrivals from the *Moho* has been achieved for the large source-receiver distances. The corrections applied were not strictly moveout ones since a real velocity function was not used. However it was much easier to identify events on the basis of their phase correlation and to determine an approximate apparent velocity for the seismic pulse as compared to the standard velocity of 8 km/s. Fig.2.6. shows a record of 12 traces before and after

removing moveout.

No elevation corrections have been applied for two reasons. Such correction requires a knowledge of the near-surface velocity which is unknown in detail. On the other hand the influence of the correction would be small (less than 0.1 sec.) because the recording line was very short, and furthermore, was laid out in flat areas.

2.3.2 Normalization

The original raw data exhibit different maximum values for the same event on different receivers. This was due to lateral inhomogeneities in the ground, different coupling between seismometers and the ground and different gain setting of the amplifiers. Thus, the next step in the processing of the data was the normalization of the amplitudes. A program was written in which the maximum value of each trace was found and multiplications factors for each trace were calculated. Each trace was multiplied by an appropriate multiplication factor to normalized the data. The result of such an operation is that the maximum amplitudes of all traces have a common value. A sample of such data is demonstrated in Fig.2.7. which shows the same records before and after normalization, respectively.

Apart from the normalization, the mean value was removed from each data set. This was achieved by writing a simple program which calculated an average value for the data set and next subtracted it from each data point.

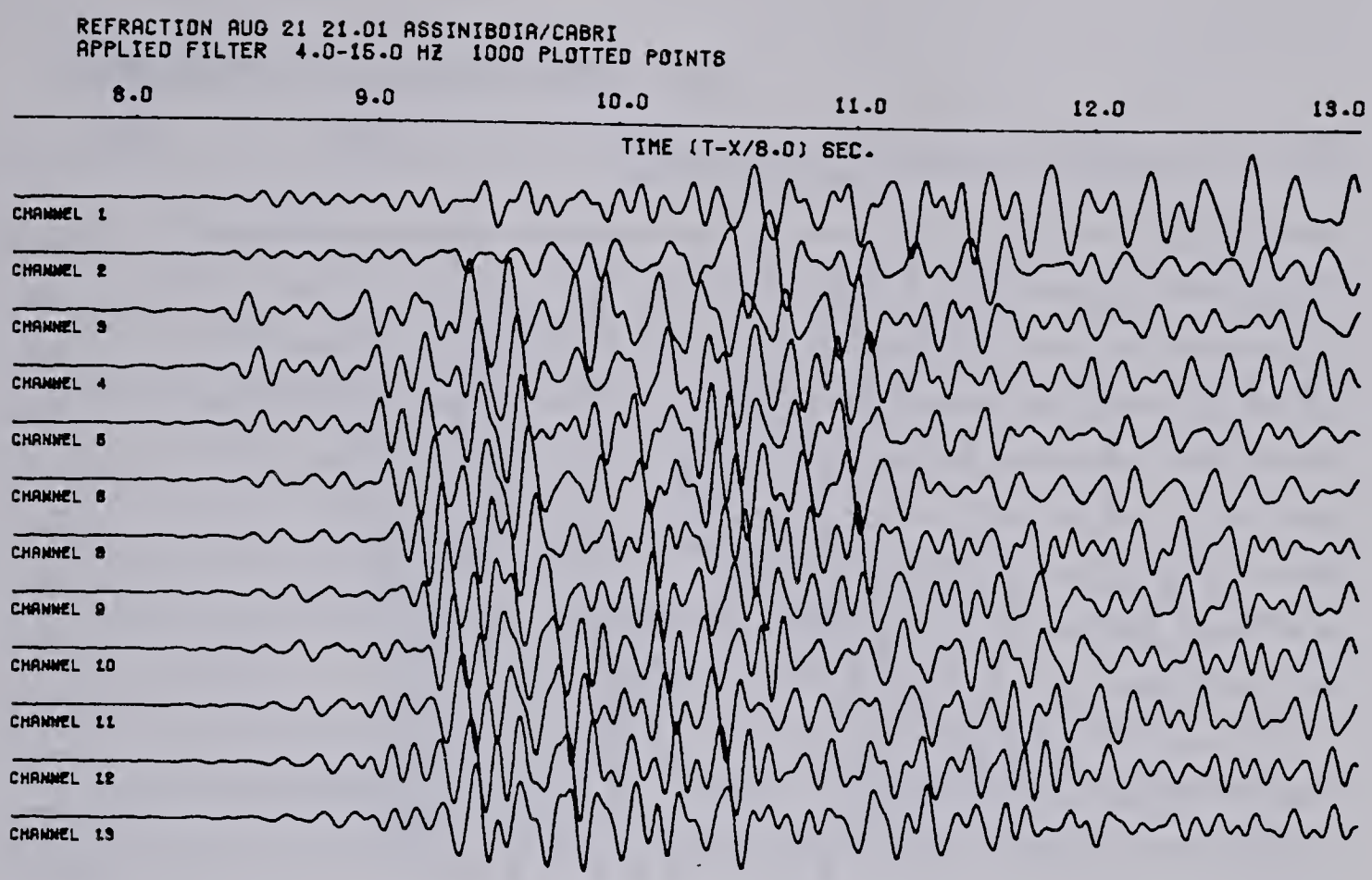

Fig.2.6. The same records displayed before and after removing moveout. The two topmost traces (channel 1 and 2) display the horizontal components and the rest are vertical component data.

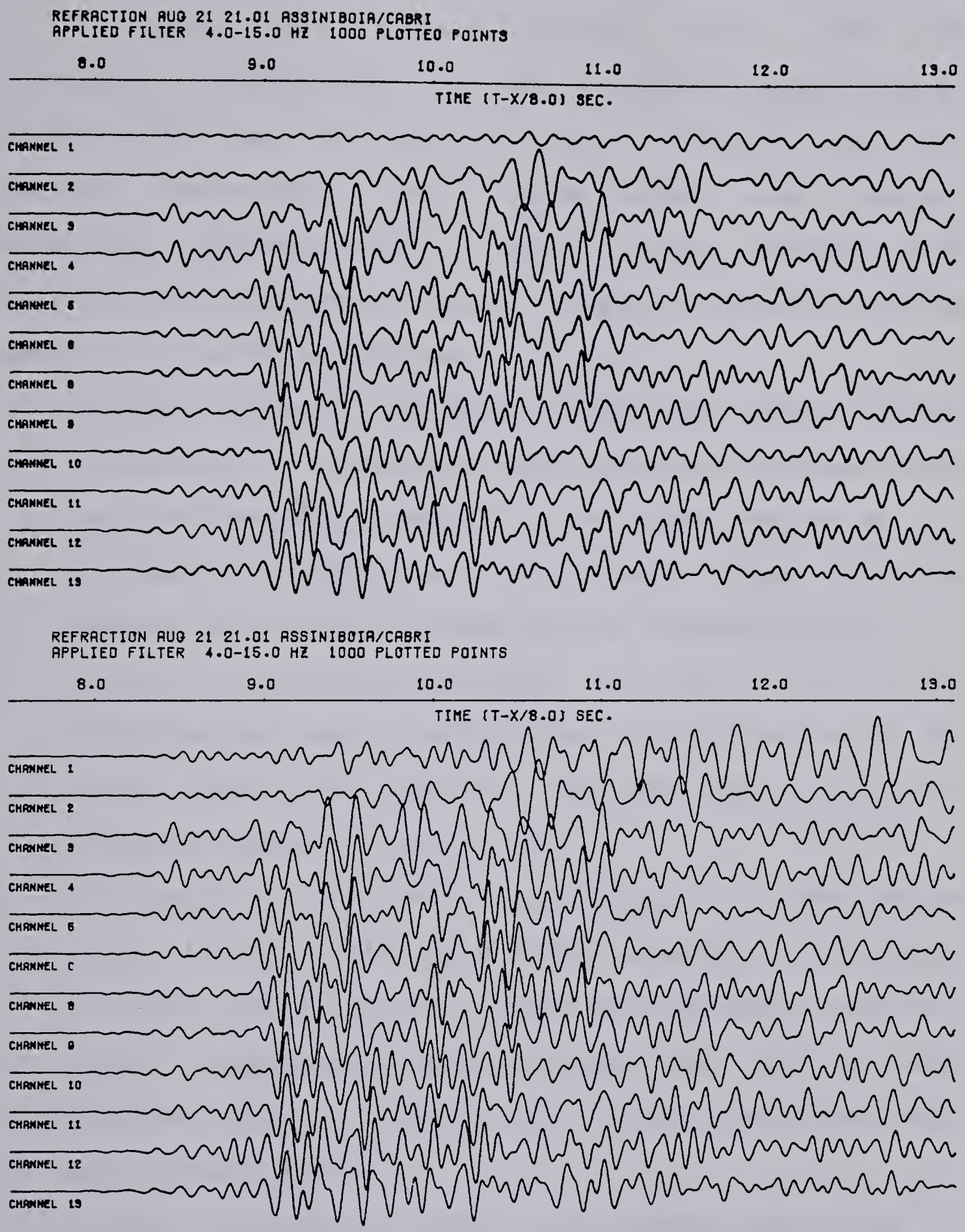

Fig.2.7. The same records displayed before and after normalization. The two topmost traces (channel 1 and 2) display the horizontal components and the rest are vertical component data.

2.3.3 Filtering

To improve the signal-to-noise ratio (SNR) of seismograms, differences in the following properties of seismic signal and noise can be used: frequency spectra, apparent velocities, wave polarization and spatial correlation (Burkhard *et al.*, 1976). Filter methods with their criteria and conditions for seismic application can be summarized briefly as follows:

1. Bandpass frequency smoothing is the most common type of filtering, in which the discrimination is done on the basis of frequency content in the signal and noise. It is especially effective in cases where signal and noise spectra do not overlap over a wide frequency band.
2. Velocity filtering can be used for an array in the direction of wave propagation. Discrimination of the signal against the noise is on the basis of their different apparent velocities.
3. Polarization filter methods can be apply to improve the signal-to-noise ratio when three component recordings are used. These type of filters are designed usually in order to suppress elliptically polarized surface wave component and to transmit only linearly polarized body wave seismic signals.
4. Filters using spatial correlation methods make use of differences in the spatial correlation of seismic signals and ambiant noise. The method proves to be particularly applicable for records with SNR>1. For

records with SNR<1 a very large number of seismometers is required to recover the signals.

Only frequency filtering has been applied to records of the 1979 survey. The power spectra of some records were plotted to find the frequency range of the refracted energy. Fig.2.8A-B show typical energy outputs as a function of frequency. The body wave energy appears to be confined always between 2 and 20 Hz (high peaks which appear around 55-60 Hz are noise caused mostly by power lines interference). It was decided, then, that a narrow band-pass filter with lower and upper cutoff frequencies of 4 and 15 Hz, respectively, would be applied, except for the Oungre/Cabri event (the largest shotpoint-receivers distance) where the lower cutoff frequency started at 2 Hz. Frequency range chosen ensured that the character of seismic pulses was not destroyed. This reduced noise considerably since signal and noise power spectra overlap only in a narrow frequency range with their peak energy widely separated.

Filtering was performed with an eight-pole, zero-phase shift, recursive Butterworth band-pass algorithm which was written by D.Ganley in 1977 during his graduate studies at the University of Alberta. A detailed analysis of this and other types of filters can be found in Kanasewich (1975). As an example of the effectiveness of the filter Fig.2.9 shows a seismic record in original form, as well as after application of the band-pass filter The improvement of the

Fig.2.8A-B Power spectra (periodograms) for two events.
a)The Assiniboia/Cabri event. Shotpoint to receiver distance was 207 Km.Charge size was 250 Kg
b)The Leross/Cabri event. Shotpoint to receiver distance was 351 Km. Charge size was 1249 Kg.

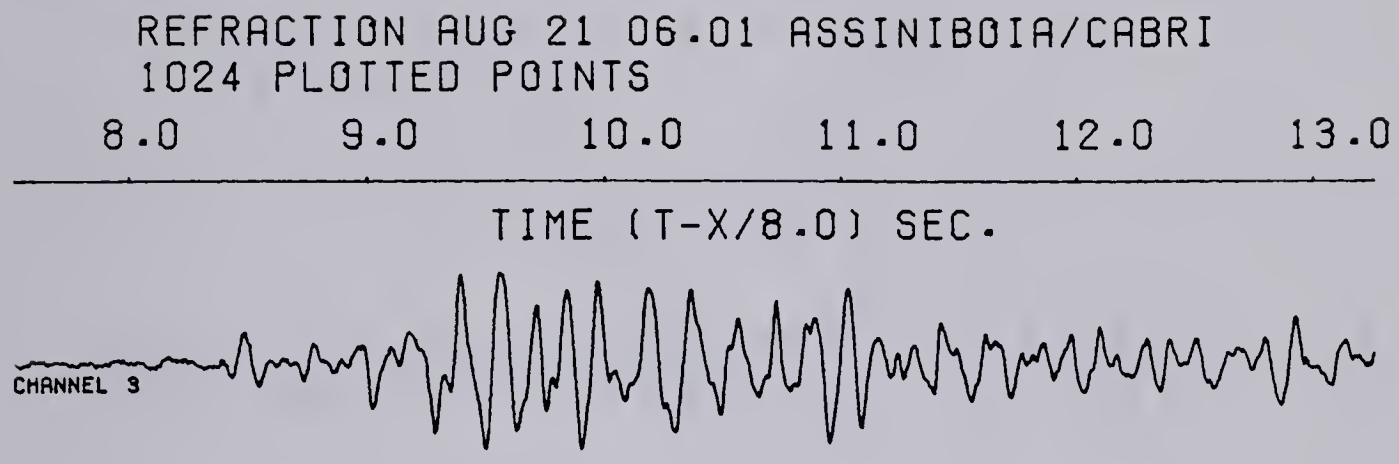

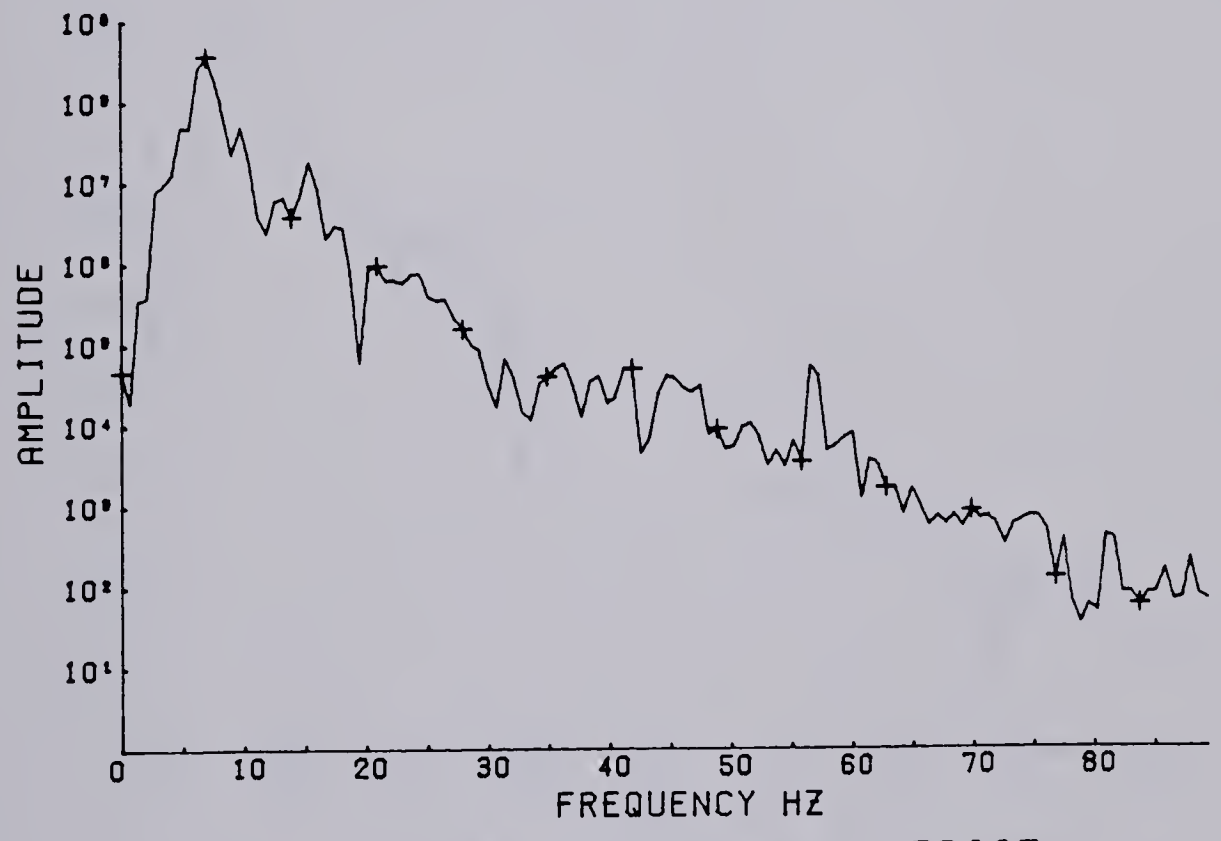

POWER SPECTRUM OF THE TRACE

(A)

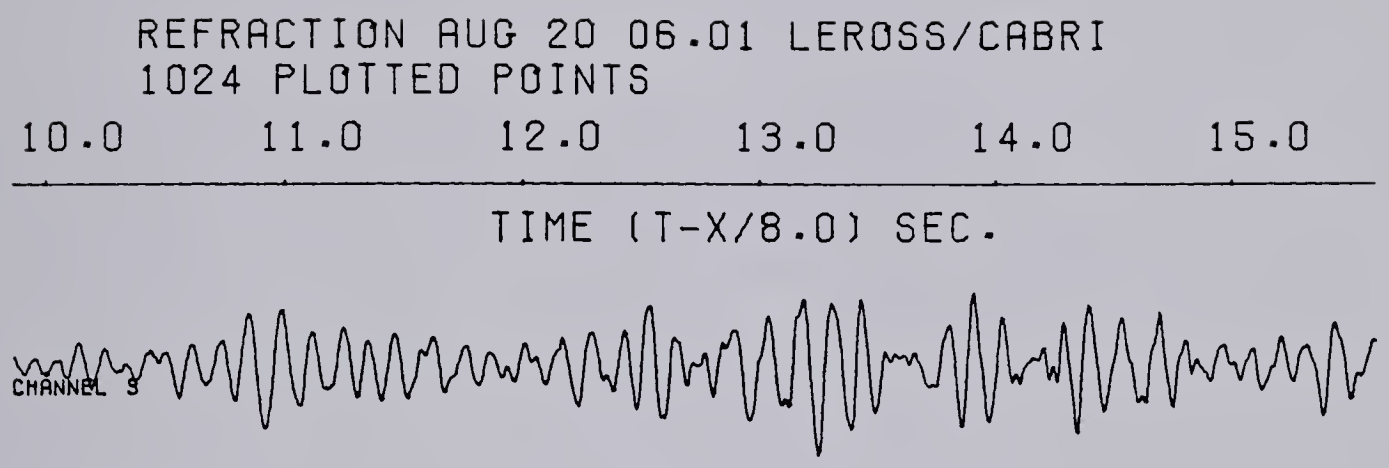

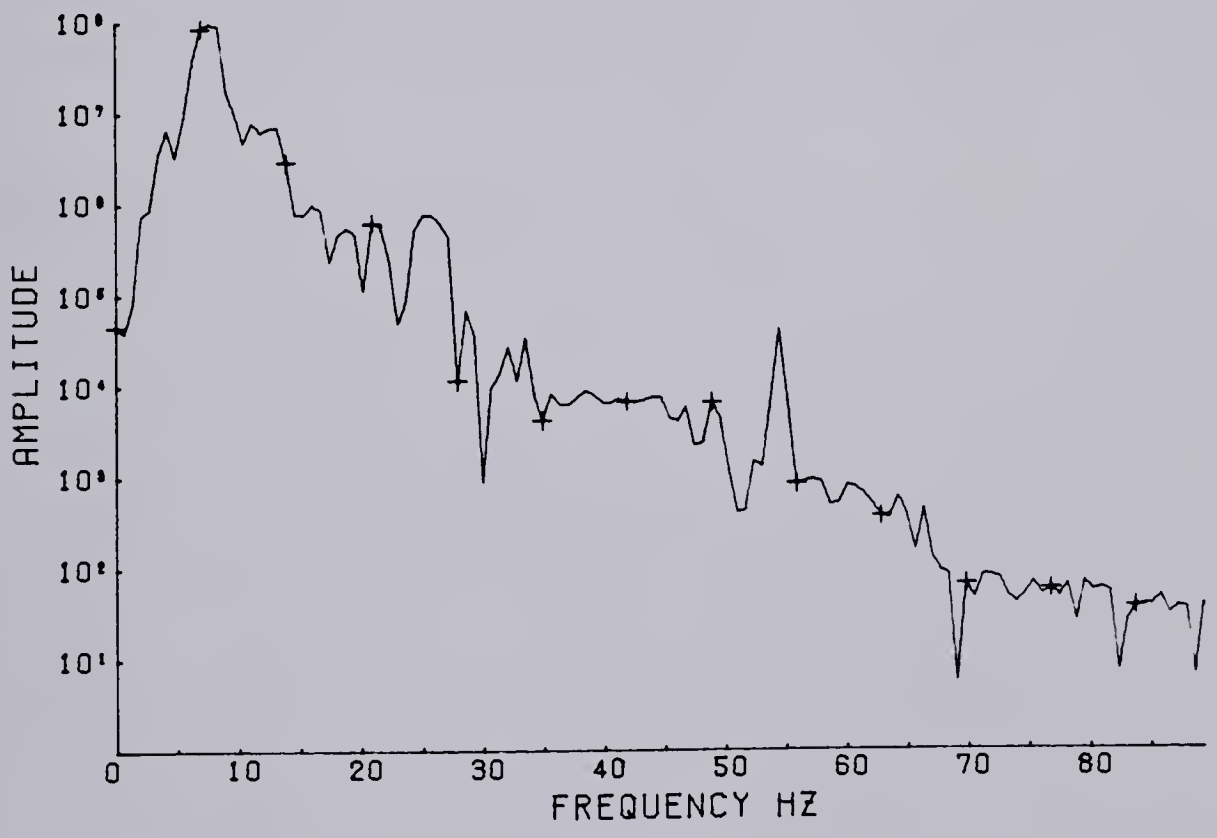

POWER SPECTRUM OF THE TRACE

(B)

Fig.2.9. The same seismic record displayed before and after filtering. The two topmost traces (channel 1 and 2) display the horizontal components and the rest are vertical component data. filtering. Higher frequencies are efficiently suppressed.

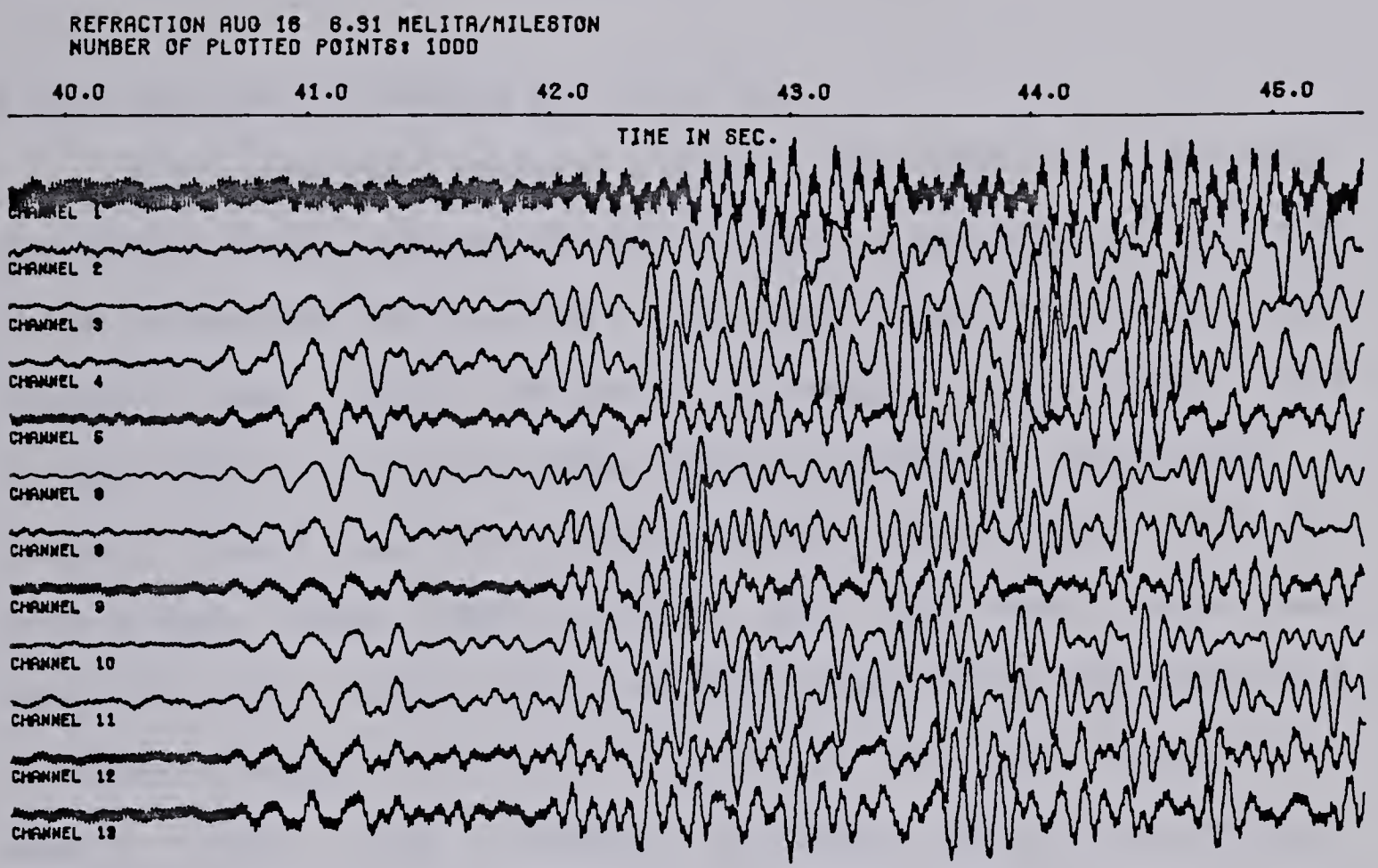
REFRACTION AUG 16 6.31 MELITA/MILESTON
NUMBER OF PLOTTED POINTS: 1000
40.0
41.0
42.0
43.0
44.0
45.0
TIME IN SEC.
CHANNEL 1
CHANNEL 2
CHANNEL 3
CHANNEL 4
CHANNEL 5
CHANNEL 6
CHANNEL 8
CHANNEL 9
CHANNEL 10
CHANNEL 11
CHANNEL 12
CHANNEL 13

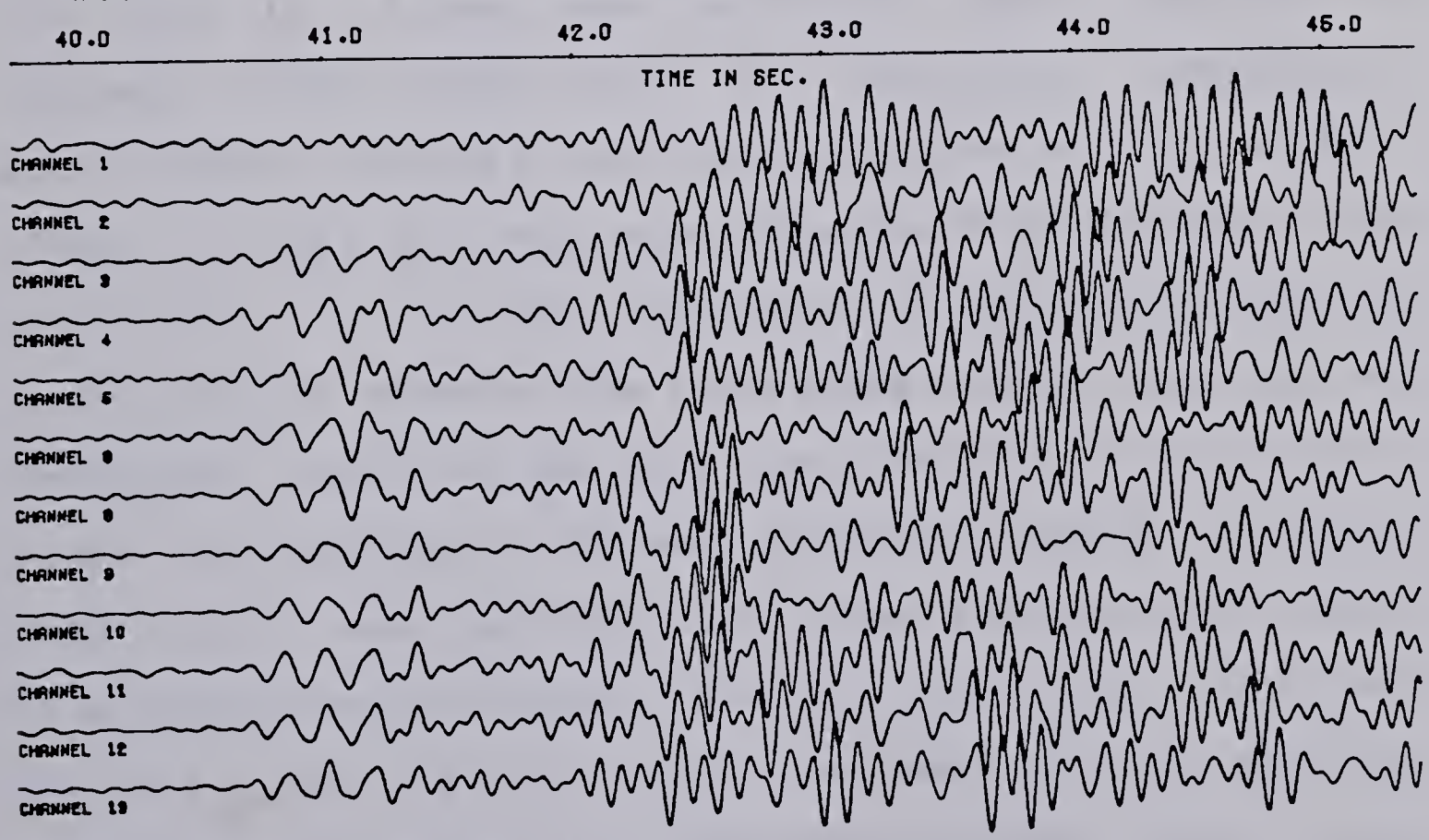
REFRACTION AUG 16 6.31 MELITA/MILESTON
APPLIED FILTER 4.0-15.0 HZ 1000 PLOTTED POINTS
40.0
41.0
42.0
43.0
44.0
45.0
TIME IN SEC.
CHANNEL 1
CHANNEL 2
CHANNEL 3
CHANNEL 4
CHANNEL 5
CHANNEL 6
CHANNEL 8
CHANNEL 9
CHANNEL 10
CHANNEL 11
CHANNEL 12
CHANNEL 13

quality is clearly visible. The high frequency parts of the noise are effectively suppressed.

2.3.4 Spatial filtering by stacking

After some preliminary analysis the need for files with processed data became obvious. Thus, a program was written which processed the raw data and next transferred them onto another tape. Only the parts of records containing P- and S-head wave arrivals have been processed resulting in compact new files. The program worked as follows: First the data points were demultiplexed and the mean value was removed. The second step was band-pass filtering using the frequency range 4.0-15.0 Hz (2.0-15.0 Hz for Oungre/Cabri event). Next, the alignment of traces was achived using a stacking velocity of 8.0 km/s for P-head wave arrivals, and 4.6 km/s for S-head wave arrivals. Then, each pair of adjacent traces (except those with horizontal components) were stacked yielding 5 new traces with the vertical motion. Since, at least two shots were detonated from the same site (see Table 1.), a further improvement of SNR was possible by correlation of records from these common shots, and stacking them again. Thus, the new tape consisted of 10 files, with 2 files corresponding to the same shotpoint-receiver distance (one with P- and the other with S-head wave arrivals). Each file consisting of 7 blocks. The first two files contained the N.S. and E.W. horizontal component and the remaining five contained the vertical components of data. Each block

was 8000 bytes long which yielded 4000 integer *2 words. About 2-3 sec. (350-500 points) of the precursor was retained in the files before the first arrivals. Fig.2.10 shows two vertical seismic records belonging to the same shot group in their original forms and next after processing as they are written on the new tape.

Fig.2.10. Two seismic records for the same profile before stacking (2 upper records), and after stacking (lower record).

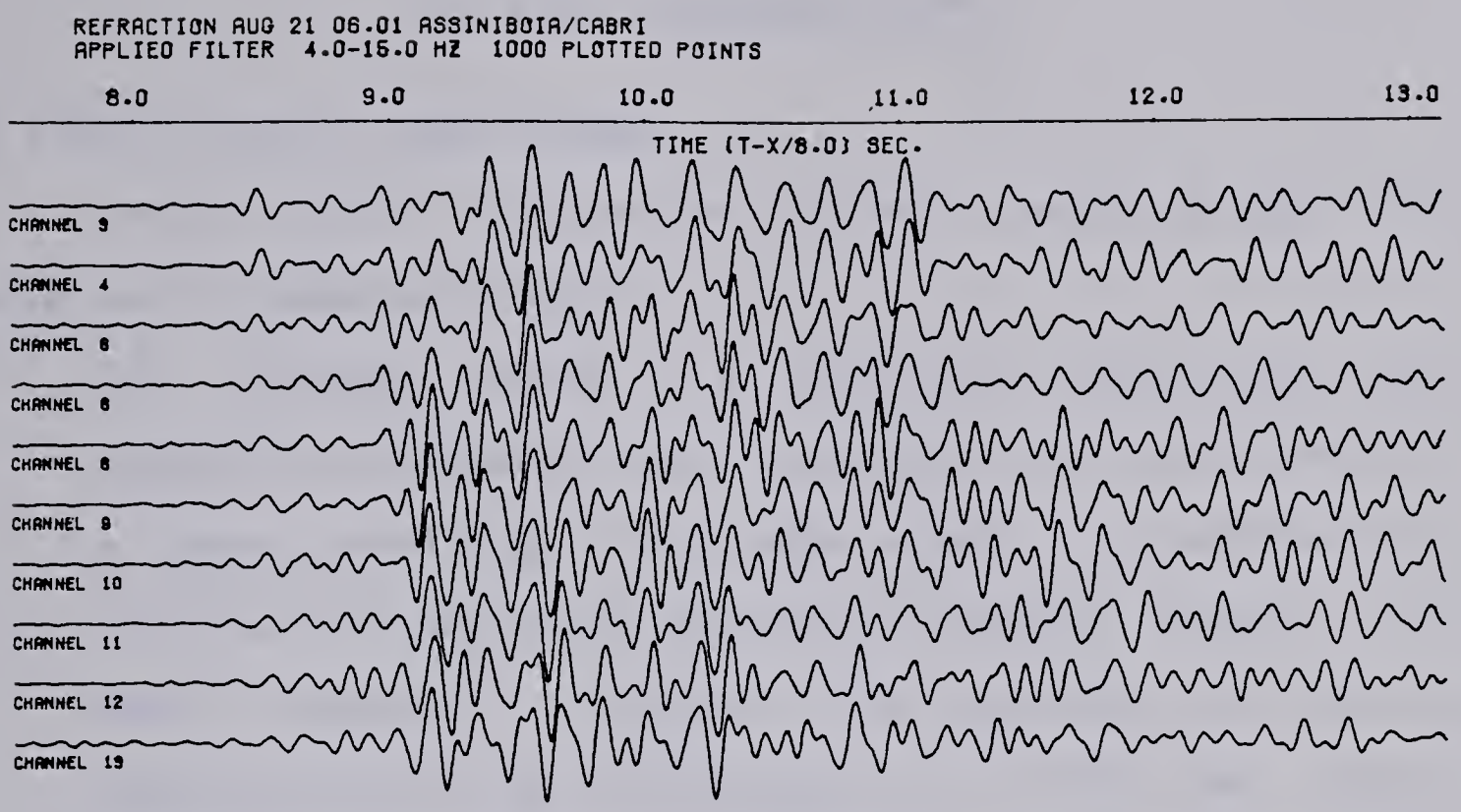
REFRACTION AUG 21 06.01 ASSINIBOIA/CABRI
APPLIED FILTER 4.0-15.0 HZ 1000 PLOTTED POINTS
8.0
9.0
10.0
11.0
12.0
13.0
TIME (T-X/8.0) SEC.
CHANNEL 3
CHANNEL 4
CHANNEL 5
CHANNEL 6
CHANNEL 8
CHANNEL 9
CHANNEL 10
CHANNEL 11
CHANNEL 12
CHANNEL 13

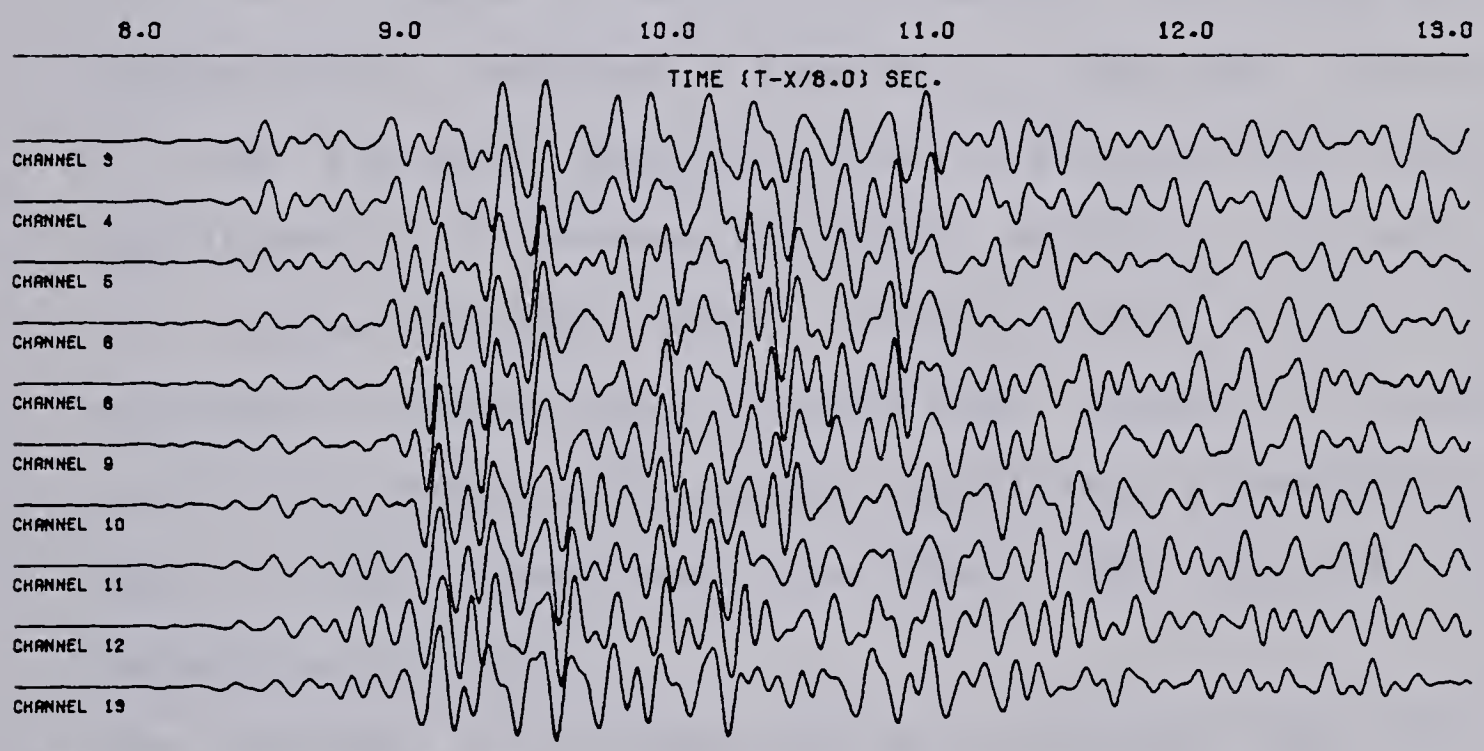
REFRACTION AUG 21 21.01 ASSINIBOIA/CABRI
APPLIED FILTER 4.0-15.0 HZ 1000 PLOTTED POINTS
8.0
9.0
10.0
11.0
12.0
13.0
TIME (T-X/8.0) SEC.
CHANNEL 3
CHANNEL 4
CHANNEL 5
CHANNEL 6
CHANNEL 8
CHANNEL 9
CHANNEL 10
CHANNEL 11
CHANNEL 12
CHANNEL 13

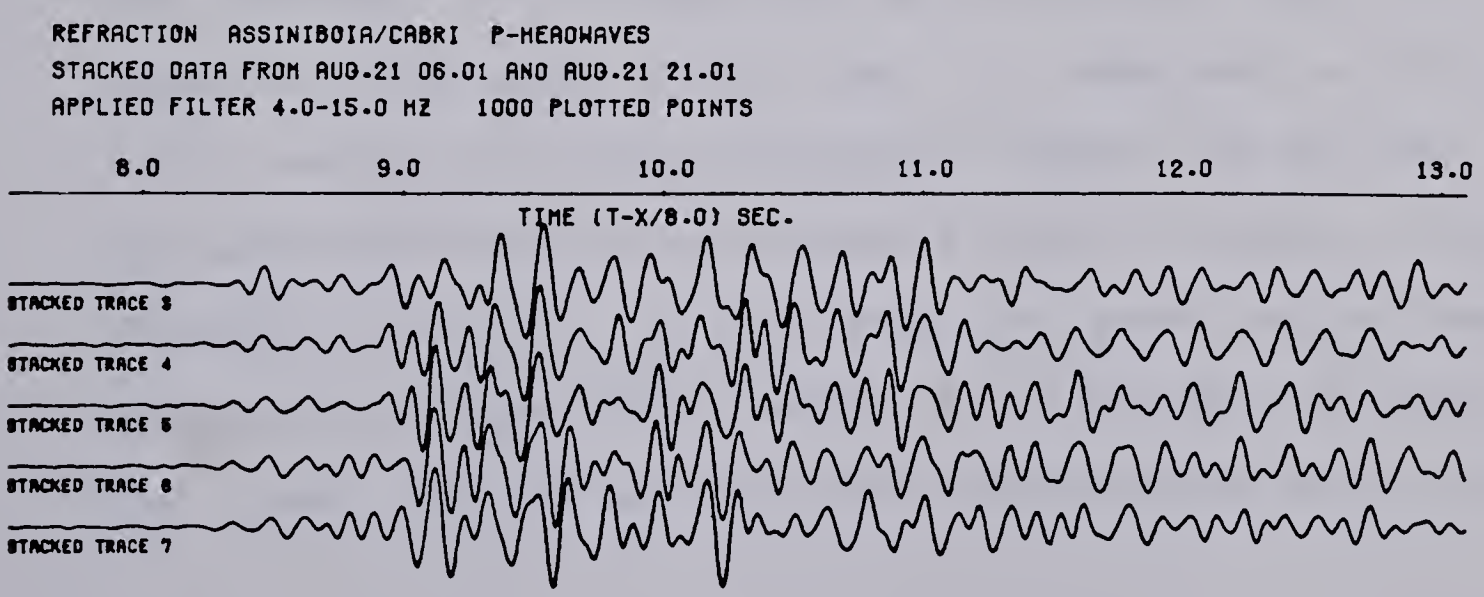
REFRACTION ASSINIBOIA/CABRI P-HEADWAVES
STACKED DATA FROM AUG.21 06.01 AND AUG.21 21.01
APPLIED FILTER 4.0-15.0 HZ 1000 PLOTTED POINTS
8.0
9.0
10.0
11.0
12.0
13.0
TIME (T-X/8.0) SEC.
STACKED TRACE 3
STACKED TRACE 4
STACKED TRACE 5
STACKED TRACE 6
STACKED TRACE 7

3. DATA INTERPRETATION

3.1 Main Crustal Wave Groups

In continental regions two dominant wave groups are observed in general (Fig.3.1.).

1. The P_g-phase which is primarily associated with crystalline basement, but in general, is considered as a wave travelling in the upper crust. If a sedimentary cover exists the phase displays a complex nature with many secondary arrivals. The P_g-phase is usually observed easily up to distances of 60-100 km. Beyond 100 km distance it becomes, in general, very weak and undetectable. The phase following P_g, sometimes called P^*, has a greater apparent velocity and can show large amplitudes as it becomes the first arrival. In turn, this phase becomes weaker with distance, and may be replaced by another one, delayed with respect to the proceding phase. Such phase splitting is frequently seen in continuous profiling where the spacing of detectors is small.
2. The P_n-phase is a head wave or a refracted wave that penetrates the upper mantle and is recorded as the first arrival at larger distances (beyond 130-200 km). Its apparent velocity is between 7.7 and 8.5 km/s. The strongest arrivals in this group are generated at the *Mohorovičić discontinuity* which is the boundary between the crust and the mantle. They are characterized by a

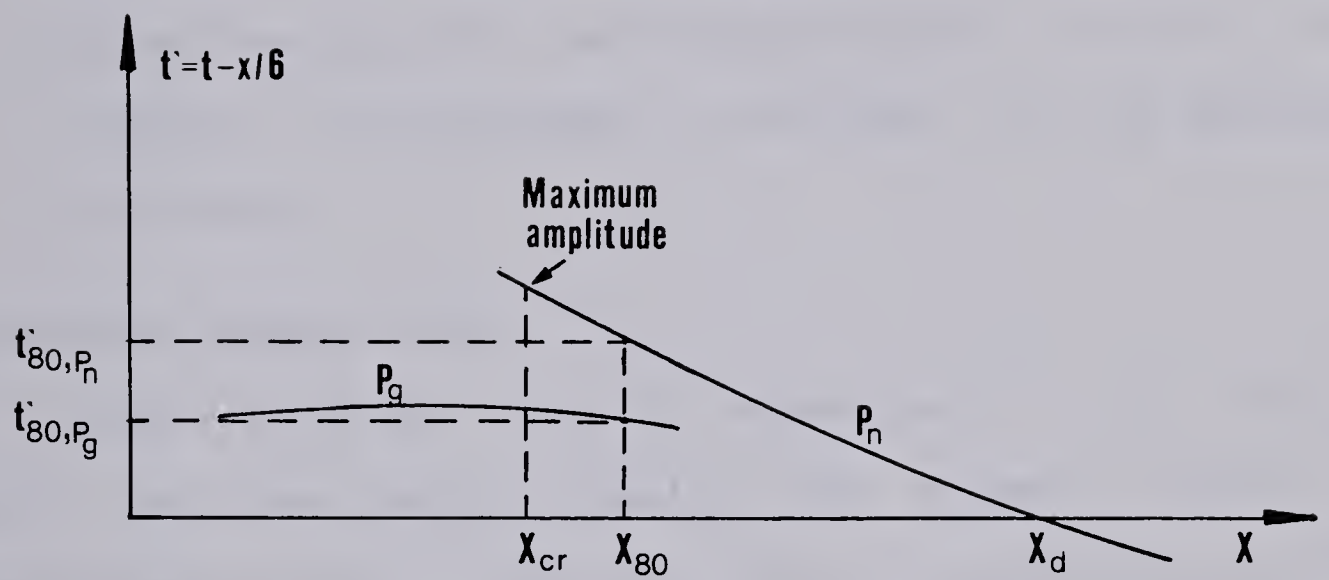

Fig.3.1 Schematic travel-time diagram with reduced time axis (reduction velocity of 6 km/s) showing two main groups P_g and P_n and the basic parameters X_{cr}, X_d and $t'(X=80)$.
X_{cr}- critical distance
X_d - crossover distance
t' - reduced travel time

large amplitude, especially near the critical point (a point at which the reflection and head wave times are equal) which, for an average continental crust, varies from 60 to 90 km. A similar feature of splitting, as for the P_g-phase, can be detected for arrivals from the *Moho* on records with continuous profiling. This is caused by variations in the elastic parameters within 1 km vertically of the discontinuity as well as by velocity or structural variation in the horizontal directions.

3.2 Record Presentation

Seismic data are usually presented in the form of record sections which display the seismic traces on a time-distance graph. The travel time is presented usually in one of two ways. In the first case it is plotted as true travel time with the source time marked as the origin for each receiver. This kind of presentation is especially useful in continuous profiling. In the second case it is scaled as a *reduced travel time* (Fig.3.1.) which is defined as follows:

$$t' = t - x/v \qquad (1)$$

where:

t' - reduced travel time

t - true travel time

x - source-receiver distance

v - reduction velocity

This type of display yields much better resolution on a small graph over large recording distances and is widely used in seismic refraction studies. If we choose the reduction velocity close to the apparent velocity of the phase of interest, the record sections show the phase arranged more or less horizontaly, which makes the correlation of seismic events much easier (Fig.3.1.). Since most crustal investigations are made by interpreting P-phases the reduction velocity should be close to the average crustal velocity of the compressional waves (i.e. about 6.0-6.5 Km/s), or it should correspond to the velocity of the most prominent and the most informative, from our point of view, refractor.

In the 1979 refraction survey the distances between shotpoints and the University of Alberta receivers were over 200 Km (Table 1.), therefore the first arrivals and many converted phases were belived to come from the Moho discontinuity. Thus, a reduction velocity of 8.0 km/s was chosen for the record presentation in all cases when a reduced time scale was used.

3.3 General Remarks on Travel Time Data

Most of problems encountered in crustal studies have been solved using the assumption that the medium under study is layered, isotropic and homogeneous in the horizontal direction. This is also assumed to hold in the following

discussion. The velocity gradient dv/dz, which influences strongly the curvature of the travel-time curve, can be either positive or negative.

1. A positive velocity gradient $0<dv/dz<+\infty$ can have three possible cases:
   a. dv/dz=0 (constant velocity layer). Here the travel-time curve exhibits a linear character. Head waves are possible at the top of the layer, and reflections are generated at both the upper and lower boundary.
   b. $0<dv/dz<+\infty$ (positive velocity gradient within a layer). A small velocity gradient makes the travel-time curve have convex curvature (normal type), while a large velocity gradient generates a cusp in the travel-time curve with concave curvature (reversed or retrograde type).
   c. $dv/dz=+\infty$ (discontinuity occurs). Recorded reflected waves produce a travel-time curve of concave curvature. A wide spectrum of velocities corresponds to the same depth value z. Many rays can bottom at this depth, which yields many points with different time corresponding to the value *z* in the travel-time diagram.
2. Negative velocity gradient $-\infty<dv/dz<0$ (velocity inversion). Such a condition rules out the possibility of refracted waves, therefore no information about the velocity value can be derived from the travel-time

diagram (shadow areas without arrivals on the travel-time diagram).

3.4 Principles of Correlation

The objective of correlation is to time the wavefronts of any phase that occur and find their travel-time branches. Here, it is common practice to use not the beginning of the event, which is usually difficult to trace, but the next pronounced amplitude minimum or maximum. It is obvious that in order to to apply true phase correlation the spacing of detectors should be smaller than one wave length. To identify in record section the regular signal from the arrivals caused only by local inhomogeneities, the following criteria must be applied:

1. Amplitudes of the correlated events should exceed those of the noise.
2. The apparent velocity should fall into a reasonable range of values.
3. The travel-time branches should have the same apparenr velocity for some length.

Phase correlation is particulary useful in reflection seismology where detector spacing is small and the apparent wavelength of the reflected pulses is relatively large. In refraction studies, where distances between receivers are usually much greater than one wavelength, the principle of group correlation is widely used. When using it, some criteria must also be followed:

1. The group correlated curve is obtained by joining of

separated phase-correlated segments and/or arrivals with clear amplitudes.

2. The resulting apparent velocity should fall into reasonable range of values.
3. The travel-time branch should have the same slope for some distance.

3.5 Ground Motion

In the 1979 refraction survey two horizontal component seismometers were included in the spread to give an indication of the type of wave involved in any particular arrivals. A usual way of analysing the ground motion is to plot particle motion diagrams of the displacements of the traces one against the other as a function of time. If both traces have a simple sinusoidal shape an ellipse is obtained with its axes corresponding to the amplitudes of the traces. The phase differance between the traces is indicated by the tilt of the axes and the sense of the motion on the figure. Plotting particle motion diagrams is based on the assumption that the output of seismometer is proportional to ground displacement for simple harmonic motion. While plotting one has to be sure that the vertical and horizontal component displacements are intercalibrated, and there is no phase differance between in-phase displacements on the vertical and horizontal component traces. Depending on circumstances, these conditions are met to varying degrees in field work. However, even when the limitations hold, particle motion diagrams can be valuable aids in the interpretation of many

features of ground motion.

Fig.3.2A-F show records of three horizontal components (N.S., E.W. and radial obtained from these two) and vertical component data for different events and various arrival times. For each case Lissajous figures of the vertical versus the radial horizontal displecements are shown. The plotting time interval was 0.59 sec. (105 points with a sampling rate of 5.6 ms.). The plotted time in Fig.3.2A and Fig.3.2D corresponds to that of the first arrival and its vicinity for these events. It is clear that the first arrivals are limited to P-wave type of motion which is what we expect. The following arrivals are still P head wave but they contain different amounts of P- and S-wave components corresponding to the various converted phases due to local inhomogeneities (Fig.3.2B and Fig.3.2E). Finally, Fig.3.2C and Fig.3.2F present ground motion at the time when the shear (S) phase is a head wave. Also here, due to phase conversion and local inhomogeneities, two types of motion at varying proportions are present.

3.6 Frequency Content of Signals

In examining the physical basis of seismic method, the following conditions should always be considered:

1. The conditions existing during waves generation.
2. The conditions prevaling along a raypath of the propagated waves.
3. The conditions under which the waves are detected.

Fig.3.2A-F Particle motion diagrams showing particle velocity for the vertical and horizontal-radial components. Units are arbitrary and the same on both axes. The horizontal-radial component was obtained from the N.S. and E.W. horizontal components.

A) and D) Plotted record time includes the first arrival

B) and E) Plotted record time includes arrivals coming in few sec. after the first break

C) and F) Plotted record time includes arrivals which are S-headwaves

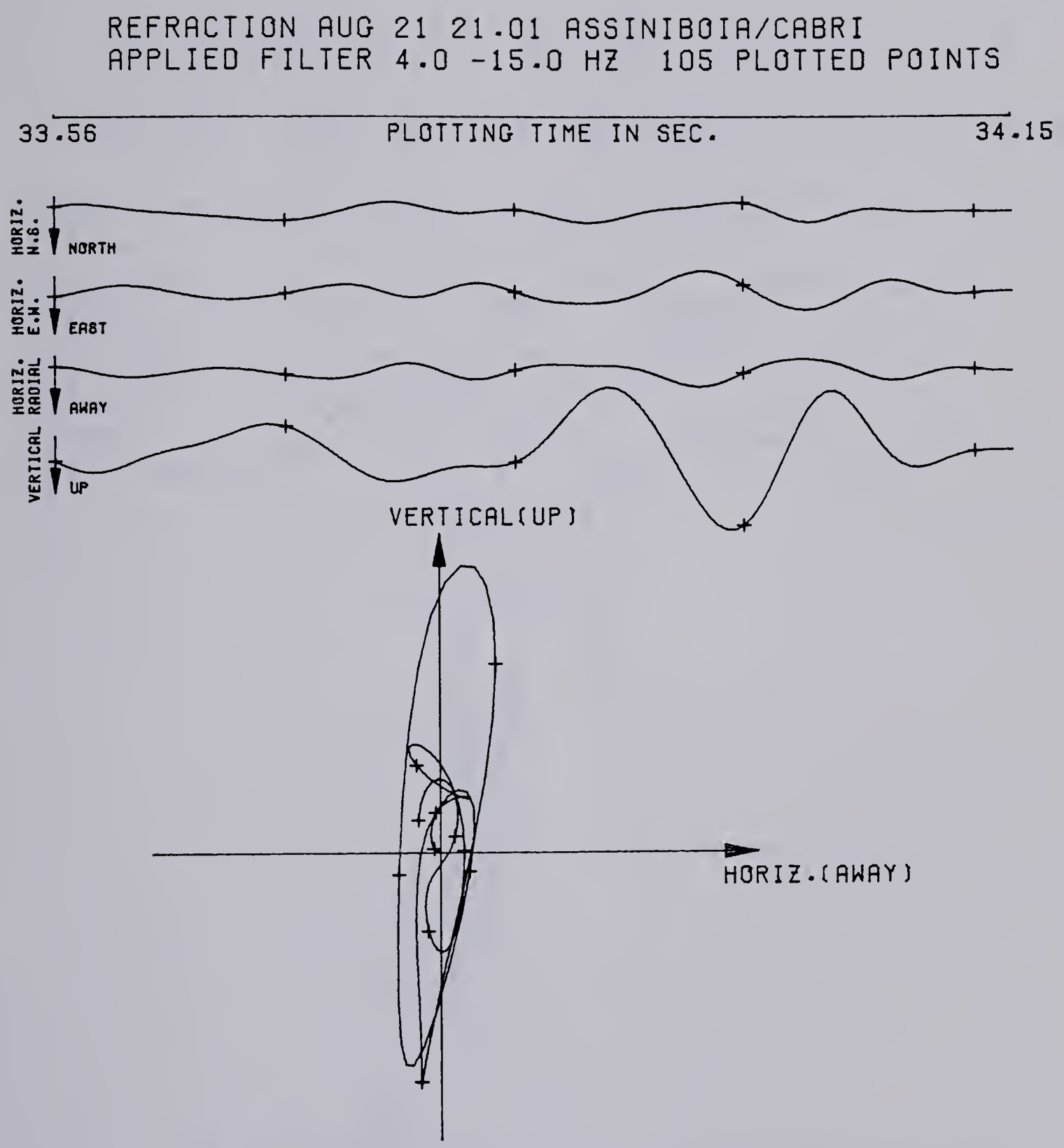

PLOT OF RADIAL(HORIZ.) VERSUS VERTICAL GROUND MOTION

(A)

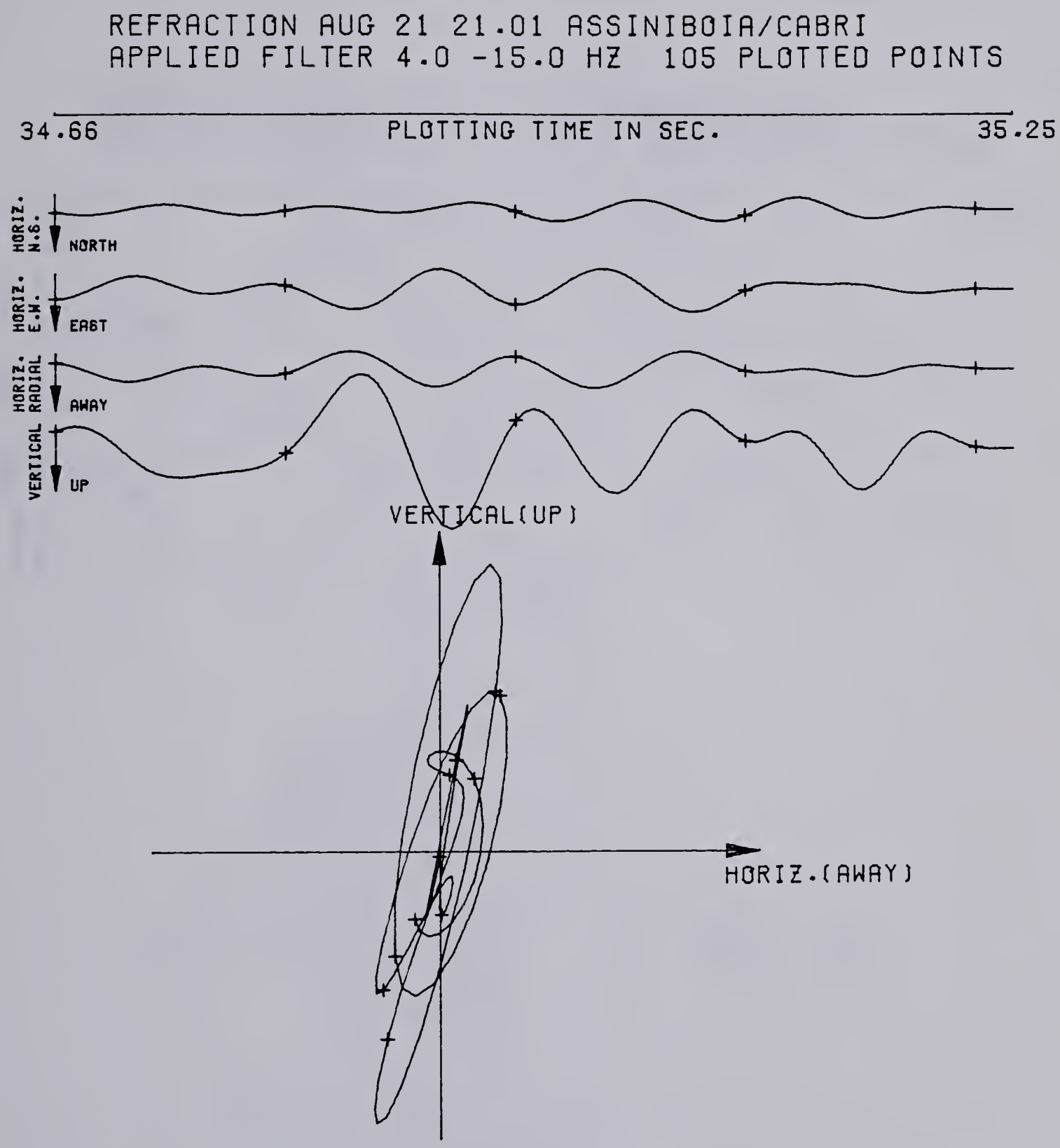

PLOT OF RADIAL(HORIZ.) VERSUS VERTICAL GROUND MOTION

(B)

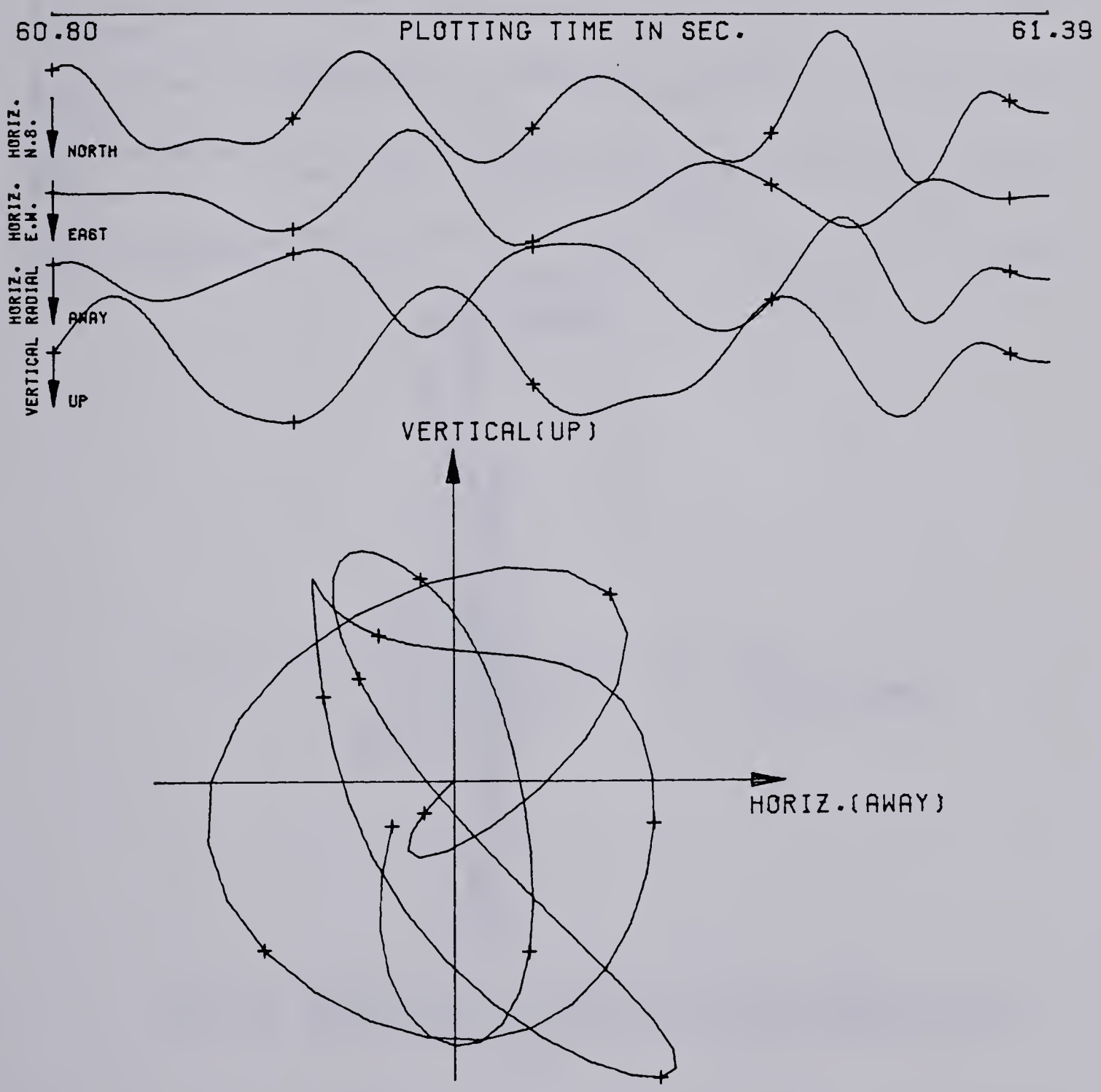

PLOT OF RADIAL(HORIZ.) VERSUS VERTICAL GROUND MOTION

(C)

REFRACTION AUG 17 5.01 ROBLIN/MILESTONE
APPLIED FILTER 4.0 -15.0 HZ 105 PLOTTED POINTS

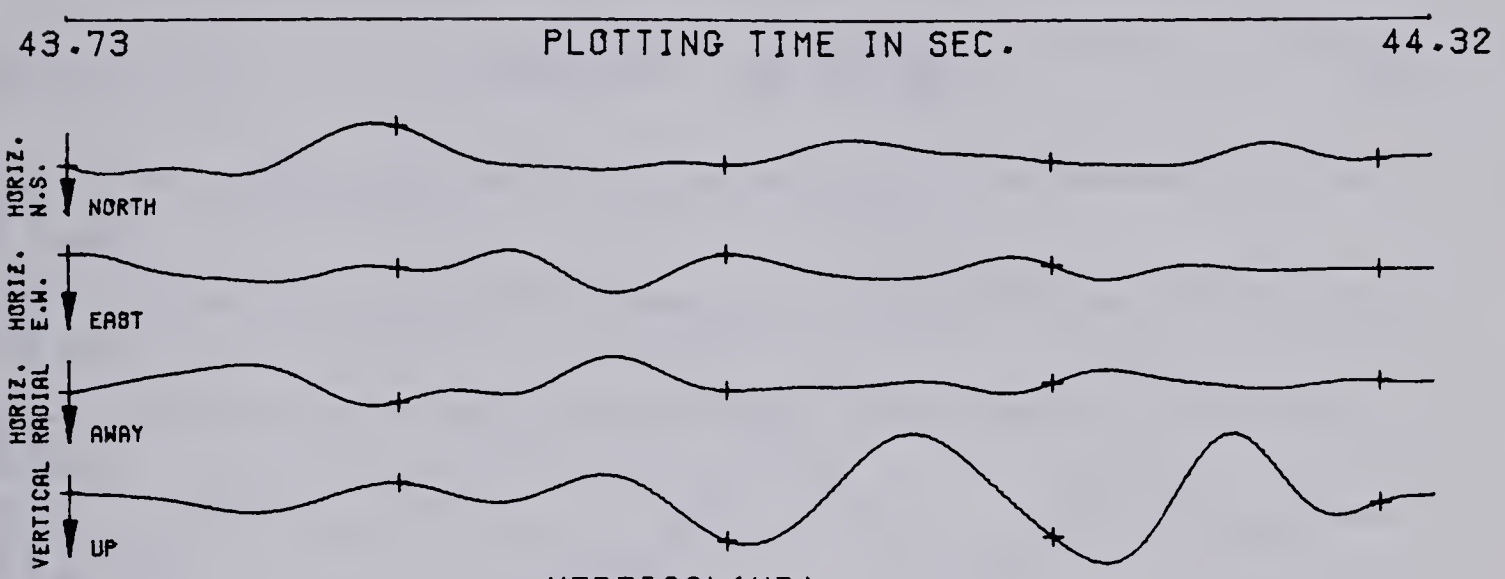

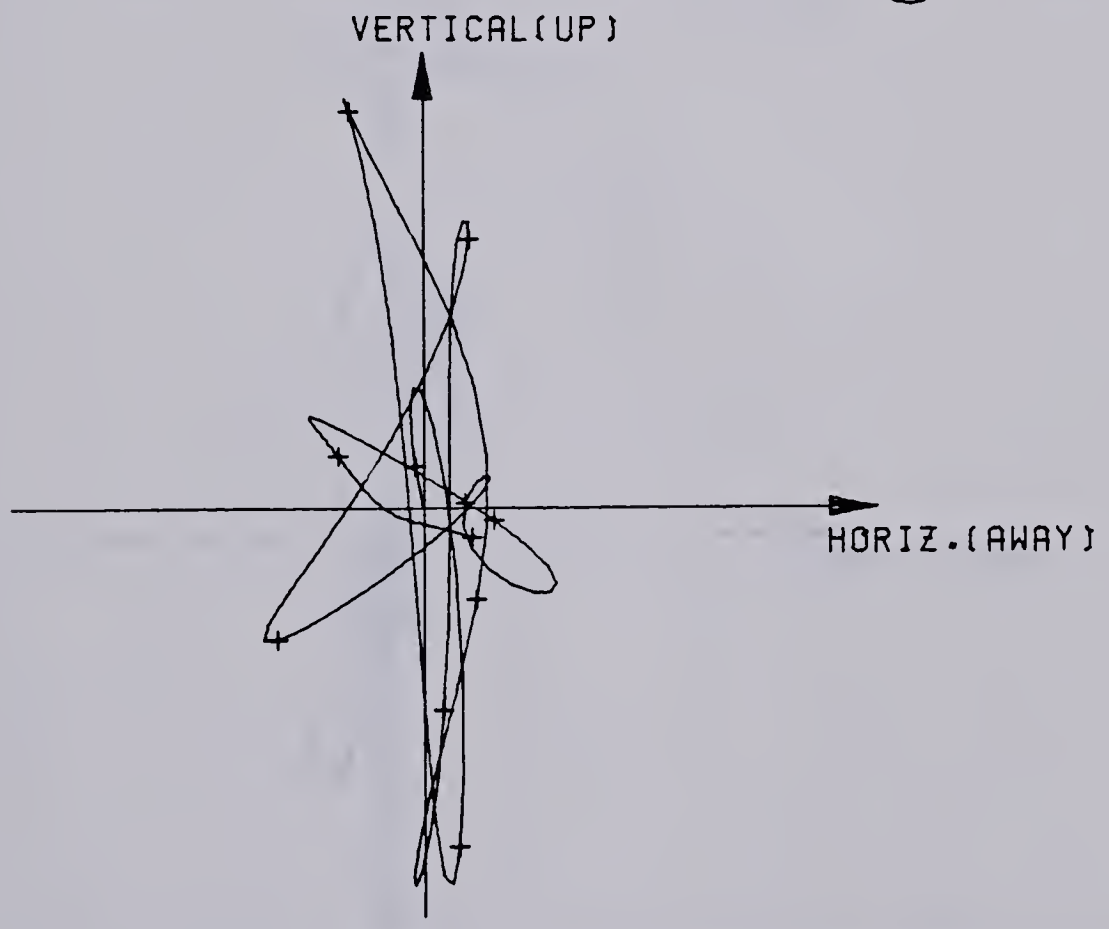

PLOT OF RADIAL(HORIZ.) VERSUS VERTICAL GROUND MOTION

(D)

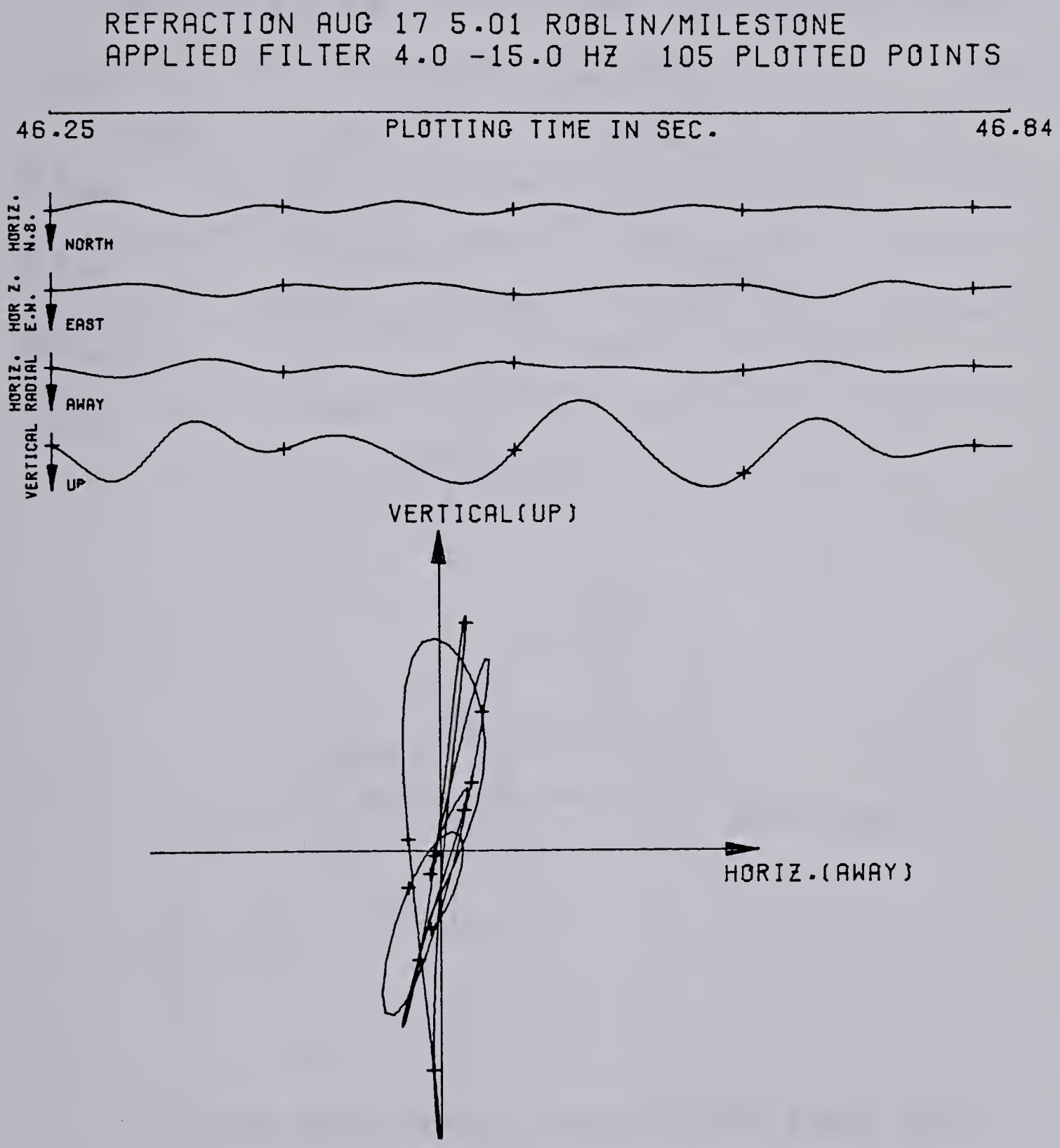

PLOT OF RADIAL(HORIZ.) VERSUS VERTICAL GROUND MOTION

(E)

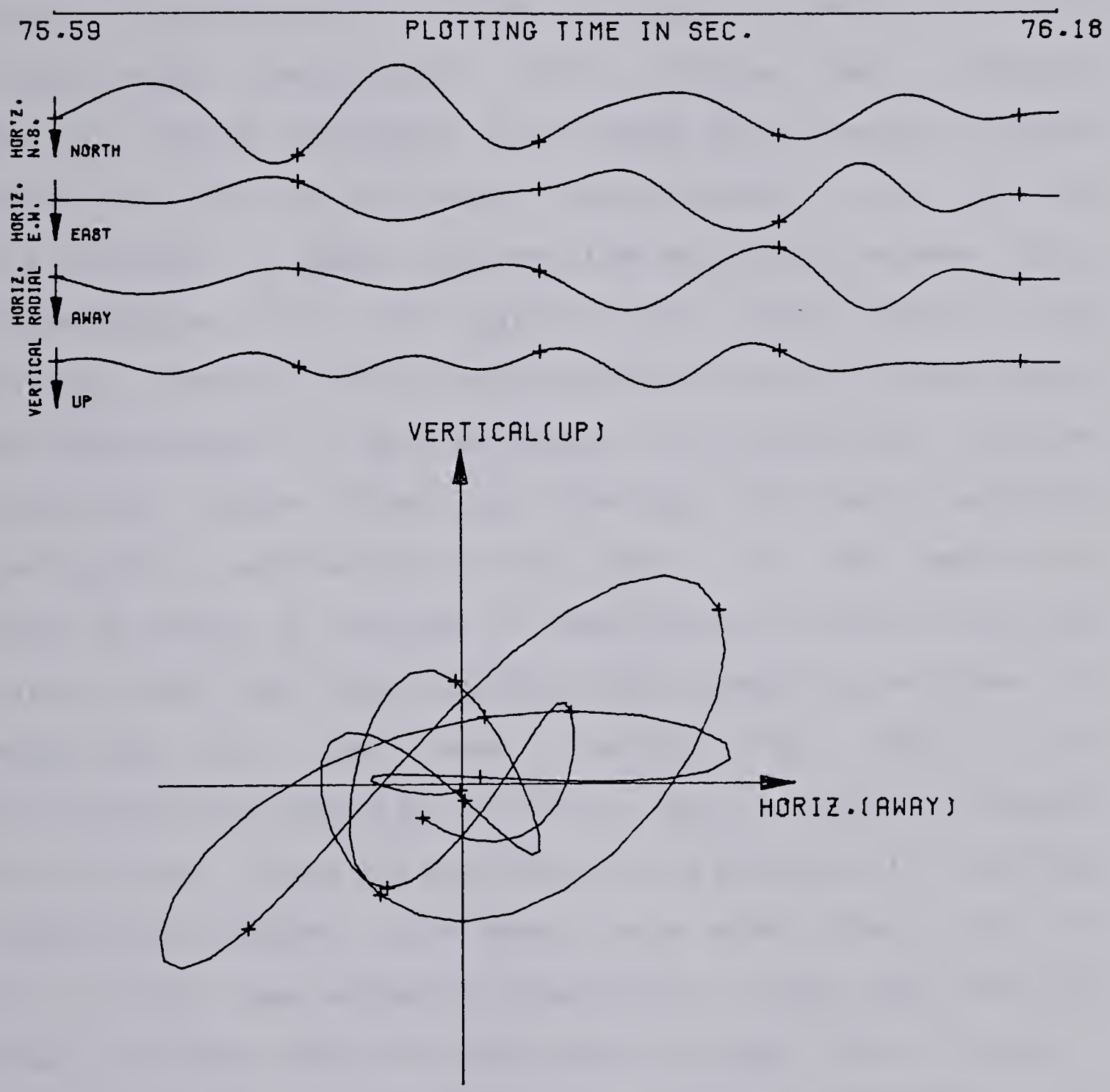

PLOT OF RADIAL(HORIZ.) VERSUS VERTICAL GROUND MOTION

(F)

In seismic crustal surveys the waves are almost always generated by explosions. Buried charges form the source which is most widely used in land operation. Elastic waves are more efficiently produced if a number of small charges (tens or hundreds of kilograms) are used instead of a single large charge (Kosminskaya, 1971). Studies have indicated that in a given geological environment the principal factors affecting shooting efficiency are hole depth, the size of the charge in each hole and the separation between holes (Kosminskaya, 1971). For a given hole depth there is an optimum charge weight which produces elastic waves with a maximum energy in a desired range of frequencies. Another important factor affecting shooting efficiency, which is particulary important for large shots, is the medium in which a charge is located. In some cases different locations yield signal amplitudes different by as much as an order of magnitude for the same charge size. There is no cost-effective method by which one can reasonably predict the optimum shooting conditions in a medium with arbitrary properties. However, experiments have shown that shots in dry rock are less effective than shots in wet rock, shots in shale are more effective than shots in sand, and so forth.

In order to maximize the shooting efficiency the spectrum of generated waves should have its peak at the frequency at which the SNR is optimum. Spectral studies have shown that despite the fact that detonation is almost instantaneous a number of resonance peaks occur. In general,

with increasing charge size the frequency at which the spectral peak occurs decreases, however the relationship is very weak (Kosminskaya, 1971). There is also observed a weak relationship between charge weight and the shape of the spectrum (Kosminskaya, 1971).

During wave propagation through the medium the spectrum of the signal changes, mainly because of scattering by inhomogeneities. Spectral analysis have revealed that:

1. The attenuation increases with frequency.
2. Near a large explosion, the thicker the sedimentary cover, the lower is the overall level of the recorded frequencies. This behavior becomes more complex if significant changes in lithology of the sedimentary cover are observed.
3. The larger the distance from the source, the lower is the dominant frequency on a record and the rate of decrease is about 1-2 Hz per 100 km for distances greater than 50 km. Usually, different types of waves exhibit similar spectra, however, at large distances (greater than 200 km) early arrivals of the first mantle waves are nearly always of higher frequency than later arriving crustal events.

Table 2. shows some characteristic parameters of spectra in the 1979 refraction records. Despite the fact that there were only 11 records to analyse it is useful to compare the experimental data with theoretical predictions. Reliable conclusions can be drawn from the data by comparing

Table 2. Spectral Analysis

Shotpoint/ Receiver	Date	Hour	Distance (km)	Charge size (kg)	F-Max (Hz)	F-Range (Hz)	Power Output $*10^5$
Ass/Cabri	Aug.21	06:01	207.2	250	7.0	4.9- 9.8	2391
Ass/Cabri	Aug.21	21:01	207.2	1375	7.0	4.2-10.5	2480
Mel/Mil	Aug.15	05:31	260.3	200	9.8	3.5-14.7	40
Mel/Mil	Aug.16	05:31	260.3	425	11.9	4.9-12.6	920
Mel/Mil	Aug.15	06:31	260.3	1000	11.9	3.5-14.7	2468
Rob/Mil	Aug.15	05:01	272.6	400	11.9	4.2-14.0	70
Rob/Mil	Aug.17	05:01	272.6	1200	5.9	4.2-11.2	1463
Ler/Cabri	Aug.18	06:01	350.7	350	7.7	5.6-13.3	82
Ler/Cabri	Aug.20	06.01	350.7	1249	7.7	6.3-10.5	921
Oun/Cabri	Aug.20	06:31	381.7	250	4.9	2.1-11.2	14
Oun/Cabri	Aug.18	06:31	381.7	400	6.3	4.2- 9.8	81

Comments:

1. F-Max - frequency at which maximum power output occurred
2. F-Range - range of frequencies within which power output was > 10% of its maximum value
3. Recording system was saturated for the Assiniboia/Cabri event of August 21 21:01
4. Power spectra were calculated for 128 points over the range of frequencies 0 to 89.3 Hz
5. Power outputs were corrected for different gain control values

the signal amplitudes and the general shape of the spectra for the same shotpoint and receiver locations for different charge sizes. It is seen that the amplitude increases with increasing charge weight. There are no significant changes in the general shape of spectra for the same distances and different charge weights (compare Fig.2.8B versus Fig.3.3). This conclusion gets another support from the fact that crosscorrelation functions for those records (Fig.3.4A-B) are very high, exceeding 0.95. From an analysis of both records and power spectra of later arrivals it is seen that later arriving events have lower frequencies than first arrivals.

3.7 Travel Times Analysis

3.7.1 Introduction

The first arrival times were read from unfiltered (applied zero-phase shift, recursive Butterworth band-pass filtering can introduce some error by altering the onset of the first break) vertical component records. It was decided that station no.1, with the two horizontal and one vertical component seismometers, would be the reference station and all times and distances would correspond to measurements at this station. The first and secondary arrivals with P head wave were read from plots with a time scale 1sec.=68mm (i.e. 1mm=0.015sec. which resulted from plotting 2001 points on 30 inches long records). Later arrivals with S head wave were read from plots with a time scale 1sec.=27.2mm (i.e.

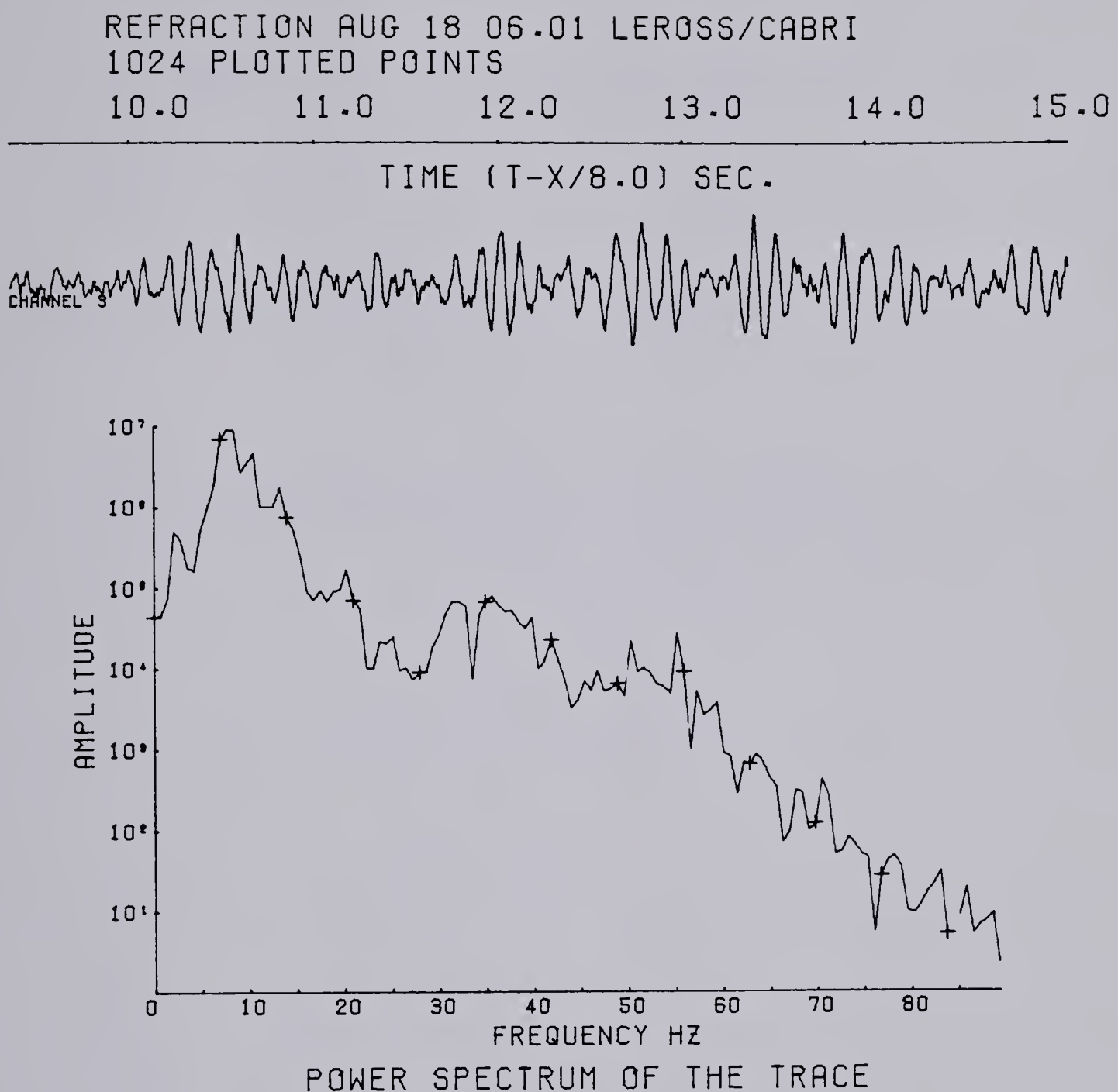

Fig.3.3 Power spectrum (periodogram) for the Leross/Cabri event. Shotpoint to receiver distance was 351 Km. Charge size was 350 kg.

Fig.3.4A-B Cross-correlation functions of events for the same profile but with different charge sizes.
a) The Assiniboia/Cabri event
b) The Leross/Cabri event

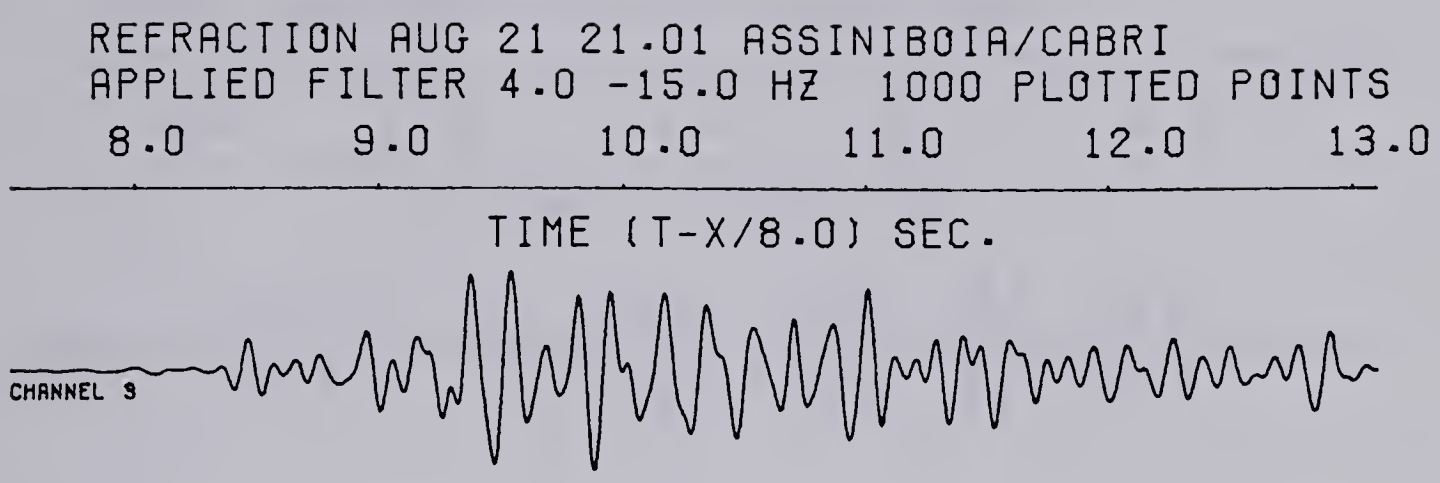

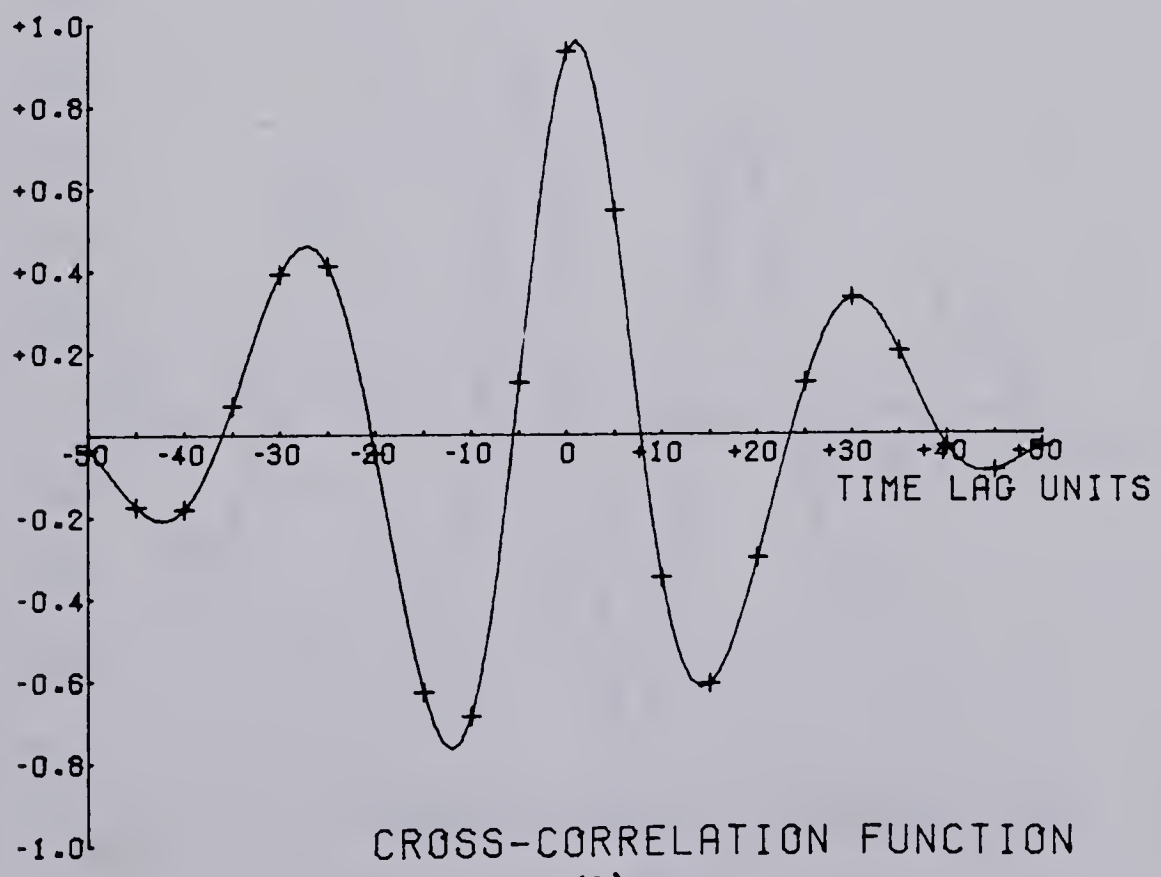

CROSS-CORRELATION FUNCTION

(A)

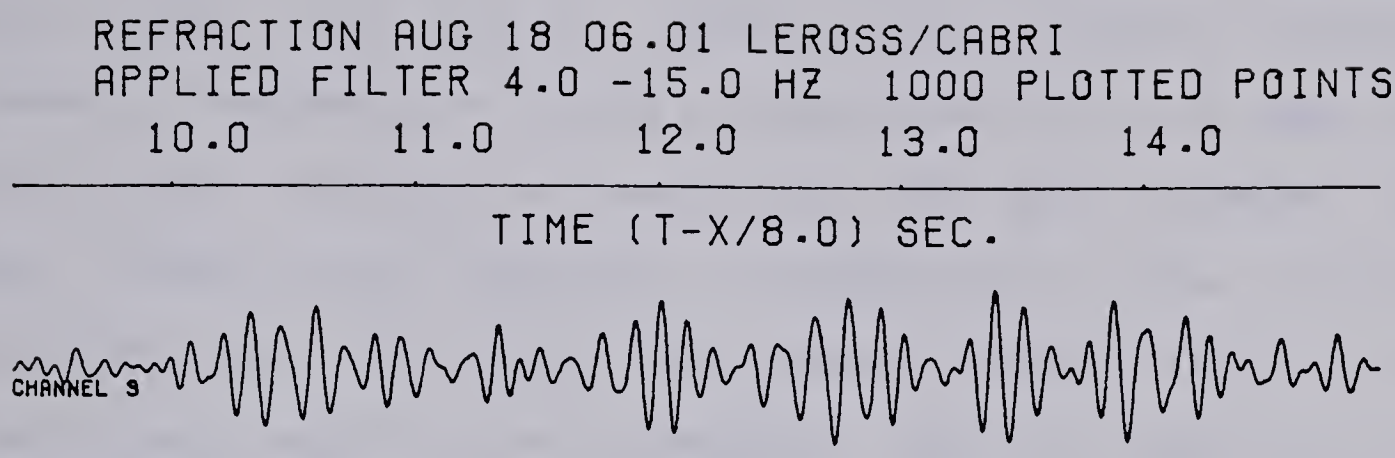
REFRACTION AUG 18 06.01 LEROSS/CABRI
APPLIED FILTER 4.0 -15.0 HZ 1000 PLOTTED POINTS
10.0 11.0 12.0 13.0 14.0
TIME (T-X/8.0) SEC.
CHANNEL 3
REFRACTION AUG 20 06.01 LEROSS/CABRI
APPLIED FILTER 4.0 -15.0 HZ 1000 PLOTTED POINTS
10.0 11.0 12.0 13.0 14.0 15.0
TIME (T-X/8.0) SEC.
CHANNEL 3
+1.0
+0.8
+0.6
+0.4
+0.2
-0.2
-0.4
-0.6
-0.8
-1.0
-50 -40 -30 -20 -10 0 +10 +20 +30 +40 +50
TIME LAG UNITS
CROSS-CORRELATION FUNCTION

(B)

1mm=0.037sec. which resulted from plotting of 5001 points on 30 inches long records). Travel time data came from so widely separated areas that no reliable conclusion can be drawn about the crustal models along profiles. The small number of records also rules out the possibility of applying statistical methods in analysing the data. However, the data, along with available information on the crustal structure of the areas from other sources, allows us to discriminate against certain models and be indicative of some major crustal features.

3.7.2 Conclusions from 1977 and 1979 refraction surveys

The main group of the 1979 COCRUST survey carried out measurements along the refraction profiles Roblin/Melita, Leross/Oungre and Assiniboia/Carlyle. Fig.3.5 shows the location of these profiles as well as crustal models derived from the data. The Roblin/Melita reversed profile covered the area of the Superior-Churchill boundary zone. The spread consisted of 38 receivers spaced an average of 6.8 km apart. The Leross-Oungre reversed profile was entirely located within the Churchill province. Thirty seven seismometers were laid out along a N-S line with an average spacing of 7.2 km. The third profile, Assiniboia/Carlyle, was unreversed with only one shot at Assiniboia and was thought as an extension to the west of the 1977 E.-W. profile. It consisted of 36 seismometers spread along a line 287.5 km long with an average spacing of about 8.0 km.

Fig.3.5 Crustal models of S.W. Manitoba and southern Saskatchewan derived from the 1979 seismic refraction survey carried out by the main COCRUST group. Values at both ends of the profiles are depths to interfaces in Km, while values placed along the profiles are velocities in layers in Km/s. The solid lines show values obtained from the coverage for a given refractor, while the dashed lines represent interpolated values.

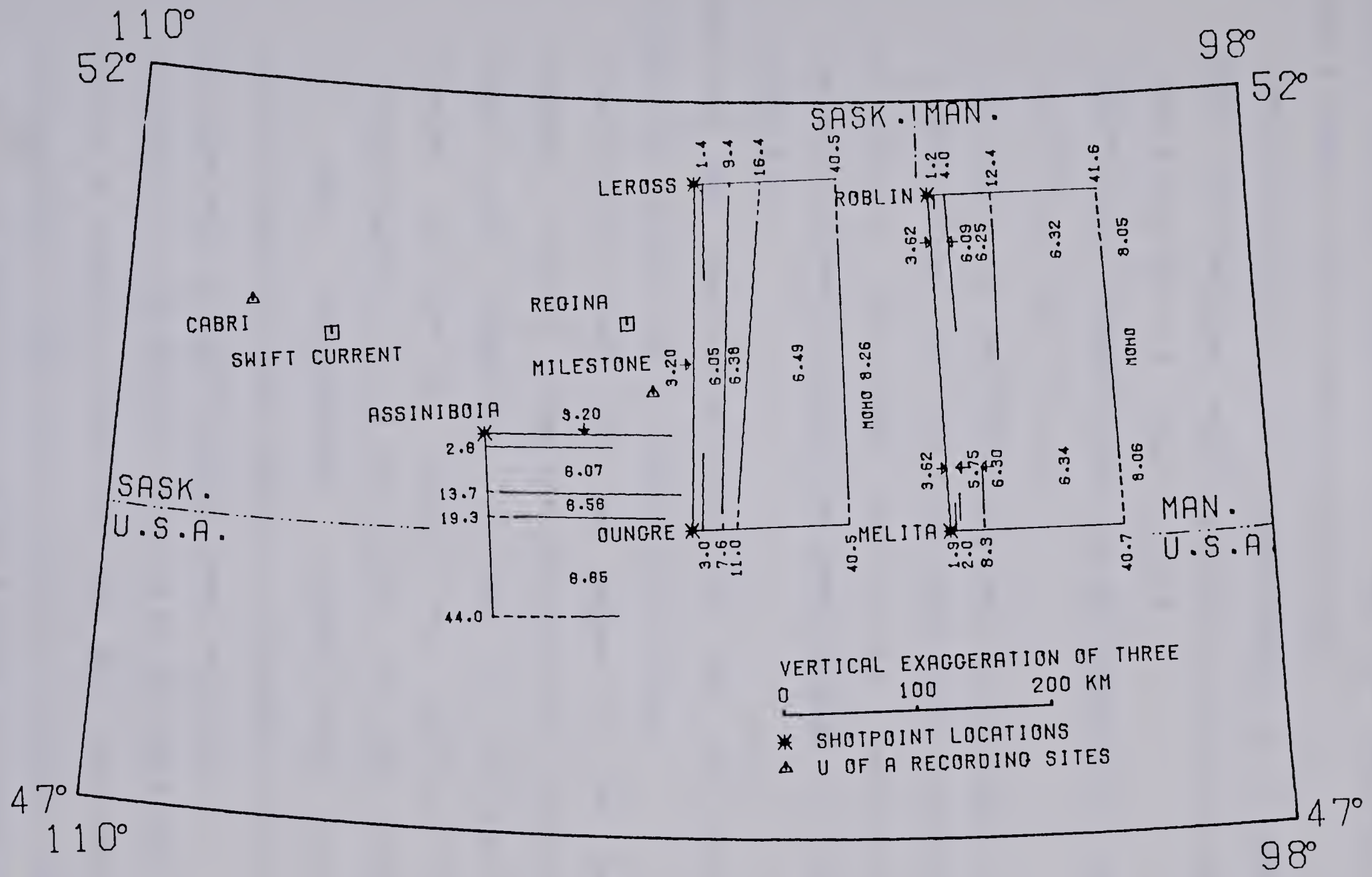
110°
52°
98°
52°
SASK. | MAN.
LEROSS
ROBLIN
1.4
9.4
16.4
40.5
1.2
4.0
12.4
41.6
3.62
6.09
6.25
6.32
8.05
REGINA
CABRI
SWIFT CURRENT
MILESTONE
3.20
6.05
6.38
6.49
MOHO 8.26
MOHO
ASSINIBOIA
3.20
2.8
6.07
13.7
6.58
19.3
8.85
44.0
SASK.
U.S.A.
OUNGRE
MELITA
3.0
7.6
11.0
40.5
1.9
2.0
8.3
40.7
3.62
5.75
6.30
6.34
8.06
MAN.
U.S.A
VERTICAL EXAGGERATION OF THREE
0
100
200 KM
SHOTPOINT LOCATIONS
U OF A RECORDING SITES
47°
110°
47°
98°

The data from these three profiles were analysed by Hajnal (personal communication) and the derived crustal models lead to the following conclusions.

1. There are no significant changes both in a depth to *Moho* and the upper mantle velocity within the boundary zone along the N.S. line (Fig.3.5).
2. *Alberta-Riel discontinuity* was not observed on any of the 1979 profiles (Fig.3.5).
3. The depth to the *Moho* along the Leross/Oungre profile is surprisingly low (40.5 km) and remains constant. The velocity of the upper mantle has a relatively high value (8.26 km/s) indicating some changes in lithology (Fig.3.5).

Comparing the results of the 1977 and 1979 refraction surveys one reaches the following conclusions.

1. The crustal model for the region to the west of Weyburn, derived from the Assiniboia/Carlyle profile, shows some resemblance to that for Suffield/Swift Current obtained by Chandra and Cumming (1972), as illustrated in Fig.1.8 and Fig.3.5. The only difference is that *Alberta-Riel discontinuity* of the Suffield/Swift Current model is replaced by a shallower horizon with a significantly lower velocity.
2. The depth to the *Moho* of 48.3 km at the west end of the 1977 E.W. profile (Fig.1.8) and 40.5 km along the Leross/Oungre 1979 profile (Fig.3.5) indicate that the vertical change is of at least 8 km over a distance of

110 km. The change in depth is accompanied by a substantial change in values of the upper mantle velocity (8.06 km/s versus 8.26 km/s). Since the data do not preclude of an abrupt change, a major crustal division might be responsible for the observed phenomena.

3. The crustal thickness in southern Saskatchewan varies from 40 to over 50 km, whereas the thickness in Manitoba is between 30 and 42 km.

The existance of a major crustal division or a fault has support from magnetic data in this area (Green *et al.*, 1979) as well as from Bouguer gravity anomaly map (Fig.4.2). Its possible location which can be traced on the magnetic map is within the range of distances which mark that abrupt change in depth to the *Moho* (the fault, as delineated by Green *et al.* (1977), cuts the 1977 and 1979 E.W. profiles about 95 km E. of Weyburn, whereas the depth to the *Moho* is 48.3 km at 110 km E. of Weyburn and 40.5 km below Weyburn).

3.7.3 Travel time analysis of data from 1979 U of A survey

Although not too much detail can be extracted from an analysis of record sections with data points coming from so widely separated points, nevertheless it is instructive to plot records on a travel time curves to obtain some approximate values characteristic of the crust in those areas. Fig.3.6A shows the record sections of the Roblin/Milestone and Leross/Cabri events (northern region),

Fig.3.6.A-B Record sections of
a) the northern profiles (Roblin/Milestone and Leross/Cabri)
b) the southern profiles (Assiniboia/Cabri, Oungre/Cabri and Melita/Milestone)
Crosses show the picks of first breakes (based on unfiltered records). Maximum amplitudes on each record have been normalized to a common value. Reduction velocity on time axis is 8 km/s.

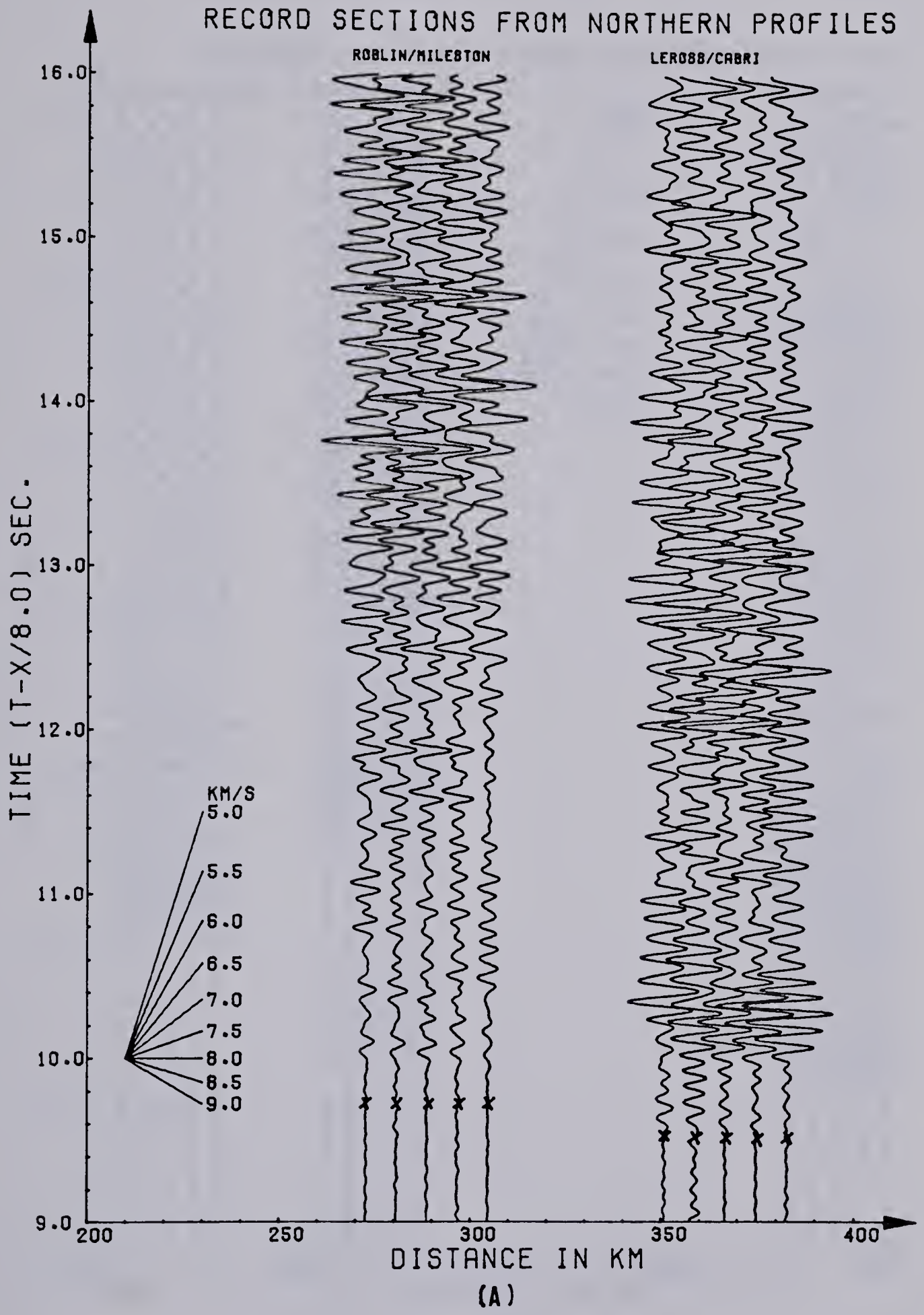
RECORD SECTIONS FROM NORTHERN PROFILES
ROBLIN/MILESTON
LEROSS/CABRI
TIME (T-X/8.0) SEC.
16.0
15.0
14.0
13.0
12.0
11.0
10.0
9.0
KM/S
5.0
5.5
6.0
6.5
7.0
7.5
8.0
8.5
9.0
200
250
300
350
400
DISTANCE IN KM

(A)

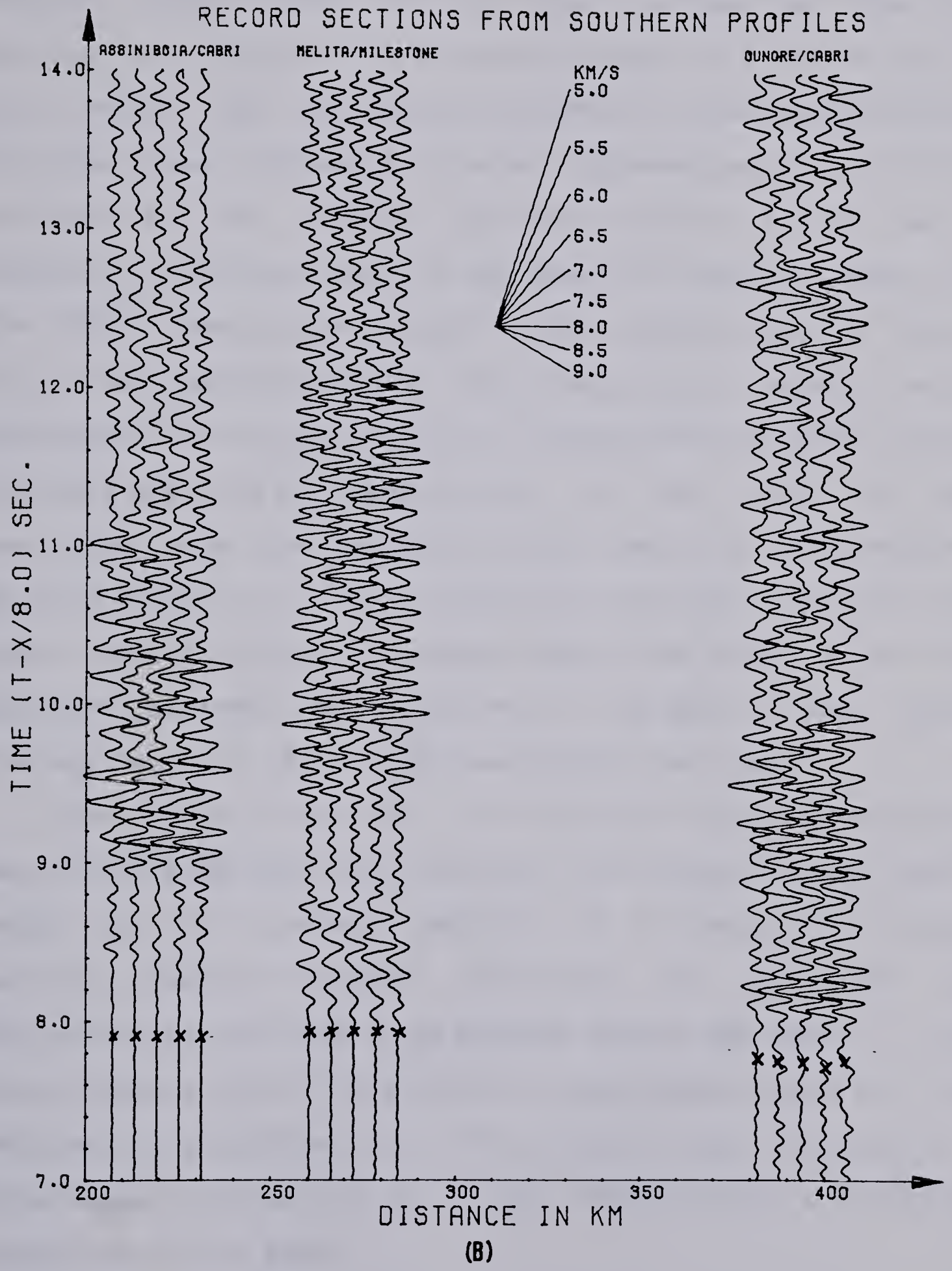
RECORD SECTIONS FROM SOUTHERN PROFILES
ASSINIBOIA/CABRI
MELITA/MILESTONE
KM/S
5.0
5.5
6.0
6.5
7.0
7.5
8.0
8.5
9.0
OUNORE/CABRI
TIME (T-X/8.0) SEC.
14.0
13.0
12.0
11.0
10.0
9.0
8.0
7.0
200
250
300
350
400
DISTANCE IN KM

(B)

whereas Fig.3.6B presents the record section of the Assiniboia/Cabri, Oungre/Cabri and Melita/Milestone events (southern region). The most striking feature is that the reduced travel times of the first arrival of the two northern profiles are significantly larger (1.5 to 1.8 sec.) than those from the southern profiles. Assuming that this resulted from different crustal thicknesses, the first arrivals of the northern section yield 8.1 Km/s as a velocity of the upper-mantle and about 53.3 Km as a depth to the *Moho*. These values found for the southern section (here only the Assiniboia/Cabri and Oungre/Cabri events were considered for reasons which will become obvious later) were 8.0 Km/s and 41.9 Km, respectively. In the light of the available data the velocity of 8.1 Km/s for the northern section appears to be very close to an average value of the upper mantle velocity between Roblin and Cabri. As to the southern section, the velocity is slightly lower than average (about 8.18 Km/s) between Oungre and Capri.

The depth values to the refractor for both sections were calculated from the intercept time using a single layer model with an average velocity of 6.4 Km/s. It is very unlikely that a crustal thickness of 53.3 Km is characteristic of large area between Roblin and Cabri. It is more probable that it indicates an approximate depth to the *Moho* on the downthrown block of a crustal fault (or faults). This supports Green's *et al*. (1979) assumption of a northern extension of the fault.

This fault could also be responsible for the Oungre/Cabri delay in the first arrival time if it changes its direction to the west instead of running to the north as assumed by Green *et al.* (1979). There is however no support for such a hypothesis when analysing the northern part of the Leross/Oungre crustal model (Hajnal, 1980) which does not show any disrupted interfaces. It is more likely that we have another major crustal fault which cuts the Leross/Cabri profile. Since the area is cut by a number of linear features trending N.W.-S.E. (Burwash and Culbert, 1976) the fault may be coincidental with one of them. Especially, an observed gravity trend at a longitude of about 105°W may be related to the fault.

The model depth to the *Moho* refractor of 41.9 km for the southern region using the intercept time seems to be a good approximation of an averaged undisturbed crustal thickness between Oungre and Cabri.

3.7.4 Computed models

Another approach to the problem is computing models which yield travel times comparable to those recorded for all events. Assuming an initial model from available data we try to fit the computed travel time to observed one by adjusting the values of a few parameters (depth, velocity) which are most likely subject to change as compared with those of the initial model. A number of models for each profile have been computed using as initial models the

closest quoted in literature, or combination of them. Table 3A-E shows the assumed initial models for each profile as well as computed ones which fit the observed travel time.

Another useful parameter which has been calculated is the critical distance for a given crustal model and refractor. It is defined here as a half of the offset at which the reflection travel time equals the refraction travel time. In case of possible crustal features which affect the travel time the critical distance allows one to narrow the range within which such a feature can occur. The values of critical distances of each model are also shown in Table 3A-E.

The computed models for the Roblin/Milestone and Leross/Cabri profiles also clearly indicate a substantial increase in the depth to the *Moho*. By keeping all parameters but the depth to *Moho* identical as in the initial model, the fit of both recorded and calculated travel times for the Roblin/Milestone event is obtained when a depth to *Moho* of 50.0 km (Table 3A). The cricical distances corresponding to this model on shotpoint and receiver sides are 62 and 63 km. It is worth noting at this point that the possible location of the crustal fault, as delineated by Green *et al*. (1979), falls within the range of the two critical distances for the Roblin/Milestone event. For the Leross/Cabri event the calculated depth to the *Moho* is 52 km, whereas the critical distances on shotpoint and receiver sides are 66 and 75 km (Table 3B).

Table 3A-E Initial and computed crustal models and their parameters. Velocities are those of compressional wave in layer. Initial crustal models below shotpoint and receiver were constructed using available data. Remaining computed models were constructed to fit observed travel times. This was done by changing one parameter (either velocity in layer or depth to refractor) of initial model. Computed critical distances ara also shown for all models.

(A) ROBLIN MILESTONE

DISTANCE (X)	272.6	KM
OBSERVED FULL TRAVEL TIME (T)	43.82	SEC.
REDUCED TRAVEL TIME (T"=T-X/8.0)	9.75	SEC.

INITIAL MODEL FROM LITERATURE AND AVAILABLE DATA

LAYER	ROBLIN DEPTH KM	ROBLIN VELOCITY KM/S	MILESTONE DEPTH KM	MILESTONE VELOCITY KM/S
1	1.2	3.62	1.2	3.20
2	4.0	6.09	10.0	6.06
3	12.4	6.25	15.0	6.47
4	41.6	6.32	44.0	6.57
HALFSPACE		8.05		8.20

CRITICAL DISTANCES (MOHO):

ROBLIN	51.2 KM
MILESTONE	54.6 KM

INITIAL MODEL TRAVEL TIME 42.6 SEC.

COMPUTED CRUSTAL MODEL WITH CHANGED DEPTH TO MOHO

LAYER	ROBLIN DEPTH KM	ROBLIN VELOCITY KM/S	MILESTONE DEPTH KM	MILESTONE VELOCITY KM/S
1	1.2	3.62	1.2	3.20
2	4.0	6.09	10.0	6.06
3	12.4	6.25	15.0	6.47
4	50.0	6.32	50.0	6.57
HALFSPACE		8.05		8.20

CRITICAL DISTANCES (MOHO):

ROBLIN	61.9 KM
MILESTONE	62.6 KM

COMPUTED TRAVEL TIME 43.9 SEC.

COMPUTED CRUSTAL MODEL WITH LOW VELOCITY LAYER

LAYER	ROBLIN DEPTH KM	ROBLIN VELOCITY KM/S	MILESTONE DEPTH KM	MILESTONE VELOCITY KM/S
1	1.2	3.62	1.2	3.20
2	4.0	6.09	10.0	6.06
3	12.4	6.25	15.0	6.47
4	41.6	5.90	44.0	5.90
HALFSPACE		8.05		8.20

CRITICAL DISTANCES (MOHO):

ROBLIN	45.5 KM
MILESTONE	45.8 KM

COMPUTED TRAVEL TIME 43.8 SEC.

(B) LEROSS CABRI

DISTANCE (X)	350.7	KM
OBSERVED FULL TRAVEL TIME (T)	53.40	SEC.
REDUCED TRAVEL TIME (T'=T-X/8.0)	9.57	SEC.

INITIAL MODEL FROM LITERATURE AND AVAILABLE DATA

LAYER	LEROSS DEPTH KM	LEROSS VELOCITY KM/S	CABRI DEPTH KM	CABRI VELOCITY KM/S
1	1.4	3.20	1.4	3.20
2	9.4	6.05	11.0	6.12
3	16.4	6.38	36.0	6.50
4	40.5	6.49	45.0	7.17
HALFSPACE		8.26		8.10

CRITICAL DISTANCES (MOHO):

LEROSS	48.3 KM
CABRI	62.0 KM

INITIAL MODEL TRAVEL TIME 51.3 SEC.

COMPUTED CRUSTAL MODEL WITH CHANGED DEPTH TO MOHO

LAYER	LEROSS DEPTH KM	LEROSS VELOCITY KM/S	CABRI DEPTH KM	CABRI VELOCITY KM/S
1	1.4	3.20	1.4	3.20
2	9.4	6.05	11.0	6.12
3	16.4	6.38	36.0	6.50
4	52.0	6.49	52.0	7.17
HALFSPACE		8.26		8.10

CRITICAL DISTANCES (MOHO):

LEROSS	64.9 KM
CABRI	78.2 KM

COMPUTED TRAVEL TIME 53.4 SEC.

COMPUTED CRUSTAL MODEL WITH LOW VELOCITY LAYER

LAYER	LEROSS DEPTH KM	LEROSS VELOCITY KM/S	CABRI DEPTH KM	CABRI VELOCITY KM/S
1	1.4	3.20	1.4	3.20
2	9.4	6.05	11.0	6.12
3	16.4	6.38	36.0	5.80
4	40.5	5.80	45.0	5.80
HALFSPACE		8.26		8.10

CRITICAL DISTANCES (MOHO):

LEROSS	41.5 KM
CABRI	46.1 KM

COMPUTED TRAVEL TIME 53.5 SEC.

(C) ASSINIBOIA CABRI

DISTANCE (X)	207.2	KM
OBSERVED FULL TRAVEL TIME (T)	33.81	SEC.
REDUCED TRAVEL TIME (T'=T-X/8.0)	7.92	SEC.

INITIAL MODEL FROM LITERATURE AND AVAILABLE DATA

	ASSINIBOIA		CABRI	
LAYER	DEPTH KM	VELOCITY KM/S	DEPTH KM	VELOCITY KM/S
1	2.6	3.20	2.6	3.20
2	13.7	6.07	11.0	6.12
3	19.3	6.56	36.0	6.50
4	44.0	6.65	45.0	7.17
HALFSPACE		8.18		8.10

CRITICAL DISTANCES (MOHO):

ASSINIBOIA	55.4 KM
CABRI	62.0 KM

INITIAL MODEL TRAVEL TIME 34.5 SEC.

COMPUTED CRUSTAL MODEL WITH CHANGED DEPTH TO MOHO

	ASSINIBOIA		CABRI	
LAYER	DEPTH KM	VELOCITY KM/S	DEPTH KM	VELOCITY KM/S
1	2.6	3.20	2.6	3.20
2	13.7	6.07	11.0	6.12
3	19.3	6.56	36.0	6.50
4	40.0	6.65	40.0	7.17
HALFSPACE		8.18		8.10

CRITICAL DISTANCES (MOHO):

ASSINIBOIA	49.8 KM
CABRI	52.5 KM

COMPUTED TRAVEL TIME 33.9 SEC.

COMPUTED CRUSTAL MODEL WITH HIGH VELOCITY LAYER

	ASSINIBOIA		CABRI	
LAYER	DEPTH KM	VELOCITY KM/S	DEPTH KM	VELOCITY KM/S
1	2.6	3.20	2.6	3.20
2	13.7	6.07	11.0	6.12
3	19.3	6.56	36.0	6.50
4	44.0	6.65	45.0	7.17
5	44.5	8.18	45.5	8.10
HALFSPACE		8.70		8.70

CRITICAL DISTANCES (MOHO):

ASSINIBOIA	48.9 KM
CABRI	52.2 KM

COMPUTED TRAVEL TIME 33.8 SEC.

(D) OUNGRE CABRI

DISTANCE (X)	381.7	KM
OBSERVED FULL TRAVEL TIME (T)	55.53	SEC.
REDUCED TRAVEL TIME (T'=T-X/8.0)	7.82	SEC.

INITIAL MODEL FROM
LITERATURE AND AVAILABLE DATA

LAYER	OUNGRE DEPTH KM	OUNGRE VELOCITY KM/S	CABRI DEPTH KM	CABRI VELOCITY KM/S
1	3.0	3.20	3.0	3.20
2	7.6	6.05	11.0	6.12
3	11.0	6.38	36.0	6.50
4	40.5	6.49	45.0	7.17
HALFSPACE		8.26		8.10

CRITICAL DISTANCES (MOHO):

OUNGRE	47.8 KM
CABRI	62.0 KM

INITIAL MODEL TRAVEL TIME 55.6 SEC.

(E) MELITA MILESTONE

DISTANCE (X)	260.3	KM
OBSERVED FULL TRAVEL TIME (T)	40.52	SEC.
REDUCED TRAVEL TIME (T"=T-X/8.0)	7.97	SEC.

INITIAL MODEL FROM LITERATURE AND AVAILABLE DATA

LAYER	MELITA DEPTH KM	MELITA VELOCITY KM/S	MILESTONE DEPTH KM	MILESTONE VELOCITY KM/S
1	1.9	3.62	1.9	3.20
2	2.0	5.75	10.0	6.06
3	8.3	6.30	15.0	6.47
4	40.7	6.34	44.0	6.57
HALFSPACE		8.06		8.20

CRITICAL DISTANCES (MOHO):

MELITA	50.2 KM
MILESTONE	54.6 KM

INITIAL MODEL TRAVEL TIME 40.9 SEC.

COMPUTED CRUSTAL MODEL WITH CHANGED DEPTH TO MOHO

LAYER	MELITA DEPTH KM	MELITA VELOCITY KM/S	MILESTONE DEPTH KM	MILESTONE VELOCITY KM/S
1	1.9	3.62	1.9	3.20
2	2.0	5.75	10.0	6.06
3	8.3	6.30	15.0	6.47
4	40.0	6.34	40.0	6.57
HALFSPACE		8.06		8.20

CRITICAL DISTANCES (MOHO):

MELITA	49.4 KM
MILESTONE	49.2 KM

COMPUTED TRAVEL TIME 40.5 SEC.

COMPUTED CRUSTAL MODEL WITH HIGH VELOCITY LAYER

LAYER	MELITA DEPTH KM	MELITA VELOCITY KM/S	MILESTONE DEPTH KM	MILESTONE VELOCITY KM/S
1	1.9	3.62	1.9	3.20
2	2.0	5.75	10.0	6.06
3	8.3	6.30	15.0	6.47
4	40.7	6.60	44.0	6.60
HALFSPACE		8.06		8.20

CRITICAL DISTANCES (MOHO):

MELITA	55.2 KM
MILESTONE	55.1 KM

COMPUTED TRAVEL TIME 40.6 SEC.

Another possible reason for such large differences in reduced travel times between the northern and southern sections might be the existance of a low velocity layer occupying the substantial portion of the crust in the northern area. However, the computed models with a low velocity layer both for the Roblin/Milestone and Oungre/Cabri profiles (Table 3A and Table 3B) clearly illustrate that such an approach is wrong. The required adjustments in the velocity of such a layer are simply too large. (a layer as thick as 29 and 33 km for the Roblin/Milestone and Oungre/Cabri profiles respectively should be introduced with velocities as low as 5.90 and 5.80 km/s to fit observed travel times).

The initial model travel time for the Assiniboia/Cabri profile turned out to be about 0.6 sec. greater than observed (Table 3C). This was rather surprising since the available data indicate rather an undisturbed and monotonous crustal structure in this region. The initial model of the Assiniboia/Cabri profile can be modified either by raising the *Moho discontinuity* to 40 km or by introducing an upper-mantle refractor with a velocity of 8.70 km/s (Table 3C). The latter case, however, represents a very improbable mantle velocity. Furthermore, the apparent velocity of the first arrivals across a recording line for the Assiniboia/Cabri event is definately lower than 8.70 km/s.

As to the Oungre/Cabri profile, the initial model travel time is in a good agreement with observations (Table

3D). This could suggest the validity of the initial model which postulates a gradual increase in the depth to *Moho* from about 40.5 km below Oungre to 45 km below Cabri.

At this point it is interesting to speculate about the causes of so low a computed depth to the *Moho* for the Assiniboia/Cabri profile which, moreover, lies in close proximity to the part of the Oungre/Cabri profile characterized by a much thicker crust. One possible answer to this might be the existance in that area of a buried Precambrian rift which was traced by Kanasewich *et al.* (1969) up to the Alberta and Saskatchewan border. If we assume its further continuation to the east, it could be responsible for these discrepencies.

The Melita/Milestone event is much more complex and difficult to analyse than the previous events. At first glance the reduced travel time of the first arrival for the Melita/Milestone event, which is within milliseconds identical to those for the Oungre/Cabri and Assiniboia/Cabri events, is difficult to reconcile with the hypothesis of a crustal fault in that area. If the fault were present we should expect the reduced travel time to be of the order of that for the Roblin/Milestone profile. Among reasons which could explain the observed value of the first arrival time for the Melita/Milestone event are:

1. Termination of the fault, or the change of its direction to the S.E., before crossing the Melita/Milestone raypath. If so, only small corrections

are required (either to raise the *Moho* about 1 km or to increase the velocity of the lower layer to about 6.60 km/s) to obtain a good agreement between computed and observed travel times (Table 3E). There are however strong arguments against this hypothesis. The Melita/Milestone profile passes through the area of the 1977 and 1979 surveys which results set some crustal parameters which should be included in any attempted crustal model of that region. In the case of the Melita/Milestone profile, as seen from Fig.1.8 and Fig.3.5, the crustal thickness gradually increases to at least 48 km over the distance 90-120 km, next sharply decreases to about 40.5 km (or lower) and finally tends to increase again to about 44 km below Milestone. Besides, the strongest support from the magnetic data for a fault comes for its southern portion (Fig.1.7).

2. The first arrival of the Melita/Milestone event does not come entirely from the *Moho* (see Fig.3.7). A relatively short distance from Melita to the possible fault and particular crustal conditions cause the waves to travel along a path marked 1 in Fig.3.7 with travel time less than that along path marked 2. This hypothesis assumes that:

   a. The *Alberta-Riel discontinuity* exists along profile (or at least between Melita and the fault) and is located very shallow near the shotpoint and very

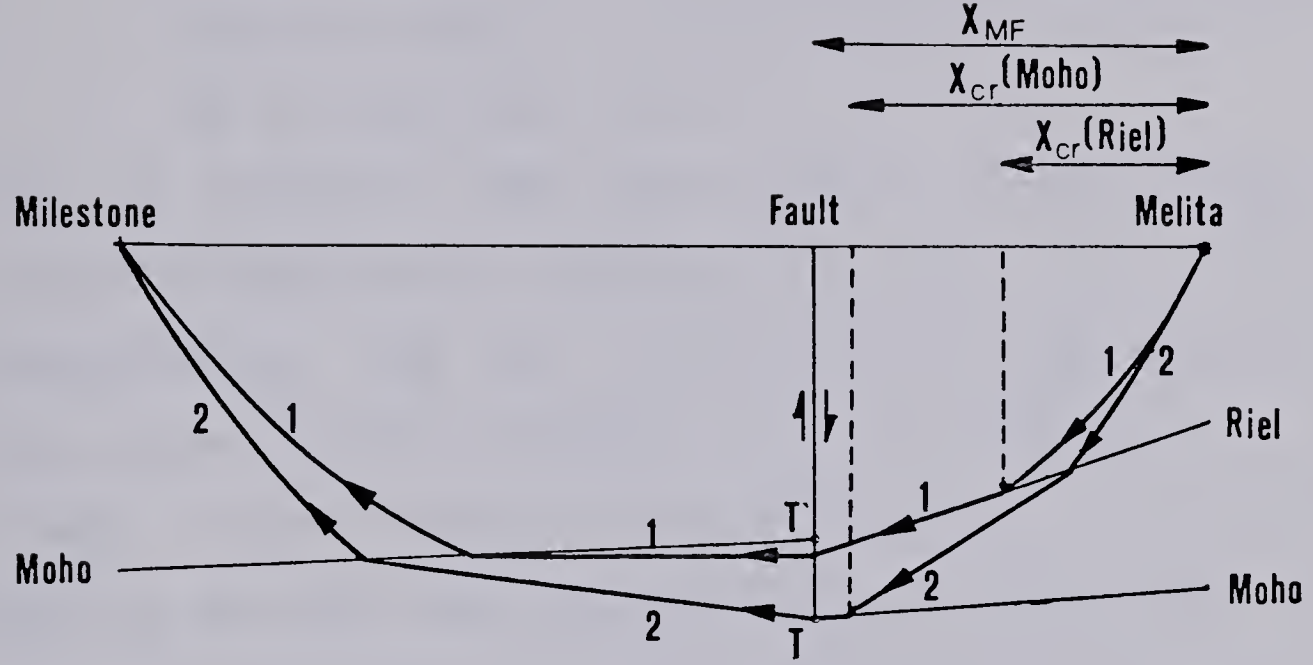

Fig.3.7 Possible raypaths between Melita and Milestone which could be responsible for the first break. The path denoted no.1 runs in some portion along *Riel discontinuity* where headwave is generated, while headwave in the path no.2 is generated along *Moho discontinuity*.

X_{cr} (Riel) - critical distance corresponding to given model with *Riel discontinuity* as refractor.

X_{cr}(Moho) - critical distance corresponding to given model with *Moho discontinuity* as refractor.

TT' - throw of the fault for *Moho discontinuity*

deep at the fault on its downthrown block (Fig.3.7).

b. The throw of the fault is such that the downthrown depth to the *Riel* is greater than the upthrown depth to the *Moho* (Fig.3.7), so that the travel time to the receiver is practically the same for various sources located along fault below the *Moho* on its upthrown block.

Table 4 presents some Melita/fault crustal models which clearly illustrate the possibility that it is the *Riel discontinuity*, not the *Moho*, which is responsible for the first arrival. With parameters set as in model no.1 in Table 4 both travel times are practically equal. By lowering the depth to the *Riel* and raising the depth to the *Moho* at their critical distances, the travel time along path 1 in Fig.3.7 becomes shorter than that along path 2. This difference increases even more with decreasing distance to the fault (model no.2 in Table 4). This hypothesis is supported additionally by the fact that records from the Melita/Milestone events exhibit a very characteristic pattern (Fig.3.8). After the first arrival (about 8.0 sec. on the reduced time scale) with a moderate amplitude there is a relatively quiet period and the next strong arrivals appear at about 9.4 sec. mark as in the Roblin/Milestone first arrival time (9.75 sec.) which definately came from *Moho*. Moreover, the apparent velocity of the first arrival across the recording line for the Melita/Milestone events is

Table 4. Crustal models for the Melita/fault profile and their computed travel times.

MELITA FAULT MODEL
DISTANCE 110 KM

LAYER	MELITA DEPTH KM	MELITA VELOCITY KM/S	FAULT DEPTH KM	FAULT VELOCITY KM/S
1	1.5	3.43	1.5	3.43
2	3.0	6.06	3.0	6.06
3	12.0	6.27	12.0	6.27
4	30.0	6.58	41.5	6.58
5	45.0	7.11	48.3	7.11
HALFSPACE		8.06		8.06

CRITICAL DISTANCE (RIEL): 64.1 KM
CRITICAL DISTANCE (MOHO): 67.1 KM

COMPUTED TRAVEL TIME (RIEL) 17.7 SEC.
COMPUTED TRAVEL TIME (MOHO) 17.7 SEC.

MELITA FAULT MODEL
DISTANCE 90 KM

LAYER	MELITA DEPTH KM	MELITA VELOCITY KM/S	FAULT DEPTH KM	FAULT VELOCITY KM/S
1	1.5	3.43	1.5	3.43
2	3.0	6.06	3.0	6.06
3	12.0	6.27	12.0	6.27
4	25.0	6.58	41.5	6.58
5	51.0	7.11	51.0	7.11
HALFSPACE		8.06		8.06

CRITICAL DISTANCE (RIEL): 51.9 KM
CRITICAL DISTANCE (MOHO): 80.6 KM

COMPUTED TRAVEL TIME (RIEL) 15.1 SEC.
COMPUTED TRAVEL TIME (MOHO) 15.5 SEC.

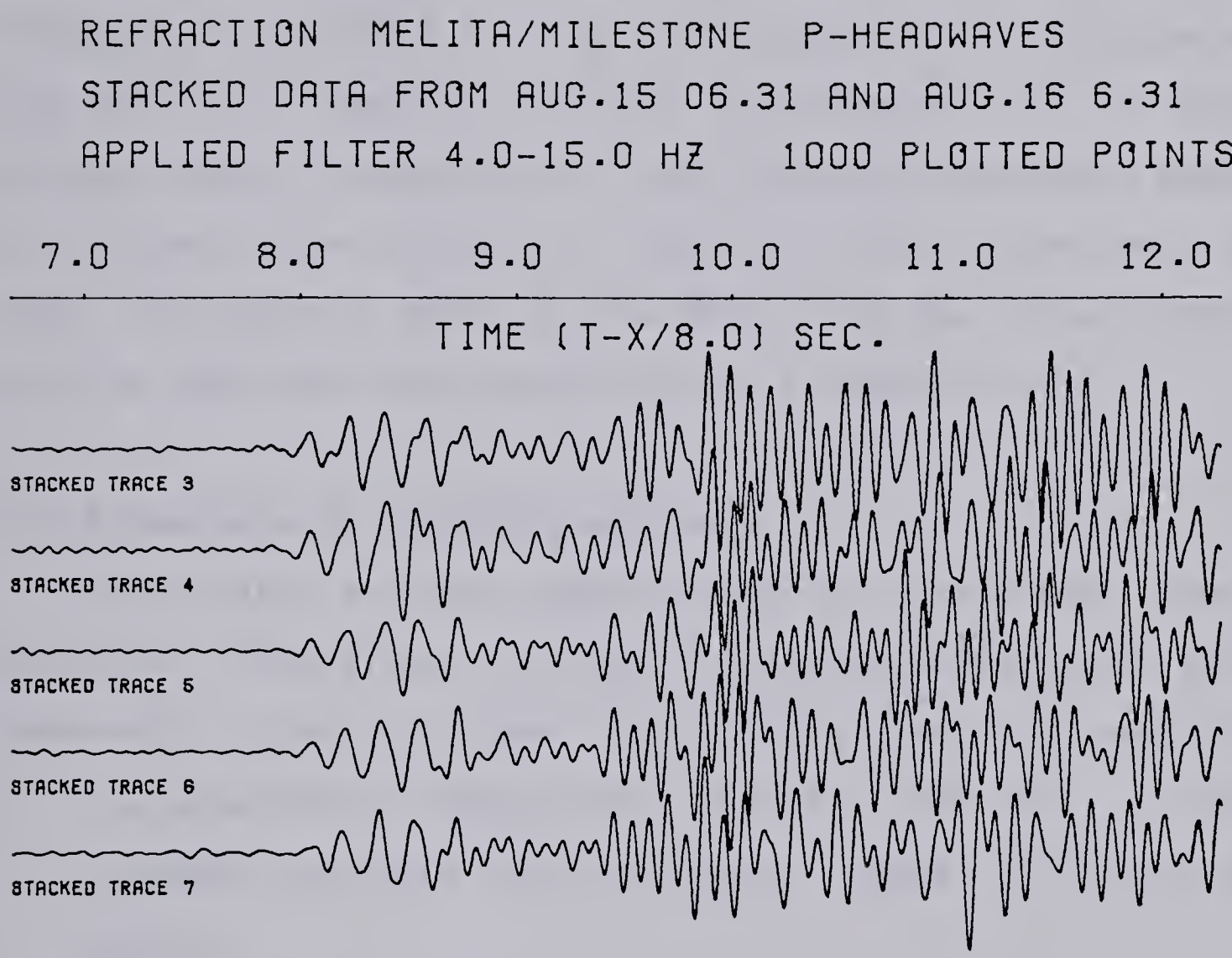

Fig.3.10 Stacked records for Melita/Milestone profile

less than 8.0 km/s.

The hypothesis presented here requires the presence of a *Riel discontinuity* within the crust between Melita and Milestone (or at least between Melita and the fault). Although both 1979 N.S. profiles do not show its existance, the 1977 E.W. profile confirms the presence of a well defined *Riel discontinuity* (Fig.1.8) which reaches a depth of 41.3 km in the vicinity of the fault. This value compared with 40.5 km as a depth to the *Moho* along the Leross/Oungre profile indicates the possibility of assumption no.2.

3.7.5 Analysis of secondary arrivals

Many later arrivals, which could be converted waves, multiple reflections or even reflected refractions, were observed. To identify them the following steps were adopted:

1. Calculation of theoretical arrival time for various assumed horizons and different types of converted waves.
2. Horizontal versus vertical ground motion was analysed to give an indication of the type of wave involved in any particular arrival.
3. Analysis of the apparent velocity of the seismic pulse across the recording line.
4. Analysis of travel time curves of later arrivals and their correlation.

The use of a line of 10 vertical seismometers along with 2 horizontal seismometers was found useful. It allowed for the

analysis of the ground motion and the apparent velocity of the seismic pulse. However, the best criterion for identification of later arrivals i.e. their apparent velocity along a profile, could not be applied. The recording line used in the survey was simply too short to yield more than one point on a traveltime versus distance curve. Consequently, only the PSP-phase (S-head waves along the *Moho discontinuity* was successfully identified. The phases yielded travel times which show a similar pattern to that for the first arrivals i.e. the reduced travel times for the northern section were greater than that for the southern section.

4. CONCLUSIONS

The results from the seismic surveys carried out in southern Saskatchewan and S.W. Manitoba have revealed a surprisingly complex structure in the crust. The crustal models derived often show a lack of uniformity when their correlation is attempted. Major conclusions inferred from analysis of available data include the following.

1. The crustal thickness in southern Saskatchewan varies from 40 to over 50 km, whereas the thickness in Manitoba is between 30 and 42 km. There is evidence for block faulting in southern Saskatchewan with a N.-S. trend in the east. There is good evidence for a major North-South fault at a longitude of about 103°W with the throw of at least 8-10 km at the *Moho discontinuity* (Fig.4.1). The trend is determined from magnetic maps. Bouguer gravity data supports this conclusion and indicates that Regina and Weyburn are situated on the upthrown block (Fig.4.2). This zone is also marked by a change in values of the upper mantle velocity from less than 8.1 km/s on the Yorkton-Melville downthrown block to 8.26 km/s on the reversed refraction line on the Regina-Weyburn upthrown block. The existance of another fault west of Regina at a longitude of about 105° is supported by our refraction data and the Bouguer gravity anomalies (Fig.4.1 and Fig.4.2).
2. Apart from the Regina-Weyburn upthrown block there is no evidence for an upper mantle compressional velocity

Fig.4.1 Crustal thickness and major crustal features in S.W. Manitoba, southern Saskatchewan and S.E. Alberta. The thick solid lines show profiles with known depth to the *Moho discontinuity* determined by previous seismic studies, whereas the thin solid lines show the 1979 University of Alberta profiles. Crustal thickness values in parenthesis were determined from this study.

MH - Medicine Hat
LE - Lethbridge
SC - Swift Current
WE - Weyburn
YO - Yorkton
ME - Melville

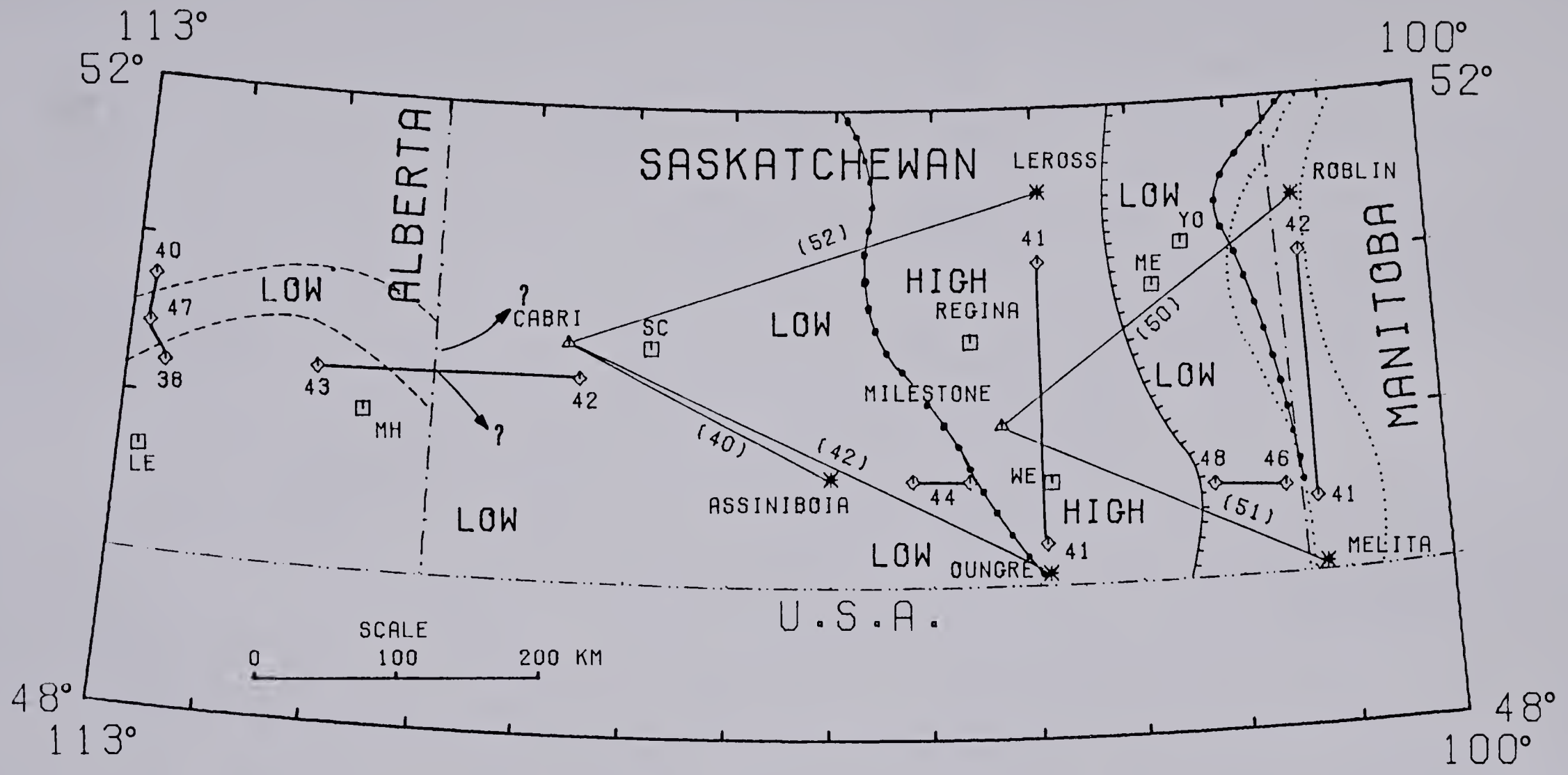

- ✱ REFRACTION SHOTPOINTS
- ⏃ U OF A RECORDING SITES
- ◈ LOCATIONS WITH KNOWN DEPTH TO MOHO
- ( ) DEPTH TO MOHO DETERMINED FROM THIS STUDY

- SUPERIOR CHURCHILL BOUNDARY ZONE
- POSSIBLE MAJOR CRUSTAL FAULT
- PRECAMBRIAN RIFT
- GRAVITY TRENDS
  LOW AND HIGH REFER TO BOUGUER GRAVITY ANOMALY

Fig.4.2 Bouguer gravity anomaly map of southern Saskatchewan, S.W. Manitoba and S.E. Alberta (after Lee, 1977)

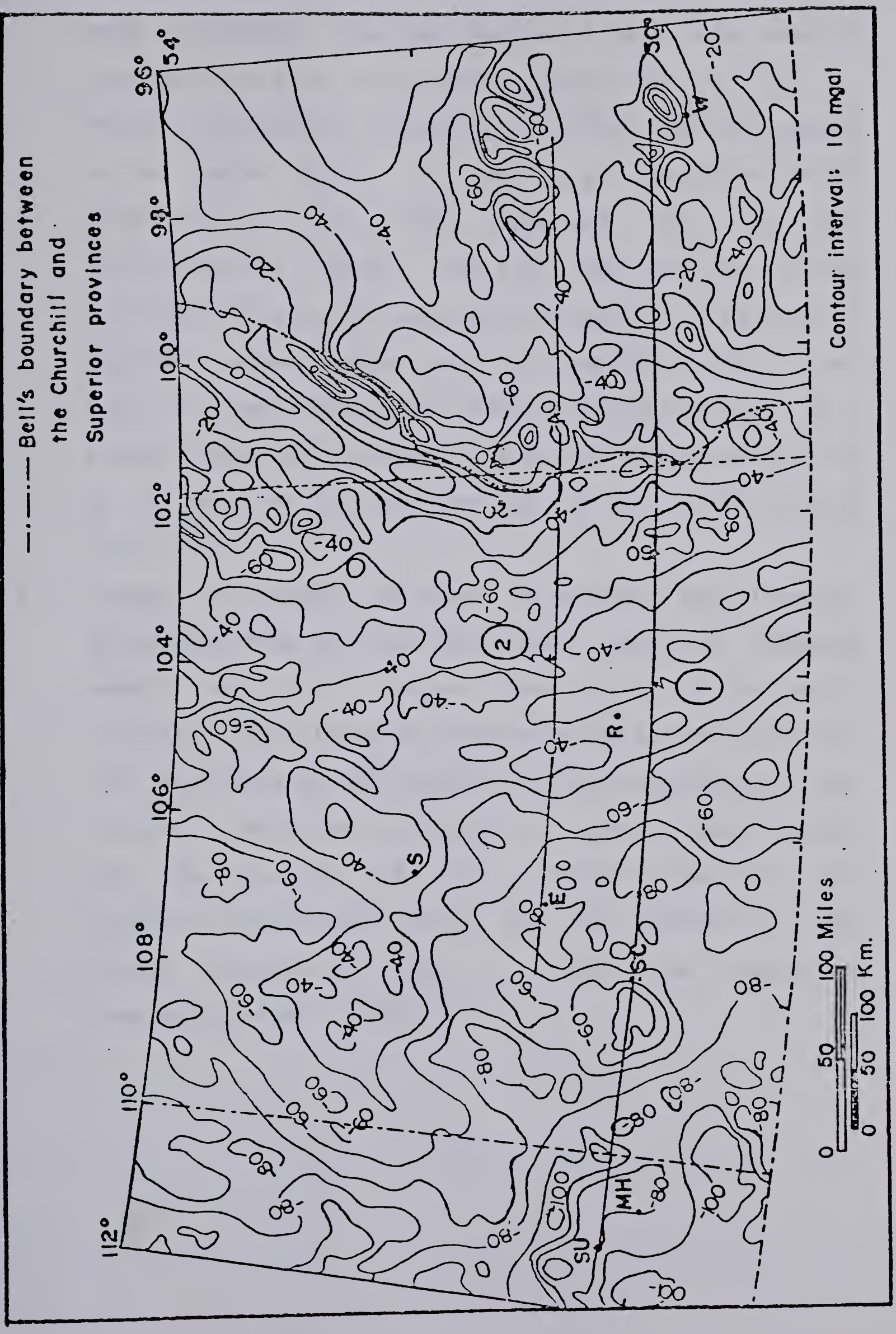
—·—·— Bell's boundary between the Churchill and Superior provinces
Contour interval: 10 mgal
0 50 100 Miles
0 50 100 Km.
96°
98°
100°
102°
104°
106°
108°
110°
112°
54°
52°
50°
R.
S.
E.
SU
MH
C100
1
2

much different from an assumed 8 km/s value used on reduced time axis in the seismic profiles.

3. Not all mid-crustal discontinuities can be correlated on a larger scale. In particular, the *Alberta-Riel discontinuity* has been observed only on the Suffield-Swift Current and E.W. 1977 profiles. It was not identified on the remaining reversed profiles in southern Saskatchewan and S.W. Manitoba (Fig.1.8 and Fig.3.5). The *Alberta-Riel discontinuity* may exist as a steeply deeping horizon on the Melita/Milestone profile or at least for its portion up to the 103°W fault (Fig.3.7).

4. Changes in crustal thickness in southern Saskatchewan, as deduced from the observed travel times and computed models, are more complex than earlier studies would indicate. The pattern of changes could be attributed to the existance of the boundary between the Superior and Churchill geological provinces in eastern Saskatchewan and the complex N.E.-S.W. trends in western and northern Saskatchewan which may be related to the buried Precambrian rift in Alberta as traced by Kanasewich *et al*. (1969).

BIBLIOGRAPHY

Allsopp, D.F., M.D.Burke, and G.L.Cumming, A digital seismic recording system, Bull. Seism. Soc. Amer., 62, 6, pp.1641-1647, 1972.

Bell, C.K., Geol. Surv. Canada Paper 66-1, p.133, 1966.

Bell, C.K., Geological Association of Canada Special Paper No. 9, p.9, 1971.

Berry, M.J., and K.Fuchs, Crustal structure of the Superior and Grenville provinces of the northeastern Canadian Shield, Bull. Seism. Soc. Amer., 63, pp.1393-1432, 1973.

Berry, M.J., Structure of the crust and upper mantle in Canada, Tectonophysic, 20, pp.183-201, 1973.

Berry, M.J., and J.A.Mair, The nature of the earth's crust in Canada, in *The Earth's Crust*, edited by J.G.Heacock, AGU, Washington, D.C., 1977.

Braile, L.W., R.B.Smith, G.R.Keller, R.M.Welch, and R.P.Meyer, Crustal structure across the Wasatch front from detailed seismic refraction studies, J. Geoph. Res., 79, pp.2669-2677, 1974.

Burkhard H., B.Buttkus, F.Keller, and R.Vees, Seismic long distance observations of quarry blasts-test measurements in Western Germany, in *Explosion Seismology in Central Europe*, pp.119-126, edited by P.Giese, C.Prodehl, and A.Stein, Springler-Verlag, 1976.

Burwash, R.A., R.R. Culbert, Multivariable geochemical and mineral patterns in the Precambrian basement of western Canada, Canadian J. of Earth Sciences, 13, pp.1-18, 1976.

Chandra, N.N., Converted wave method for crustal structure. Unpubl.M.Sc. thesis, Univ. of Alberta, 110p., 1964.

Chandra, N.N., G.L.Cumming, Seismic refraction studies in Western Canada, Canadian J. of Earth Sciences, 9, p.1099, 1972.

Clowes, R.M., E.R.Kanasewich, and G.L.Cumming, Deep crustal reflections at near vertical incidence, Geophysics, 33, pp.441-451, 1968.

Clowes, R.M., E.R.Kanasewich, Seismic attenuation and the nature of reflecting horizons within the crust, J.

Geophys. Res., 75, pp.6693-6705, 1970.

Conrad, V., Lauftzeitkurven des Tauernbebens vom 28 November 1923, Mitt. Erdb. Komm. Wienner Akad. Wiss., 59, pp.1-23, 1925.

Cranstone, D.A., and Turek, A., Canadian J. of Earth Sciences, 13, p.1058, 1976

Cumming, G.L., and E.R.Kanasewich, Crustal structure in Western Canada. Final report; May 1, 1963 - April 30, 1966. Advanced Research Projects Agency on contract AF19(628)-2835. Task no. 865202, Document no. AFCRL-66-519, pp.1-126.

Douglas, R.J.W., Introduction in *Geology and Economic Minerals of Canada*, Department of Energy, Mines and Resources Canada, 1970.

Edel, J.B., K.Fuchs, C.Gelbke, and C.Prodehl, Deep structure of the southern Rhinegraben area from seismic refraction investigation, J. Geophys., 41, pp.333-356, 1975.

Green, A.G., Cumming, G.L., and D.Cedarwell, The Superior-Churchill boundary zone in suthern Canada, Centre for Precambrian Studies, Publication No.34.

Green, A.G., A cooperative near vertical incident reflection and refraction/wide angle reflection seismic survey across the Superior-Churchill boundary zone in southern Canada, Part 1. A technical report, 1977.

Green, A.G., D.G.Stephenson, Cooperative near vertical incident reflection and refraction/wide angle reflection seismic survey across the Superior-Churchill boundary zone in southern Canada, Part 2. Data and preliminary results, 1978.

Green, A.G., O.G.Stephenson, G.D.Mann, E.R.Kanasewich, G.L.Cumming, Z.Hajnal, J.A.Mair, G.F.West, Cooperative Seismic Survey across the Superior-Churchill boundary zone in southern Canada, A final report, 1979.

Hall, D.H., and W.C.Brisbin, A study of the Mohorovicic discontinuity near Flin Flon, Manitoba. Final report for Geophysics Research Directorate, Air Force Cambridge Research Laboratories: U.S. Department of Commerce, Office of Technical Services, Washington 25, D.C., 1961.

Hall, D.H., and W.C.Brisbin, Crustal structure from converted head waves in Central Western Manitoba, Geophysics, 30, 6, pp.1053-1067, 1972.

Heacock, J.G., Intermediate and deep properties of the earth's crust, A possible electromagnetic wave guide, in *The Structure and Physical Properties of the Earth's Crust*, Geophys. Monogr. Ser., vol.14, edited by J.G.Heackock, pp.1-9, AGU, Washington, D.C., 1971.

Hodgson, J.H., Analysis of travel times from rock bursts at Kirkland Lake, Ontario, Bull. Seism. Soc. Amer., 37, pp.5-17.

Jeffreys, H., On the materials and density of the earth's crust, Mon. Not. R. A. S. Geophys. Suppl., 4, 50, 1937.

Kanasewich, E.R., Deep crustal structure under the plains and Rocky Mountains, Canadian J. of Earth Science, 3, p.937, 1966.

Kanasewich, E.R., R.M.Clowes, and C.H.Mc Clougham, A buried Precambrian rift in Western Canada, Tectonophysics, 8, pp.513-527, 1969.

Kanasewich, E.R., *Time Series Analysis in Geophysics*, University of Alberta Press, Edmonton, 1975.

Keller, G.R., R.B.Smith, and L.W.Braile, Crustal structure along the Great Basin-Colorado plateau transition from seismic refraction stadies, J. Geophys. Res., 80, pp.1093-1098, 1975.

Kosminskaya, I.P., Deep crustal sounding of the earth's crust and upper mantle, Consultant Bureau, pp.15-31, New York, 1971.

Lee, S.K.J.,Multilayer gravity inversion using Fourier transforms, M.Sc. thesis, Univ. of Alberta, 141 p., 1977.

Liebscher, H., Reflexionshorizonte der triferen Erdkruste im Bayrischem Alpenforland, abgeleitet aus Ergebrussen der Reflexionseismik, Z.Geophys., 28, pp.162-184, 1962.

Liebscher, H., Deutungsversuche fur die Structur der tieferen Erdkruste nach reflexionsseismischen und gravimetrischen Messungen im deutschen Alpenforland, 1, 2, Z.Gephys., 30, pp.51-96, pp.115-126, 1964.

Mann, G.D., Multichannel signal enhancement techniques for reflection seismic records. Unpubl. M.Sc. thesis, Univ. of Alberta, 164 p., 1979.

Maureau, G.T.F.R., Crustal structure in western Canada. Unpubl. M.Sc. thesis, Univ. of Alberta, 110 p., 1964.

Meissner, R., H.Berckhemer, and A.Glocke, Results from deep-seismic sounding in the Rhine-Mainarea, in *Explosion seismology in Central Europe-Data and Results*, edited by P.Giese, C.Prodehl, and A.Stein, pp.303-312, Springer, New York, 1976.

Milne, W.G., and W.R.H.White, A seismic survey in the vicinity of Vancouver Island, British Columbia, Publ. Dom. Obs. Ottawa, Ontario, 24, pp.145-154, 1960.

Mohorovicic, A., Das Beben vom 8.10.1909, Jahrb. Meteorol. Observ. Zagreb 9(4), 63, 1910.

Mueller, S., E.Peterschmitt, K.Fuchs, D.Emter, and J.Ansorge, Crustal structure of the Rhinegraben area, Tectonophysics, 20, pp.381-392, 1973.

Mueller, S., A new model of the continental crust, in*The Earth's Crust*, Geophys. Monogr. Ser., vol.20, edited by J.G.Heacock, pp.289-317, A.G.U., Washington, D.C., 1977.

Oliver, J., M.Dobrin, S.Kaufman, R.Meyer and R.Phinney, Continuous seismic reflection profiling of the deep basement, Hardeman County, Texas, Geol. Soc. Amer. Bull., 87, 1537-1546, 1976.

Polshkov, M.K., N.B.Bulin, and B.E.Sherbakova, Crustal investigation of the U.S.S.R. by means of earthquake-generated converted waves, Tectonophysic, 20, pp.57-66, 1973.

Prodehl, C., J.Ansorge, J.B.Edel, D.Emter, K.Fuchs, S.Mueller, and E.Peterschmitt, Explosion-seismology research in the central and southern Rhinegraben -A case history, in *Explosion Seismology in Central Europe -Data and Results*, edited by P.Giese, C.Prodehl, and A.Stein, pp.313-328, Springer, New York, 1976.

Richards, T.C. and D.J.Walker, Measurements of the thickness of the earth's crust in the Albertan plains of Western Canada, Geophysics, 24, pp.262-284, 1959.

Schilt, S., J.Oliver, L.Brown, S.Kaufman, D.Albaugh, J.Brewer, F.Cook, L.Jensen, P.Krumhansl, G.Long and D.Steiner, The heterogeneity of the continental crust:Results from deep crustal seismic reflection profiling using the VIBROSEIS technique, Papers in Seismology, U.S. National Report to the IUGG, vol.17, no.2, pp.354-368, 1979.

Weaver, D.F., Seismological determination of crustal thickness in southern Alberta. Unpubl. M.Sc. thesis, Univ. of Alberta, 210 p., 1962.

White, W.R.H., and J.C.Savage, A seismic refraction and gravity study of the earth'scrust in British Columbia, Bull. Seism. Soc. Amer., 55, pp.463-468, 1965.

Wilson, H.D.B., Geological Association of Canada Special Paper No.9, p.41, 1971.

APPENDIX

LISTING OF COMPUTER PROGRAMS

1. The power spectrum
2. The cross-correlation function
3. The ground motion
4. The traveltime for n-layer system

This program plots seismic trace and calculates
and plots its power spectrum

****

****

```
C...    THIS ROUTINE PLOTS SEISMIC TRACE AND COMPUTES AND
C...    PLOTS ITS POWER SPECTRUM
      INTEGER IWK(8)
      REAL X(5003),PSX(129),WK(128),FA(129),F(129),
      REAL PSLC(140),PSL(140),XX(5003)
      COMPLEX CWK(258)
      DIMENSION REC1(20),REC2(20),REC3(20)
      READ(5,1000) REC1
      READ(5,1000) REC2
      READ(5,1000) REC3
 1000 FORMAT(20A4)
      READ(5,1001) LL,IND,NN,NTR,NB,NS
 1001 FORMAT(16I5)
      READ(5,1002) TL,SCL,CSP,RP,TSR,FDIST
 1002 FORMAT(10F8.2)
C...    LL IS PARAMETER WHICH AFFECTS NUMBER OF FREQUENCES
C...    AT WHICH POWER SPECTRA ARE CALCULATED
C...      IND IS INPUT CONTROL PARAMETER
C...    NN IS NUMBER OF POINTS WE READ.MUST BE EVENLY
C...    DIVISIBLE BY LL
C...    NTR IS TRACE NUMBER WE READ DATA FROM
C...    NB IS STARTING BLOCK TO READ DATA FROM
C...    NS IS STARTING POINT WITHIN BLOCK
C...    TL IS LENGTH OF TIME AXIS
C...    SCL IS HEIGHT OF SEISMIC TRACE ON PLOT
C...    CSP IS CHANNEL SEPARATION
C...    RP IS FACTOR AFFECTING POLARITY
C...    TSR IS TIME BETWEEN SHOT AND FIRST RECORDED POINT
C...    FDIST IS DISTANCE BETWEEN SHOT POINT AND RECEIVER
      CALL READTR(NTR,NB,NS,NN,XX)
      CALL MEANR(XX,NN,X)
      IF (RP.EQ.1.00)GO TO 1
      DO 2 I=1,NN
      X(I)=-X(I)
    2 CONTINUE
    1 CONTINUE
      CALL MAXMIN(X,NN,XMAX,XMIN,BIG)
      CALL PLOTS
      CALL FACTOR(0.9)
      CALL PLOT(0.0,0.4,-3)
      CALL SYMBOL(0.2,0.2,0.12,REC1,90.0,80)
      CALL SYMBOL(0.4,0.2,0.12,REC2,90.0,80)
      CALL TAXIS2(NB,NS,NN,TSR,FDIST,CSP,TL)
      CALL PLOTCH(X,NN,TL,SCL,NTR,CSP,BIG)
      CALL FTFPS(X,Y,NN,LL,IND,PSX,PSY,XPS,IWK,WK,
     &CWK,IER)
```

```
C...    CALCULATES FREQUENCES AT WHICH POWER SPECTRUM
C...    WAS FOUND
      TDIG=0.0056
      TDG=LL*TDIG
      II=LL/2+1
      DO 3 I=1,II
      F(I)=(I-1)/TDG
    3 CONTINUE
      WRITE(6,1003)
 1003 FORMAT(//5X,'FREQUENCY(HZ)',20X,'AMPLITUDE'//)
      DO 4 K=1,II
      WRITE(6,1004) F(K),PSX(K)
 1004 FORMAT(5X,F10.4,15X,F20.4)
    4 CONTINUE
C...    PLOTTING POWER SPECTRUM IN LOG SCALE
      CALL PLOT(5*CSP,CSP,-3)
      FB=(6*CSP)/FLOAT(II-1)
C...    FB IS DISTANCE BETWEEN TWO SUCCESIVE POINTS
C...    ON FREQUENCY AXIS
      FA(1)=0.0
      DO 6 K=2,II
      FA(K)=FA(K-1)+FB
    6 CONTINUE
      FA(II+1)=0.0
      FA(II+2)=1.0
      CALL PLOT(0.0,6*CSP,2)
      CALL PLOT(0.0,0.0,3)
      CALL PLOT((-4)*CSP,0.0,2)
      DO 10 K=1,II
      PSL(K)=ALOG10(PSX(K))
   10 CONTINUE
      CALL MAXMIN(PSL,II,PS1,PS2,PS3)
      IPS=IFIX(PS1)+1
      ALS=4*CSP/IPS
      DO 12 I=1,II
      PSLC(I)=-(IFIX(PSL(I))+ALOG10((PSL(I)-IFIX(PSL(I)))
     &*10))
   12 CONTINUE
      PSLC(II+1)=0.0
      PSLC(II+2)=IPS/(4.*CSP)
      CALL LINE(PSLC,FA,II,1,10,3)
C...    PLOTS SYMBOLS FOR FREQUENCY AXIS
      HZL=(6*CSP)/F(II)
C...    HZL IS LENGTH OF 1 HZ
      IFF=IFIX(F(II)/5)
      IFF=IFF+1
      DO 7 I=1,IFF
      CALL SYMBOL(0.0,(I-1)*HZL*5.,0.05,16,90.0,-1)
    7 CONTINUE
      IFG=IFIX(F(II)/10)
      IFG=IFG+1
      DO 20 I=1,IFG
      CALL NUMBER(0.12,(I-1)*HZL*10.-0.05,0.08,(I-1)*10.,
     &90.0,-1)
```

```
   20 CONTINUE
      CALL SYMBOL(0.30,0.4*6*CSP,0.1,'FREQUENCY HZ',90.0,12)
C...    PLOTS SYMBOLS FOR LOG AMPLITUDE AXIS
      IPSS=IPS+1
      DO 8 I=2,IPSS
      CALL SYMBOL((-1)*(I-1)*ALS,0.0,0.05,16,0.0,-1)
      CALL NUMBER((-1)*(I-1)*ALS+0.04,-0.25,0.08,10.,
     &90.0,-1)
      CALL NUMBER((-1)*(I-1)*ALS,-0.08,0.04,FLOAT(I-1),
    &90.0,-1)
    8 CONTINUE
      CALL SYMBOL((-0.4)*4*CSP,-0.35,0.1,'AMPLITUDE',
     &180.0,9)
      CALL SYMBOL(0.55,0.5,0.12,REC3,90.0,80)
      CALL PLOT(0.0,0.0,999)
      STOP
      END



      SUBROUTINE READTR(NTR,NB,NS,NN,X1)
C...    READS RAW DATA FROM ONE SPECIFIED CHANNEL AND
C...    DEMULTIPLEXES IT
      INTEGER *2 ID(1792),L1
      REAL X1(5003)
      NBB=NB-1
      CALL SKIP(0,NBB,8)
C...    SKIPS AT BEGINNING OF BLOCK WE WANT TO READ
C...    DATA FROM
      NAA=NS+NN-1
      NA=(NAA/128)+1
C...    NA IS NUMBER OF BLOCKS REQUIRED TO READ DATA
      IDP=NA*128
      M=0
      DO 101 I=1,NA
      CALL READ(ID,L1,0,LNR,8)
      DO 102 J=NTR,1792,14
      M=M+1
  102 X1(M)=ID(J)/4.0
  101 CONTINUE
      DO 103 I=1,NN
      IN=I+(NS-1)
      X1(I)=X1(IN)
  103 CONTINUE
      WRITE(6,1110) NTR,NS,NB,NN
 1110 FORMAT(//'DATA ARE READ FROM CHANNEL',I3/'FIRST',
     &' POINT TO READ IS',I4,' IN BLOCK',I4/'NUMBER OF',
     &' DATA POINTS READ IS',I5)
      NBC=NBB+NA
      CALL SKIP(0,-NBC,8)
      RETURN
      END
```

```
      SUBROUTINE MAXMIN(X1,NN,XMAX,XMIN,BIG)
C...    FINDS MAXIMUM  AND MINIMUM VALUES
      REAL X1(5003)
      XMAX=X1(1)
      XMIN=X1(1)
      DO 201 I=2,NN
      IF(X1(I) .GT. XMAX) XMAX=X1(I)
      IF(X1(I) .LT. XMIN) XMIN=X1(I)
  201 CONTINUE
      BIG=XMAX
      IF(ABS(XMIN) .GT.BIG) BIG=ABS(XMIN)
      WRITE(6,1210) NN,XMAX,XMIN
 1210 FORMAT(//'MAXIMUM AND MINIMUM VALUES OF',I5,' DATA',
     &' POINTS ARE RESPECTIVELY',2F15.4)
      RETURN
      END



      SUBROUTINE PLOTCH(X1,NN,TL,SCL,NTR,CSP,BIG)
C...    PLOTS DATA FROM ONE SPECIFIED CHANNEL NTR
C...    START AND END OF PLOTTING HAVE TO BE CALLED
C...    IN MAIN ROUTINE
      DIMENSION T(5003),X1(5003)
      CALL PLOT(SCL+0.4,0.0,-3)
      TBP=TL/FLOAT(NN-1)
C...    TBP IS DISTANCE BETWEEN TWO SUCCESIVE POINTS
C...    ON TIME AXIS
      T(1)=0.0
      DO 301 I=2,NN
      T(I)=T(I-1)+TBP
  301 CONTINUE
      T(NN+1)=0.0
      T(NN+2)=1.0
      X1(NN+1)=0.0
      X1(NN+2)=BIG/SCL
      CALL LINE(X1,T,NN,1,0,0)
      CALL SYMBOL(0.15*CSP,0.0,0.06,'CHANNEL',90.0,7)
      CALL NUMBER(0.15*CSP,0.5,0.06,FLOAT(NTR),90.0,-1)
      RETURN
      END



      SUBROUTINE MEANR(X1,NN,Y1)
C...    REMOVES MEAN VALUE FROM DATA
      REAL Y1(5003),X1(5003)
      XSUM=0.0
      DO 151 I=1,NN
      XSUM=XSUM+X1(I)
  151 CONTINUE
      XSUM=XSUM/NN
      DO 152 I=1,NN
      Y1(I)=X1(I)-XSUM
```

```
  152 CONTINUE
      WRITE(6,1160) NN,XSUM
 1160 FORMAT(//'MEAN VALUE OF',I5,' DATA POINTS IS',F10.0)
      RETURN
      END


      SUBROUTINE TAXIS2(NB,NS,NN,TSR,FDIST,CSP,TL)
C...    PLOTS REDUCED TIME AXIS (T-X/8.0) FOR GIVEN
C...    DISTANCE X=FDIST AND TIME OF SHOT STARTING AT
C...    REQUIRED BLOCK AND POINT
      TSF=(NB*128+NS)*0.0056+TSR-FDIST/8.0
C...   TSF IS TIME BETWEEN SHOT AND FIRST PLOTTED POINT
C...    ON REDUCED TIME AXIS
      ITSF=IFIX(TSF)+1
C...   ITSF IS TIME BETWEEN SHOT AND FIRST PLOTTED POINT
C...   WITH FULL NUMBER OF SEC.
      TT=ITSF-TSF
      RDIG=178.5714
      UTL=(RDIG*TL)/FLOAT(NN)
C...   UTL IS LENGTH OF 1S ON PLOT
      UTTL=TT*UTL
      NTT=IFIX(TT*RDIG)
      IKT=(NN-NTT)/IFIX(RDIG)
      IKT=IKT+1
      CALL PLOT(0.8,0.0,-3)
      CALL PLOT(0.0,TL,2)
      DO 155 I=1,IKT
      CALL SYMBOL(0.0,UTTL+(I-1)*UTL,0.05,16,90.0,-1)
  155 CALL NUMBER(-0.15,UTTL-0.1+(I-1)*UTL,0.12,
     &FLOAT(ITSF+I-1),90.0,1)
      CALL SYMBOL (0.25,0.35*TL,0.12,'TIME (T-X/8.0) SEC.',
     &90.0,19)
      RETURN
      END
```

```
This program plots two traces, calculates their variances,
cross-covariances and cross-correlations and also
plots the cross-correlation function

**************************************************************


**************************************************************
C...    THIS ROUTINE PLOTS TWO FILTERED SEISMIC TRACES,
C...    FINDS VARIANCES AND
C...    CROSS-COVARIANCES AND ALSO CALCULATES AND PLOTS
C...    CROSS-CORRELATION
      INTEGER NC(4)
      REAL XX(5003),X(5003),XXX(5003),YY(5003),Y(5003)
      REAL XY(10003),EMUSIG(4),ACV(1,1,51),AC(1,1,51)
      REAL ACL(200),D(8),YX(10003),EMU(4),ACV1(1,1,51)
      REAL YYY(5003),TLU(200),AC1(1,1,51)
      DIMENSION REC1(20),REC2(20),REC3(20),REC4(20),REC5(20)
      DATA NC/1000,1000,1,50/
      NC5=NC(4)
      READ(5,1000) REC1
      READ(5,1000) REC2
      READ(5,1000) REC3
      READ(5,1000) REC4
      READ(5,1000) REC5
 1000 FORMAT(20A4)
      READ(5,1001)NTR1,NB1,NS1,NN1,NF,NTR2,NB2,NS2,NN2
      READ(5,1001) ISW,IA,IB,IC,ID,NC4
      READ(5,1002) RP1,TL1,SCL1,CSP1,RP2,TL2
      READ(5,1002) SCL2,CSP2,TSR1,FDIST1,TSR2,FDIST2
      READ(5,1002) F1,F2,DELT
 1001 FORMAT(16I5)
 1002 FORMAT(8F10.2)
C...    NF IS FILE NUMBER OF SECOND RECORD
C...    NN IS NUMBER OF POINTS WE READ.MUST BE EVENLY
C...    DIVISIBLE BY LL
C...    NTR IS TRACE NUMBER WE READ DATA FROM
C...    NB IS STARTING BLOCK TO READ DATA FROM
C...    NS IS STARTING POINT WITHIN BLOCK
C...    TL IS LENGTH OF TIME AXIS
C...    SCL IS HEIGHT OF SEISMIC TRACE ON PLOT
C...    CSP IS CHANNEL SEPARATION
C...    RP IS FACTOR AFFECTING POLARITY
C...    TSR IS TIME BETWEEN SHOT AND FIRST RECORDED POINT
C...    FDIST IS DISTANCE BETWEEN SHOT POINT AND RECEIVER
C...    F1 IS LOW CUT-OFF FREQUENCY
C...    F2 IS HIGHT CUT-OFF FREQUENCY
C...    DELT IS SAMPLING INTERVAL IN MS
      CALL BNDPAS(F1,F2,DELT,D,G)
      CALL READTR(NTR1,NB1,NS1,NN1,XX)
      CALL MEANR(XX,NN1,X)
      CALL MAXMIN(X,NN1,XMAX,XMIN,BIG1)
      CALL FILTER(X,NN1,D,G,1)
```

```
      REWIND 8
      NFA=NF-1
      CALL SKIP(NFA,0,8)
      CALL READTR(NTR2,NB2,NS2,NN2,YY)
      CALL MEANR(YY,NN2,Y)
      CALL MAXMIN(Y,NN2,YMAX,YMIN,BIG2)
      CALL FILTER(Y,NN2,D,G,1)
C...    NORMALIZES VALIUES BOTH TRACES
      BIGG=BIG1
      IF(BIG2 .GT.BIGG) BIGG=BIG2
      BIGX=BIGG/BIG1
      BIGY=BIGG/BIG2
      CALL NORM(X,BIGX,RP1,NN1,XXX)
      CALL NORM(Y,BIGY,RP2,NN2,YYY)
      CALL PLOTS
      CALL FACTOR(0.9)
      CALL PLOT(0.0,0.4,-3)
      CALL SYMBOL(0.2,0.0,0.12,REC1,90.0,80)
      CALL SYMBOL(0.4,0.0,0.12,REC2,90.0,80)
      CALL TAXIS2(NB1,NS1,NN1,TSR1,FDIST1,CSP1,TL1)
      CALL PLOTCH(XXX,NN1,TL1,SCL1,NTR1,CSP1,BIGG)
      CALL PLOT(SCL1+0.4,0.0,-3)
      CALL SYMBOL(0.2,0.0,0.12,REC3,90.0,80)
      CALL SYMBOL(0.4,0.0,0.12,REC4,90.0,80)
      CALL TAXIS2(NB2,NS2,NN2,TSR2,FDIST2,CSP2,TL2)
      CALL PLOTCH(YYY,NN2,TL2,SCL2,NTR2,CSP2,BIGG)
C...    CALCULATES REQUIRED VALUES IN FORWARD DIRECTION
      DO 1 I=1,NN1
      XY(I)=XXX(I)
    1 CONTINUE
      NN3=NN1+NN2
      NN4=NN1+1
      DO 2 I=NN4,NN3
      XY(I)=YYY(I-NN1)
    2 CONTINUE
      CALL FTCROS(XY,NC,ISW,EMUSIG,ACV,IA,IB,AC,IC,ID,IER)
      WRITE(6,1009)
1009 FORMAT(///10X,'FORWARD DIRECTION'///)
      WRITE(6,1010) EMUSIG
1010 FORMAT(//'MEAN VALUE OF FIRST TIME SERIES IS',F5.0/
     &'MEAN VALUE',
     &' OF SECOND TIME SERIES IS',F5.0/'VARIANCE OF',
     &'FIRST TIME SERIES',
     &' IS',F12.0/'VARIANCE OF SECOND TIME SERIES IS',F12.0)
      WRITE(6,1011) NC5
1011 FORMAT(//'CROSS-COVARIANCES OF ',I5,
     &' TIME LAG UNITS ARE'//)
      WRITE(6,1012) ACV
1012 FORMAT(5F15.0)
      WRITE(6,1013) NC5
1013 FORMAT(//'CROS-CORRELATIONS OF',I5,
     &' TIME LAG UNITS ARE'//)
      WRITE(6,1014)AC
1014 FORMAT(10F8.4)
```

```
      WRITE(6,1015) IER
 1015 FORMAT(//'ERROR PARAMETER IS',I5)
C...    CALCULATES REQUIRED VALUES IN REVERSED DIRECTION
      DO 20 I=1,NN1
      YX(I)=YYY(I)
   20 CONTINUE
      NN5=NN2+1
      DO 21 I=NN5,NN3
      YX(I)=XXX(I-NN2)
   21 CONTINUE
      CALL FTCROS(YX,NC,ISW,EMU,ACV1,IA,IB,AC1,IC,ID,IER1)
      WRITE(6,1019)
 1019 FORMAT(///10X,'REVERSED DIRECTION'///)
      WRITE(6,1020) EMU
 1020 FORMAT(//'MEAN VALUE OF FIRST TIME SERIES IS',F5.0/
     &'MEAN VALUE',
     &' OF SECOND TIME SERIES IS',F5.0/'VARIANCE OF',
     &'FIRST TIME SERIES',
     &' IS',F12.0/'VARIANCE OF SECOND TIME SERIES IS',F12.0)
      WRITE(6,1011) NC5
      WRITE(6,1021) ACV1
 1021 FORMAT(5F15.0)
      WRITE(6,1013) NC5
      WRITE(6,1022)AC1
 1022 FORMAT(10F8.4)
      WRITE(6,1015) IER1
C...    PLOTS CROS-CORRELATION FUNCTION
      TDL=(0.7*TL1)/FLOAT(NC4-1)
C...    TDL IS DISTANCE BETWEEN TWO SUCCESIVE
C...    POINTS ON TIME LAG AXIS
      TLU(1)=0.0
      DO 4 K=2,NC4
      TLU(K)=TLU(K-1)+TDL
    4 CONTINUE
      TLU(NC4+1)=0.0
      TLU(NC4+2)=1.0
      CALL PLOT(0.40*TL1,0.1*TL1,-3)
      CALL PLOT(0.0,0.7*TL1,2)
      CALL PLOT((-0.3)*TL1,0.0,3)
      CALL PLOT(0.3*TL1,0.0,2)
      NC6=NC5+1
      NC7=NC6+1
      DO 16 I=1,NC6
      II=NC7-I
      ACL(I)=-AC1(1,1,II)
   16 CONTINUE
      DO 17 I=NC7,NC4
      III=I-NC5
      ACL(I)=-AC(1,1,III)
   17 CONTINUE
      ACL(NC4+1)=0.0
      ACL(NC4+2)=1./(0.3*TL1)
      CALL LINE(ACL,TLU,NC4,1,5,3)
C...    PLOTS SYMBOLS AND NUMBERS ON CROSS-CORRELATION
```

```
C...     VALUE AXIS
         DO 12 I=1,5
         CALL SYMBOL((-0.3)*TL1*I/5.,0.0,0.05,16,0.0,-1)
         CALL SYMBOL(0.3*TL1*I/5.,0.0,0.05,16,0.0,-1)
         CALL SYMBOL((-0.3)*TL1*I/5.,-0.3,0.04,3,90.0,-1)
         CALL SYMBOL(0.3*TL1*I/5.,-0.3,0.04,15,90.0,-1)
         CALL NUMBER((-0.30)*TL1*I/5.+0.04,-0.24,0.08,I*0.2,
         90.0,1)
         CALL NUMBER(0.3*TL1*I/5.+0.04,-0.24,0.08,I*0.2,90.0,1)
      12 CONTINUE
C...     PLOTS SYMBOLS AND NUMBERS FOR TIME LAG AXIS
         ILU=NC4/5+1
         DO 6 I=1,ILU
         CALL SYMBOL(0.0,5*(I-1)*TDL,0.05,16,90.0,-1)
       6 CONTINUE
         CALL PLOT(0.0,0.7*TL1/2,-3)
         CALL SYMBOL(0.12,-0.02,0.08,'0',90.0,1)
         ILW=ILU/4
         DO 14 I=1,ILW
         CALL SYMBOL(0.08,10*I*TDL-0.1,0.05,3,90.0,-1)
         CALL SYMBOL(0.08,(-10)*I*TDL-0.1,0.05,15,90.0,-1)
         CALL NUMBER(0.12,10*I*TDL-0.05,0.08,I*10.,90.0,-1)
         CALL NUMBER(0.12,(-10)*I*TDL-0.05,0.08,I*10.,90.0,-1)
      14 CONTINUE
         CALL SYMBOL(0.30,(0.2)*TL1,0.1,'TIME LAG UNITS',
         90.0,14)
         CALL SYMBOL(0.31*TL1,(-0.2)*TL1,0.12,REC5,90.0,80)
         CALL PLOT(0.0,0.0,999)
         STOP
         END


         SUBROUTINE NORM(X1,FN,RPOL,NN,Y1)
C...     NORMALIZES AND REVERSES POLARITY
C...     COEFFICIENT OF NORMALIZATION SHOULD BE CALCULATED
C...     IN MAIN ROUTINE USING OUTPUT OF SUBROUTINE MAXMIN
         REAL Y1(5003),X1(5003)
         FNA=FN*RPOL
         DO 251 I=1,NN
         Y1(I)=X1(I)*FNA
       251 CONTINUE
         IF(RPOL .EQ. 1.00) GO TO 252
         WRITE(6,1260) NN,FN
      1260 FORMAT(//'MULTIPLYING FACTOR OF',I5,' DATA POINTS IS',
        &F7.4,5X,'POLARITY IS REVERSED')
         GO TO 253
       252 CONTINUE
         WRITE(6,1270)NN,FN
      1270 FORMAT(//'MULTIPLYING FACTOR OF',I5,' DATA POINTS IS',
        &F7.4,5X,' POLARITY IS NOT CHANGE')
       253 CONTINUE
         RETURN
         END
```

This program first plots traces of horizontal N.S., E.W. and radial components as well as vertical component of the ground motion. Next it plots Lissajous figure of vertical versus radial horizontal components

****

****

```
C...     THIS ROUTINE PLOTS HORIZONTAL N.S., E.W.
C...      AND RADIAL COMPONENTS AS WELL AS
C...     VERTICAL COMPONENT OF GROUND MOTION.
C...     RADIAL HORIZONTAL IS CALCULATED FROM
C...     THE OTHER TWO HORIZONTAL.
C...     PLOTS LISSAJOUS FIGURE OF VERTICAL
C...     COMPONENT VERSUS HORIZONTAL RADIAL
      REAL XX1(1000),XX2(1000),XX3(1000),X1(1000),X2(1000)
      REAL XR(1002),XUP(1002),D(8),X3(1000)
      DIMENSION REC1(20),REC2(20),REC3(20)
      READ(5,1003) REC1
      READ(5,1003) REC2
      READ(5,1003) REC3
 1003 FORMAT(20A4)
      READ(5,1000) NB,NS,NN
 1000 FORMAT(16I5)
      READ(5,1001) F1,F2,DELT,TL,SCL,CSP,TSR,AZR
 1001 FORMAT(10F8.2)
      CALL BNDPAS(F1,F2,DELT,D,G)
      CALL READTR(1,NB,NS,NN,XX1)
      CALL READTR(2,NB,NS,NN,XX2)
      CALL READTR(3,NB,NS,NN,XX3)
      CALL MEANR(XX1,NN,X1)
      CALL MEANR(XX2,NN,X2)
      CALL MEANR(XX3,NN,X3)
      CALL FILTER(X1,NN,D,G,1)
      CALL FILTER(X2,NN,D,G,1)
      CALL FILTER(X3,NN,D,G,1)
      DO 1 I=1,NN
      XR(I)=-X1(I)*COS(AZR)-X2(I)*SIN(AZR)
      XUP(I)=-X3(I)
    1 CONTINUE
      CALL MAXMIN(X1,NN,X1B,X1S,X1L)
      CALL MAXMIN(X2,NN,X2B,X2S,X2L)
      CALL MAXMIN(X3,NN,X3B,X3S,XUPL)
      CALL MAXMIN(XR,NN,XRB,XRS,XRL)
      SC=X1L
      IF(X2L .GT. SC) SC=X2L
      IF(XUPL .GT. SC) SC=XUPL
      IF(XRL .GT. SC) SC=XRL
      SC1=SC/X1L
      SC2=SC/X2L
      SCUP=SC/XUPL
      SCR=SC/XRL
```

```
      BIG=XUPL
      IF(XRL .GT. BIG) BIG=XRL
      CALL PLOTS
      CALL FACTOR(0.9)
      CALL PLOT(0.0,0.4,-3)
      CALL SYMBOL(0.2,0.0,0.12,REC1,90.0,80)
      CALL SYMBOL(0.4,0.0,0.12,REC2,90.0,80)
      CALL TAXIS3(NB,NS,NN,TSR,CSP,TL)
      CALL PLOT(0.10,0.0,-3)
      CALL PLOTCH(X1,NN,TL,SCL,CSP,SC1,X1L)
      CALL SYMBOL(0.5*CSP,-0.20,0.06,'HORIZ.',180.0,6)
      CALL SYMBOL(0.5*CSP,-0.10,0.06,'N.S.',180.0,4)
      CALL AROHD(-0.2*CSP,0.0,0.5*CSP,0.0,0.3*CSP,
     &0.12*CSP,16)
      CALL SYMBOL(0.5*CSP,0.10,0.06,'NORTH',90.0,5)
      CALL PLOTCH(X2,NN,TL,SCL,CSP,SC2,X2L)
      CALL SYMBOL(0.5*CSP,-0.20,0.06,'HORIZ.',180.0,6)
      CALL SYMBOL(0.5*CSP,-0.10,0.06,'E.W.',180.0,4)
      CALL AROHD(-0.2*CSP,0.0,0.5*CSP,0.0,0.3*CSP,
     &0.12*CSP,16)
      CALL SYMBOL(0.5*CSP,0.10,0.06,'EAST',90.0,4)
      CALL PLOTCH(XR,NN,TL,SCL,CSP,SCR,XRL)
      CALL SYMBOL(0.5*CSP,-0.20,0.06,'HORIZ.',180.0,6)
      CALL SYMBOL(0.5*CSP,-0.10,0.06,'RADIAL',180.0,6)
      CALL AROHD(-0.2*CSP,0.0,0.5*CSP,0.0,0.3*CSP,
     &0.12*CSP,16)
      CALL SYMBOL(0.5*CSP,0.10,0.06,'AWAY',90.0,4)
      CALL PLOTCH(X3,NN,TL,SCL,CSP,SCUP,XUPL)
      CALL SYMBOL(0.6*CSP,-0.10,0.06,'VERTICAL',180.0,8)
      CALL AROHD(-0.2*CSP,0.0,0.5*CSP,0.0,0.3*CSP,
     &0.12*CSP,16)
      CALL SYMBOL(0.5*CSP,0.10,0.06,'UP',90.0,2)
      CALL PLOT(0.42*TL,0.1*TL,-3)
      CALL PLOT(0.0,0.6*TL,2)
      CALL AROHD(0.0,0.6*TL,0.0,0.6*TL+0.2,0.2,0.08,16)
      CALL PLOT(0.30*TL,0.30*TL,3)
      CALL PLOT(-0.30*TL,0.30*TL,2)
      CALL AROHD(-0.30*TL,0.30*TL,-0.30*TL-0.2,0.30*TL,0.2,
     &0.08,16)
      CALL SYMBOL(-0.31*TL-0.2,0.25*TL,0.1,'VERTICAL(UP)',
     &90.0,12)
      CALL SYMBOL(0.20,0.6*TL,0.1,'HORIZ.(AWAY)',90.0,12)
      CALL PLOT(0.0,0.30*TL,-3)
      XR(NN+1)=0.0
      XR(NN+2)=BIG/(0.30*TL)
      XUP(NN+1)=0.0
      XUP(NN+2)=BIG/(0.30*TL)
      CALL LINE(XUP,XR,NN,1,10,3)
      CALL SYMBOL(0.35*TL,-0.35*TL,0.1,REC3,90.0,80)
      CALL PLOT(0.0,0.0,999)
      STOP
      END
```

```
      SUBROUTINE PLOTCH(X1,NN,TL,SCL,CSP,SCF,A)
C...    PLOTS DATA POINTS WITHOUT LABEL FROM ONE CHANNEL
C...    START AND END OF PLOTTING HAVE TO BE CALLED
C...    IN MAIN ROUTINE
      DIMENSION T(5003),X1(5003)
      CALL PLOT(CSP,0.0,-3)
      TBP=TL/FLOAT(NN-1)
C...    TBP IS DISTANCE BETWEEN TWO SUCCESIVE POINTS
C...    ON TIME AXIS
      T(1)=0.0
      DO 301 I=2,NN
      T(I)=T(I-1)+TBP
  301 CONTINUE
      T(NN+1)=0.0
      T(NN+2)=1.0
      X1(NN+1)=0.0
      X1(NN+2)=(A*SCF)/SCL
      CALL LINE(X1,T,NN,1,25,3)
      RETURN
      END



      SUBROUTINE TAXIS3(NB,NS,NN,TSR,CSP,TL)
C...    PLOTS TIME AXIS WITH TWO VALUES ON IT
C...    (FIRST AND LAST POINTS)
      TSF=(NB*128+NS)*0.0056+TSR
      TSL=(NB*128+NS+NN)*0.0056+TSR
      CALL PLOT(0.7,0.0,-3)
      CALL PLOT(0.0,TL,2)
      CALL SYMBOL(0.0,0.0,0.05,16,90.0,-1)
      CALL SYMBOL(0.0,TL,0.05,16,90.0,-1)
      CALL NUMBER(0.15,-0.20,0.1,TSF,90.0,2)
      CALL NUMBER(0.15,TL-0.20,0.1,TSL,90.0,2)
      CALL SYMBOL(0.15,0.35*TL,0.10,'PLOTTING TIME IN SEC.',
     &90.0,21)
      RETURN
      END
```

```
This program calculates traveltime of a given phase of
n-layer system given a velocity in each layer, depth to
the bottom of each layer and a velocity of a halfspace

**********************************************************


**********************************************************

C...     THIS PROGRAM CALCULATES IN MOST GENERAL CASE
C...     TRAVELTIME OF A GIVEN PHASE IN N-LAYER SYSTEM
C...     GIVEN VELOCITY IN EACH LAYER, DEPTH TO
C...     BOTTOM OF EACH LAYER AND VELOCITY OF
C...     HALFSPACE
       INTEGER ICSP(10),ICRP(10) ,REC(20),REC1(20)
       REAL VSP(11),VRP(11),HSP(10),HRP(10)
       READ(5,1000) REC
 1000  FORMAT(20A4)
       WRITE(6,1000) REC
       READ(5,1002) X
 1002  FORMAT(F10.3)
       WRITE(6,1003) X
 1003  FORMAT(//'DISTANCE',F10.3,' KM')
       READ(5,1004) NL
 1004  FORMAT(I5)
       WRITE(6,1005) NL
 1005  FORMAT(//'NUMBER OF LAYERS',I3,' PLUS HALFSPACE')
       READ(5,1000) REC1
       WRITE(6,1006) REC1
 1006  FORMAT(/'PHASE',2X,20A4)
       NL1=NL+1
       READ(5,1007)( ICSP(K),K=1,NL)
 1007  FORMAT(10I1)
       READ(5,1007) (ICRP(K),K=1,NL)
       READ(5,1008) ICHS
 1008  FORMAT(I1)
       READ(5,1009) (VSP(K),K=1,NL1)
 1009  FORMAT(11F5.2)
       READ(5,1009) (VRP(K),K=1,NL1)
       READ(5,1010) (HSP(K),K=1,NL)
 1010  FORMAT(10F5.2)
       READ(5,1010) (HRP(K),K=1,NL)
       WRITE(6,1020)
 1020  FORMAT(//20X,'VELOCITY BELOW SHOTPOINT',10X,'DEPTH',
      &'  BELOW SHOTPOINT')
C...     X IS DISTANCE BETWEEN SHOTPOINT AND RECEIVER
C...     NL IS NUMBER OF LAYERS ABOVE HALF-SPACE
C...     ICSP IS COD NUMBER FOR PHASES BELOW SHOTPOINT
C...     BEGINNING WITH UPPERMOST LAYER NUMBER 1 IS
C...     DESIGNATED FOR P-WAVES; ANY OTHER NUMBER FOR S-WAVES
C...     ICRP IS COD NUMBER FOR PHASES BELOW RECEIVER
C...     ICHS IS COD NUMBER FOR HEAD-WAVES IN HALF-SPACE
C...     VSP ARE VELOCITIES IN SUCCESSIVE LAYERS AND
C...     HALFSPACE BELOW SHOTPOINT
```

```
C...    VRP ARE VELOCITIES IN SUCCESSIVE LAYERS AND
C...    HALFSPACE BELOW RECEIVER
C...    HSP ARE DEPTHS TO SUCCESSIVE HORIZONS BELOW
C...    SHOTPOINT
C...    HRP ARE DEPTHS TO SUCCESSIVE HORIZONS BELOW RECEIVER
      TSPS=0.0
      TCSP=0.0
      XCSP=0.0
      IF(ICHS .EQ. 1) GO TO 4
      VSP2=VSP(NL1)/1.73
      GO TO 5
    4 CONTINUE
      VSP2=VSP(NL1)
    5 CONTINUE
      DO 1 I=1,NL
      IF(ICSP(I) .EQ. 1) GO TO 2
      V1=VSP(I)/1.73
      GO TO 3
    2 CONTINUE
      V1=VSP(I)
    3 CONTINUE
      IF(I .GT. 1) GO TO 7
      H=HSP(1)
      GO TO 8
    7 CONTINUE
      H=HSP(I)-HSP(I-1)
    8 CONTINUE
      IF(VSP2 .GT. V1) GO TO 10
      GO TO 100
   10 CONTINUE
      WRITE (6,1021)I,V1,HSP(I)
 1021 FORMAT(/I2,' LAYER',10X,F15.2,15X,F15.2)
      TSP=SQRT(VSP2*VSP2-V1*V1)/(VSP2*V1)
      TSPS=TSPS+TSP*H
      COS=SQRT(1-((V1*V1)/(VSP2*VSP2)))
      TCSP=TCSP+H/(V1*COS)
      TAN=(V1/VSP2)/COS
      XCSP=XCSP+H*TAN
    1 CONTINUE
      WRITE(6,1022) VSP2
 1022 FORMAT(/' HALFSPACE',8X,F15.2)
      WRITE(6,1023)
 1023 FORMAT(//20X,'VELOCITY BELOW RECEIVER',10X,
     &'DEPTH BELOW RECEIVER')
      TRPS=0.0
      TCRP=0.0
      XCRP=0.0
      IF(ICHS .EQ. 1) GO TO 20
      VRP2=VRP(NL1)/1.73
      GO TO 21
   20 CONTINUE
      VRP2=VRP(NL1)
   21 CONTINUE
      DO 22 I=1,NL
```

```
      IF(ICRP(I) .EQ. 1) GO TO 23
      V1=VRP(I)/1.73
      GO TO 24
   23 CONTINUE
      V1=VRP(I)
   24 CONTINUE
      IF(I .GT. 1) GO TO 27
      H=HRP(1)
      GO TO 28
   27 CONTINUE
      H=HRP(I)-HRP(I-1)
   28 CONTINUE
      IF(VRP2 .GT. V1) GO TO 25
      GO TO 100
   25 CONTINUE
      WRITE (6,1021)I,V1,HRP(I)
      TRP=SQRT(VRP2*VRP2-V1*V1)/(VRP2*V1)
      TRPS=TRPS+TRP*H
      COS=SQRT(1-((V1*V1)/(VRP2*VRP2)))
      TCRP=TCRP+H/(V1*COS)
      TAN=(V1/VRP2)/COS
      XCRP=XCRP+H*TAN
   22 CONTINUE
      WRITE(6,1022) VRP2
      TCT=TCSP+TCRP
      XCT=XCSP+XCRP
      WRITE(6,1050) XCT,XCSP,XCRP,TCT,TCSP,TCRP
 1050 FORMAT(//'CRITICAL DISTANCE FOR THIS RAY IS',F10.3,
     &' KM'/'(',F7.3,' AND',F7.3,' KM FOR SHOTPOINT AND',
     &'RECEIVER BRANCHES RESPECTIVELY)'
     &//'CRITICAL TIME FOR THIS RAY IS',F7.2,' S'
     &/'(',F7.3,' AND',F7.3,' S FOR SHOTPOINT AND',
     &' RECEIVER BRANCHES RESPECTIVELY)')
      READ(5,1055) WFSP,WFRP
 1055 FORMAT(2F5.2)
      WRITE(6,1026) WFSP,VSP2,WFRP,VRP2
 1026 FORMAT(//F5.2,' OF HEAD WAVE PATH IS WITH VELOCITY',
     &F5.2,' KM/S'
     &/F5.2,' OF HEAD WAVE PATH IS WITH VELOCITY',)
     &F5.2,' KM/S'
C...     WFSP AND WFRP ARE WEIGHTING FACTORS FOR VELOCITY
C...     DISTRIBUTION OF HEAD WAVES
      V2=WFSP*VSP2+WFRP*VRP2
      T=X/V2+TSPS+TRPS
      WRITE(6,1060)T
 1060 FORMAT(//'TRAVELTIME IS',F10.2,' S'//)
      GO TO 101
  100 WRITE(6,1070) VSP2,I,V1
 1070 FORMAT(//'VELOCITY OF ASSUMED HEADWAVES',F5.2,' KM/S'
     &' IS LOWER THAN THAT IN LAYER',I3,'(',F5.2,' KM/S)')
  101 CONTINUE
      STOP
      END
```